Introduction/All

Robot Design Studio 2025: Mechanical Documentation Index

The HAND ERC is developing a robotic hand that is robust, easy to assemble and maintain, minimizes open space when opening and closing, features a soft, durable, conforming tactile sensing skin, and includes forearms capable of resting and sliding over supports. The goal is to create a hand capable of performing a range of dexterous tasks such as hammering, power-grasp jar capping, and drilling. The class researched various hand architectures before settling on a design that is not a complete hand, but rather tests design ideas to help evaluate future full-hand designs. For RDS 2025, the class was tasked with designing four key components: a wrist, a dexterous finger, a power-grasp finger, and a forearm. These components would be integrated into a simple hand design with a dummy thumb and palm. This document provides an index for documentation files, all stored within the class google drive.

Forearm

Forearm

Design Objectives

The following were set as the design objectives for the Series Elastic Actuator (SEA) modules:

- Enable **force-control** without force sensors, via angular deflection of a torsion spring
- Ensure **compliance** of up to 60° at 1 Nm of torque
- Allow **unlimited rotation** of motors (i.e. no absolute motor travel limits)

Those SEA modules fit into a forearm designed with the following objectives:

- **Package** 7 SEA modules securely and rigidly
- Fit in a **compact envelope** (approx. width, height, length of human forearm) and weight (1kg)
- Maintain **ease of manufacturing** and **assembly**

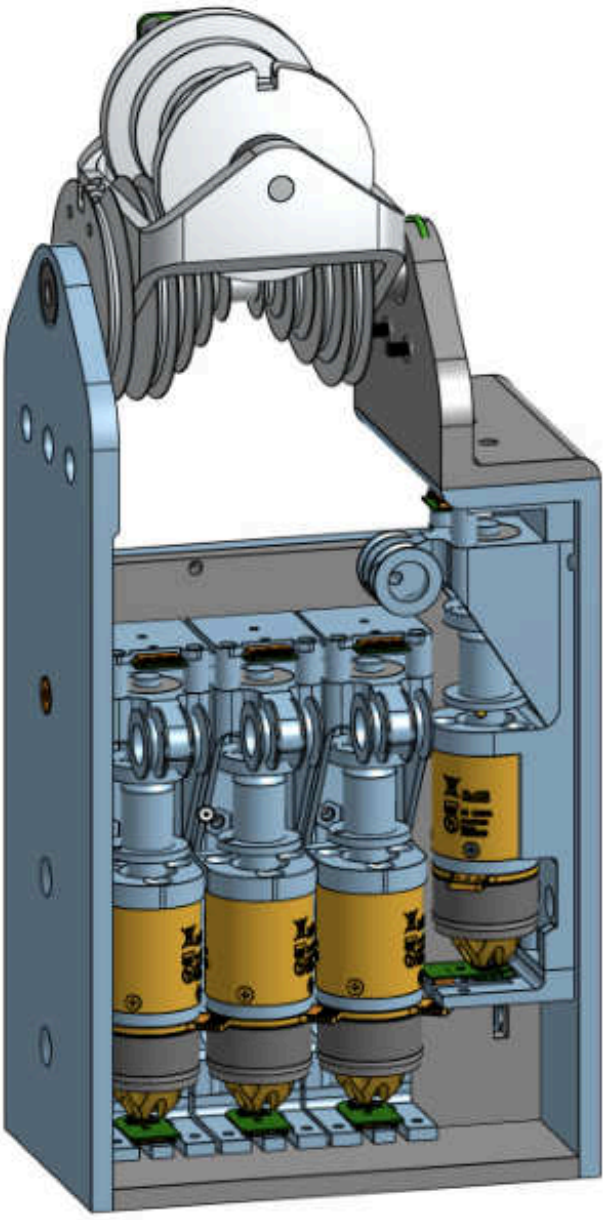
Overview of Forearm

The SEA modules enable force-control by inserting, as an intermediate between the motor and the tendon, a torsion spring whose angular deflection can be measured with magnetic encoders and used to infer tension in the tendon.

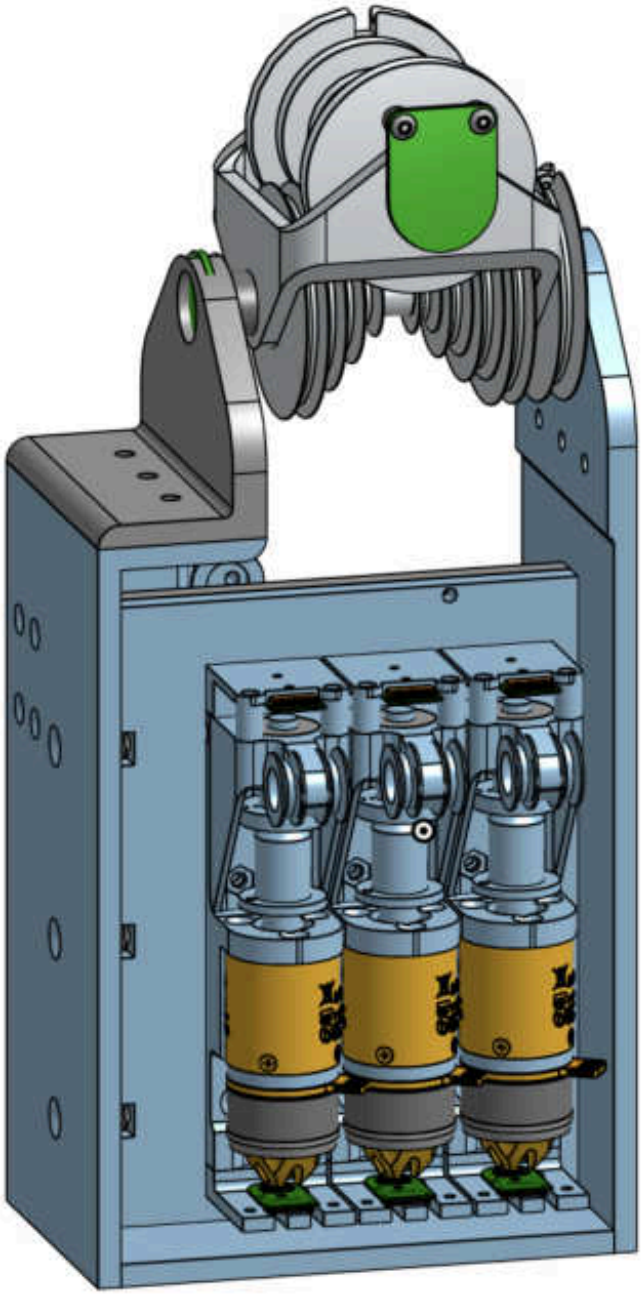


In this picture, you can see 3 distinct components directly above the motor: the motor pulley (bottom, inside spring), the spring, and the tendon pulley (above spring, wrapped with green fishing line). While it may look like all the aluminum parts above the motor are connected, they are in fact two separate pulleys, linked only by their connections to either end of the spring. This allows them to rotate relative to each other (i.e. when the finger is prevented from moving, yet the motor is applying torque), and this rotation is measured by comparing objective motor encoder values on the motor shaft versus the shaft of the tendon pulley. The motor encoders can be seen in green at the bottom, as well as in black at the top.

Originating from the tendon pulley, the tendon travels up over a redirection pulley which can be seen jutting out to the right and towards the viewer. The tendon then travels up, directly into its respective pulley in the wrist, without any further redirection. (With the exception of one wrist tendon, which requires one redirection pulley [not pictured] mounted onto the back plate.)



In this image, the orientation of 4 of the 7 SEA modules can be seen. The three on the left correspond to the wrist pitch, power finger, and one of the dextrous finger tendons, respectively. The SEA module on the right, which is raised above the others, controls the wrist yaw direction. It is the only SEA used in an "N" configuration, such that the one tendon pulley has two tendons coming off of opposite sides, which move in opposite directions as the motor spins. All other SEA's are in the "N+1" configuration (or, in the case of the power finger, actuate against antagonistic springs), and only have one tendon coming out of them.



In this image, the other 3 of the 7 SEA modules are shown. They are all used by the dextrous finger.

The SEA modules screw onto two back plates, which are then fixed to each other and to two side plates which provide a place for the wrist to mount. To screw the SEA modules onto the backplates, nuts are placed inside the hexagonal holes below the spring, and countersunk screws are screwed in from the back of the back plate. The back plates are attached to each other via four nuts and bolts, on the corners. The side plates are attached by bolts which screw into nuts placed inside the rectangular cutouts, which can be seen on the left half of the figure.

While the backplates are printed from PLA, they are sufficiently rigid to ensure that the compliance in the SEA module comes primarily from the spring, and not from any deflection of the module or forearm itself.

Not pictured is one additional redirection pulley, which fits into the small hole at the top of the backplate. One tendon from the unique SEA module (the one which is turned 90 degrees relative to the other modules) must cross over the back plate to reach a wrist pulley on the other side; therefore, this redirection pulley was mounted on a shaft bent by hand to accommodate the tendon's angle of attack. The pulley itself is exactly the same as all pulleys on the SEA modules.

Specifications

The following are the full SEA specifications:

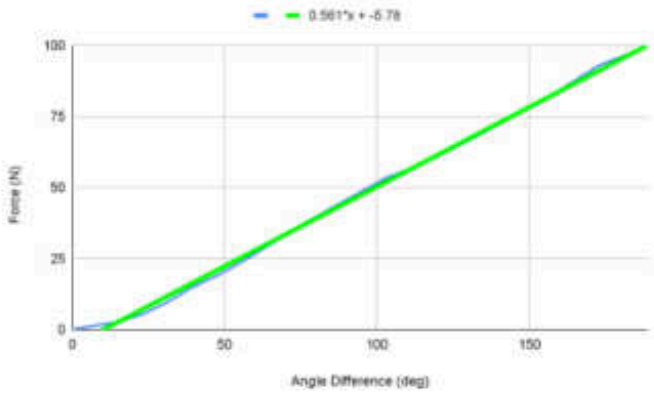
Item	Quantity
Compliance	120º @ 0.7 Nm
Motor	RoboMaster M2006 P36 Brushless DC Gear Motor
Assembly Time (per module)	~30 min
Manufacturing Time (per module)	~3 hours

Forearm specifications:

Item	Quantity
Width	4.75 in ≈ 121 mm
Length	3 in ≈ 76 mm
Height	6.5 in ≈ 165 mm
Weight	~1 kg

Experimental Results

All design objectives were achieved except the compliance level of the Series Elastic Actuator (SEA) modules. Our springs were hand-wound, which resulted in their spring constants being both substantially different from each other, and from our desired value.



MCP tendon SEA

Reflections

Regarding ease of manufacturing and assembly, we are generally satisfied due to:

- Standardized parts which can be machined in bulk
- Modular design which allow incremental assembly, as well as use by other teams for testing electronics and software

Areas of improvement include:

- Standardized springs (off-the-shelf) and iterative improvements to the spring packaging, both of which should result in more consistent spring behavior which aligns more closely with our goals.
- A way of mounting the SEA modules to the packaging which does not require total forearm disassembly to remove one SEA
- A better magnet and magnetic-encoder mounting design; the current design relies on hot gluing the magnets to the motor shaft, which is difficult and inconsistent, and making it necessary to shim the encoder mounts so that they are the correct distance from the magnet.
- [Minor fix] By rotating the motor mounting holes (the holes through which screws attach the motors to the SEA module), the motor wires can be made to come straight out, instead of diagonally out. These wires interfered with the other motors, causing packaging issues. This is an easy fix.

Beyond those brief and general notes, there are some overarching reflections regarding the course as a whole and the design process. This was a wild ride, with many all nighters pulled, and in my opinion, unnecessarily. There could have been a lot done early to try to streamline this

entire process, but I think a key step I would've taken early on is integrating all teams together sooner. It seemed like every team was off working on their own thing practically until right before final assembly. As the forearm team, this is frustrating. It felt as though we were the only subteam (besides palm, but that complex palm was only necessary as a result of our failure to integrate sooner) that actually had to take into account anyone else's design. Everyone was designing in their own black box until it came time to put everything together. As a result, we had to make rapid iterations to our design to accommodate changes in the fingers and wrists and palm with very little communication from any team. All of this while trying to juggle handling the SEA module, which in and of itself could have been an entire design project.

It feels like we barely scratched the surface with the SEAs. There was a lot of promise in the design we ended up with, and it could really use another quarter or two in the oven for perfecting. I am excited to see where that goes. But considering that our whole mechanical and software systems were reliant on these SEAs to work properly, maybe a dedicated subteam would have been nice.

That's not to say I'm not proud of the way everything turned out… I certainly am. This is one of the coolest things I've ever gotten to work on, and has inspired me in my own personal projects in so many ways. I just wish our team had worked more like a team earlier on. I can't blame anyone for the way things turned out, communication is a two way street. I think some structure would have been nice.

I think the forearm is well designed, with a good form factor and overall promising SEA design. It could've used another iteration or two to be perfect, but I don't think the goal of this project was to have something perfect. Either way, I'm rambling. Fun project and fun team, I definitely learned a lot. Hopefully this is useful to the Hand ERC in the future.

-Shishir

The fundamental design of the SEA modules is promising.
Future work for this project should include iterating on the design of the SEA modules to improve spring consistency and stiffness, as well as magnet and encoder mounting.

For future work in RDS, I recommend that the forearm team create for themselves early deadlines for the prototyping of SEA modules—even if their design does not intend to be "modular"—so the software team can begin testing and characterizing much earlier than they were able to in this project. We went through multiple iterations of the forearm, most of which did not include an easily "modularized" version of the SEA, and by focusing on getting to an end product of the forearm instead of a useable SEA subsystem, we blocked the software team from

progressing. A prototype of the SEA which at least works in a similar way to what is anticipated for the final design of the forearm should be forearm team's initial priority—the actual mechanical design, including motors, encoders, etc., can certainly be changed later. Thanks to Davin for pointing this out and assisting the forearm team—and therefore the whole team—in progressing.

-Michael Miller

Bill of Materials

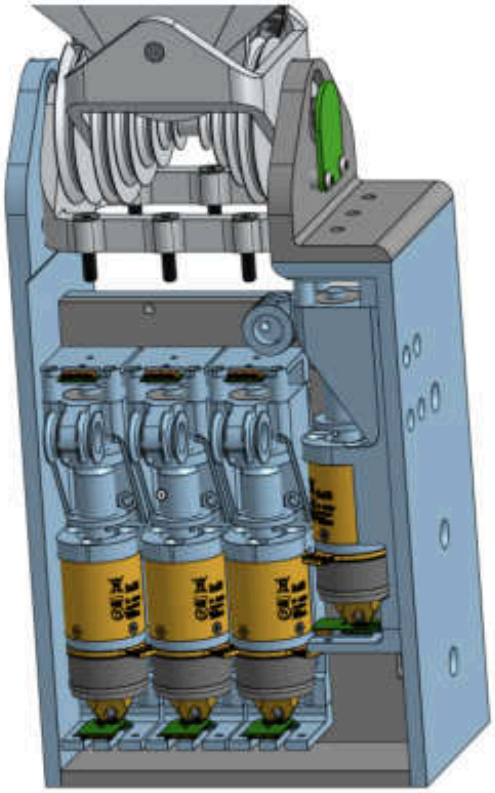
Table 1 shows the parts that make up the Forearm.

Part Number	Quantity	Title	Description
6000	1	Left Mounting Plate	PLA plate which mounts the wrist, does not mount an SEA
6001	1	Right Mounting Plate	PLA printed, mounts wrist and an SEA module for wrist yaw
6002	1	Left Wrist Mount	PLA, fastens to left mounting plate and holds pitch shaft bearing
6003	1	Right Wrist Mount	PLA, fastens to right mounting plate and holds pitch shaft bearing
6004	1	Center Mounting Plate 1	PLA, mounts three SEAs, fastens to Center Mounting Plate 2 via clearance holes
6005	1	Center Mounting Plate 2	PLA, mounts three SEAs, fastens to Center Mounting Plate 1 via clearance holes
6006	7	SEA Module Base	SLA Printed, contain mounting holes for both Encoder Mounts, Idler Pulley Mount, and have nut shaped cutouts for mounting to Center Mounting Plates
6007	7	Idler Pulley Mount	SLA Printed, contain hole for double R4 bearings and another hole to mount idler pulleys via a bolt and nut
6008	15	Idler Pulley	Redirect tendons towards wrist, or back towards SeA in the case of yaw redirection pulley. Aluminum, 30 degree V-groove, .0625in landing.

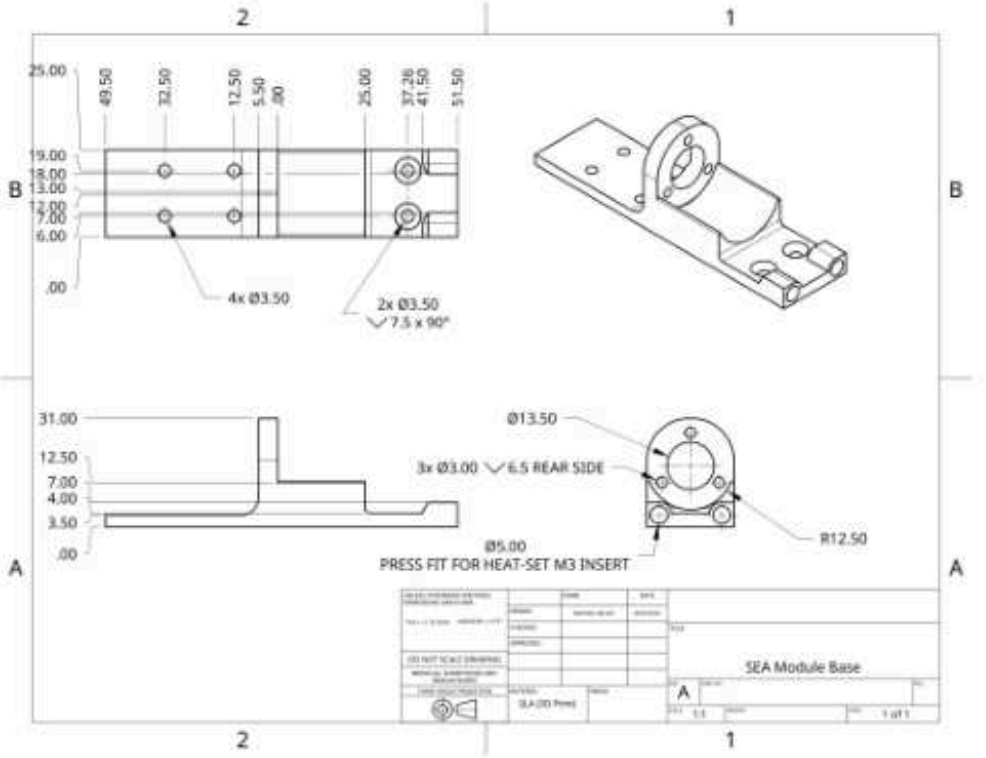
6009	7	Motor Pulley	Aluminum, fit over motor drive shaft and contain holes for dowel pin and fastener mounting, to eliminate backlash. Mounting hole for SEA spring
6010	7	SEA Pulley	Aluminum, contain mounting hole for SEA spring and two sets of tendon termination holes
6011	14	R4 Bearing	Double stacked in SEA module for cantilevered SEA Pulley
6012	15	R2 Bearing	Fit inside of idler pulleys
6013	7	Dowel Pins	.125'x.5' steel pins. Lock rotation onto motors
6014	7	SEA Encoder Mounts	PLA, mount via heat set inserts to SEA Module Base
6015	7	Motor Encoder Mounts	PLA, mount via heat set inserts to SEA Module Base
6016	7	SEA Springs	Music wire, hand wound "to spec"
6017	7	Prefab Encoders	Encoders mounted to Motor Encoder Mounts
6018	7	Circular Encoders	Designed by Electrical team, mount to SEA Encoder Mounts
6019	14	Countersink M4	M4x18mm screws, used for mounting side plates to center plates, wrist mounts to side plates, and center mounting plates together
6020	56	Countersink M3	M3x12mm screws, used for mounting SEA Modules to Center Mounting Plates, M3x6mm screws used for mounting motors to SEA Module Base, M3x16mm screws used for mounting Motor Pulleys to motor drive shaft
6021	14	Neodymium Magnets	¼"x1/16", used in conjunction with all encoders on respective shaft
6022	10	M3 Machine Head Bolt	Used to mount Idler Pulleys to Idler Pulley Mount, and mount wrist yaw redirection pulley
6023	7	RoboMaster M2006 P36	Star of the show, mounts to SEA Module Base
6024	35	M3 Nuts	Steel, used for all SEA mounting bolts and Idler Pulley Bolt
6025	14	M4 Nuts	Used for all M4 Countersink Screws

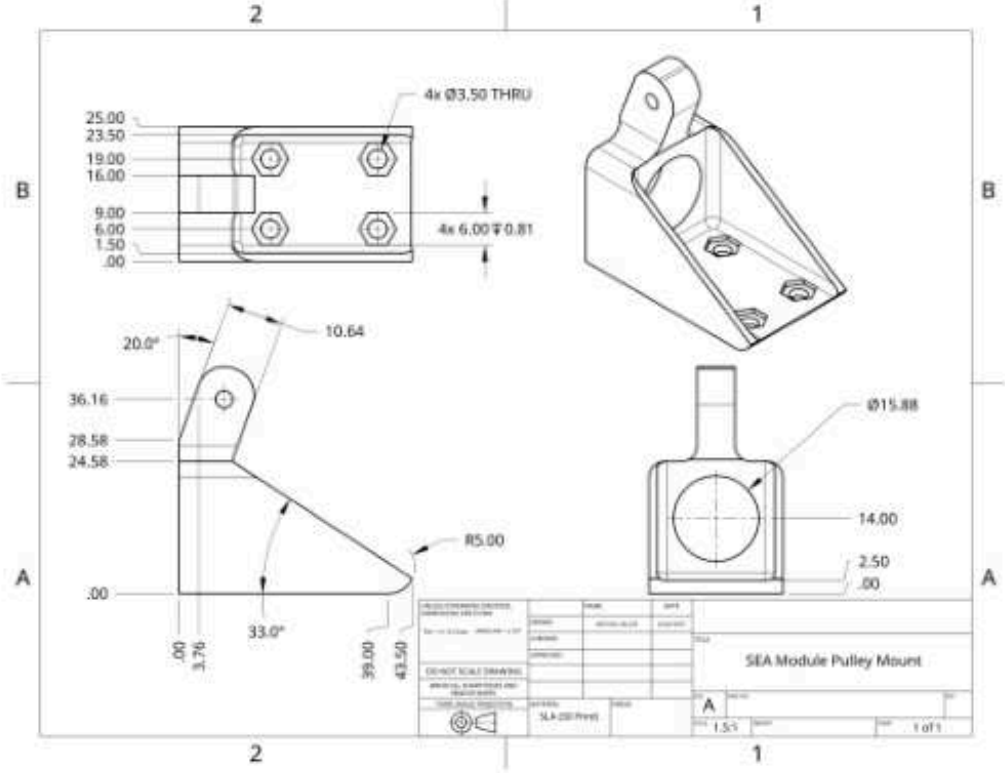
CAD Models

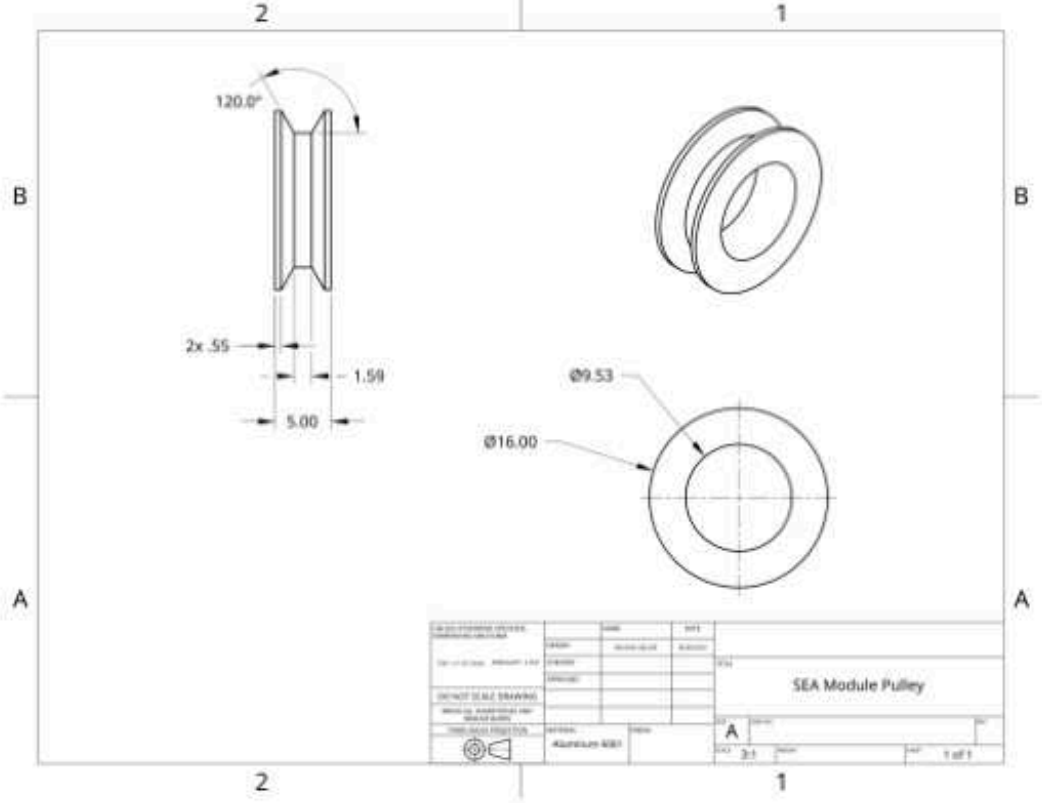
The nearly-full CAD assembly (containing forearm, dextrous finger, power finger, but not the palm) can be downloaded as a .step file at: https://drive.google.com/file/d/1mDD1UYY1RPnousOtAR7atOJPsXN8e4-G/view?usp=sharing.

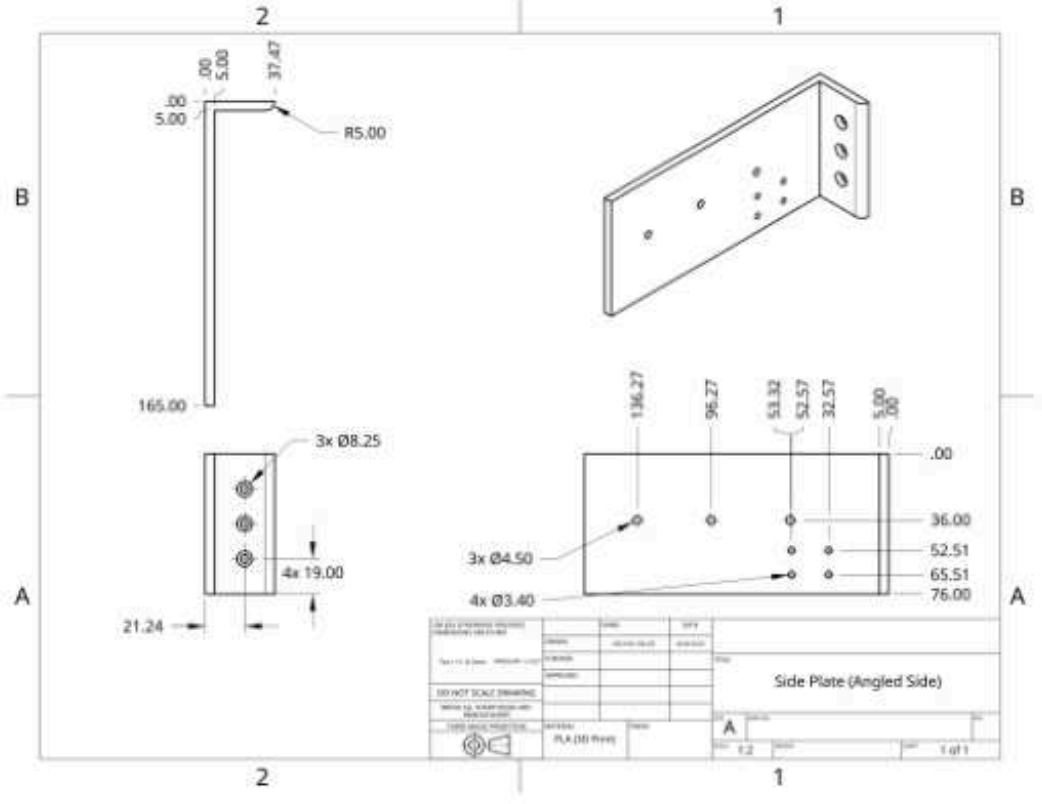


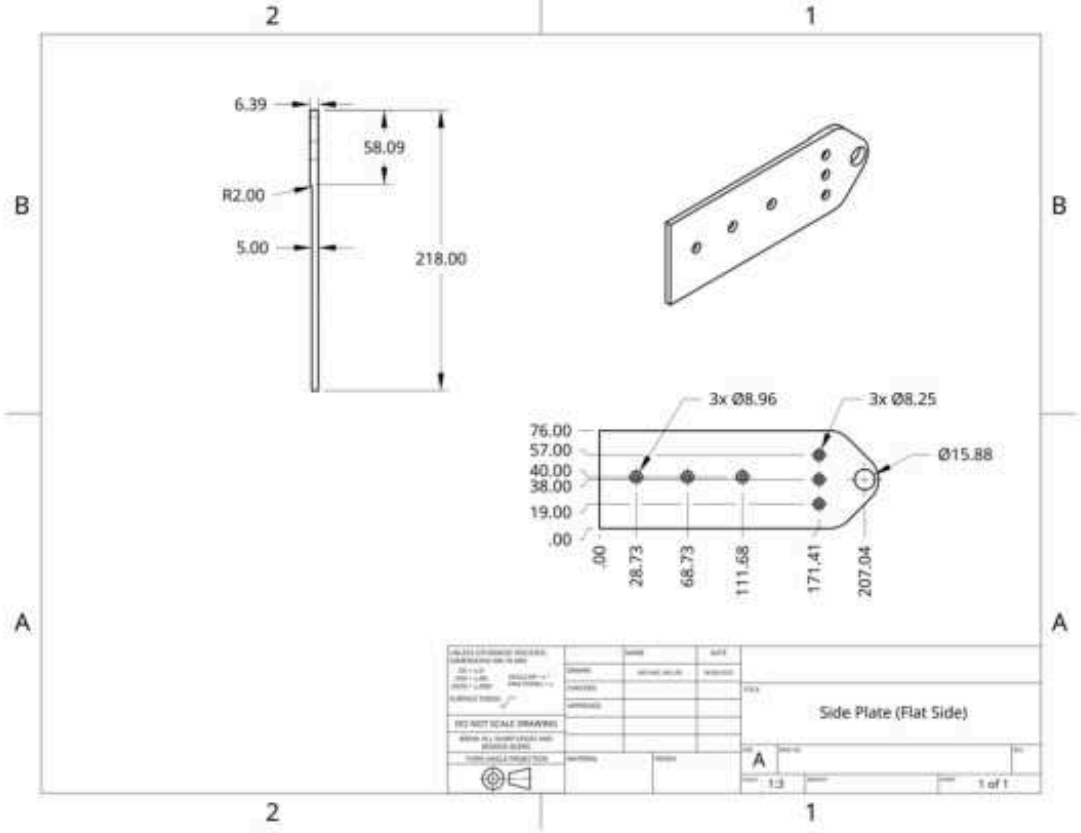
Part Drawings

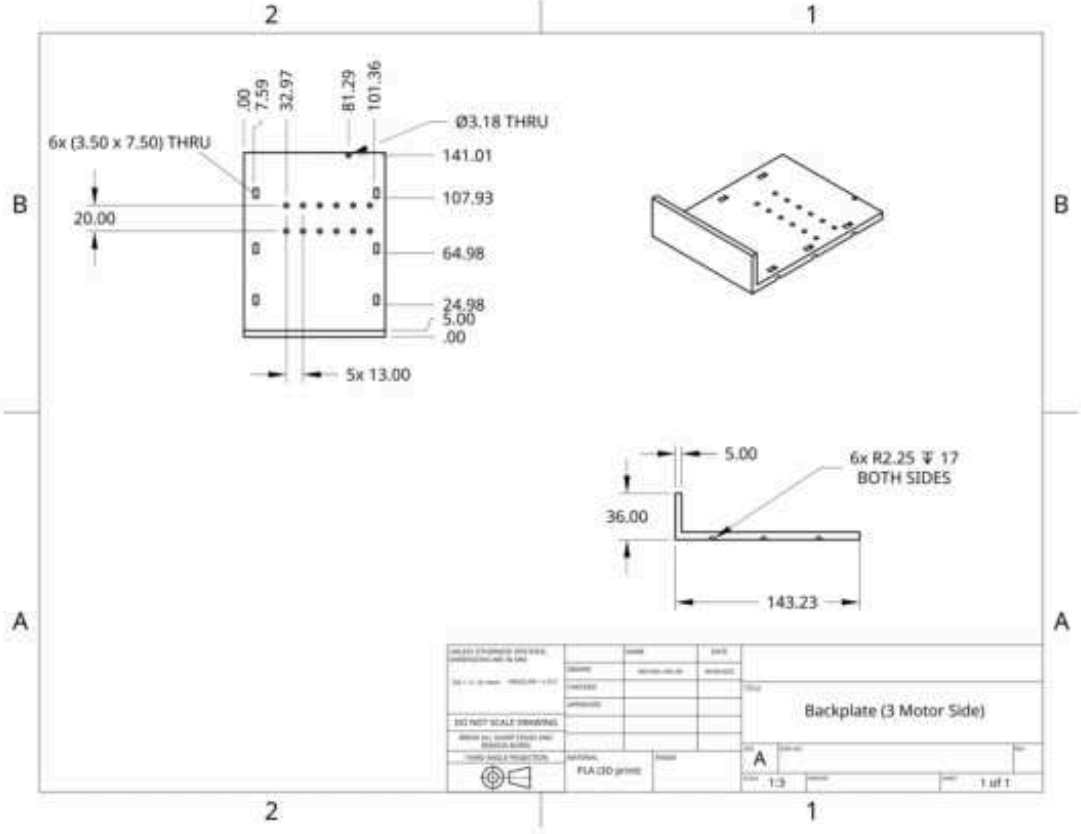


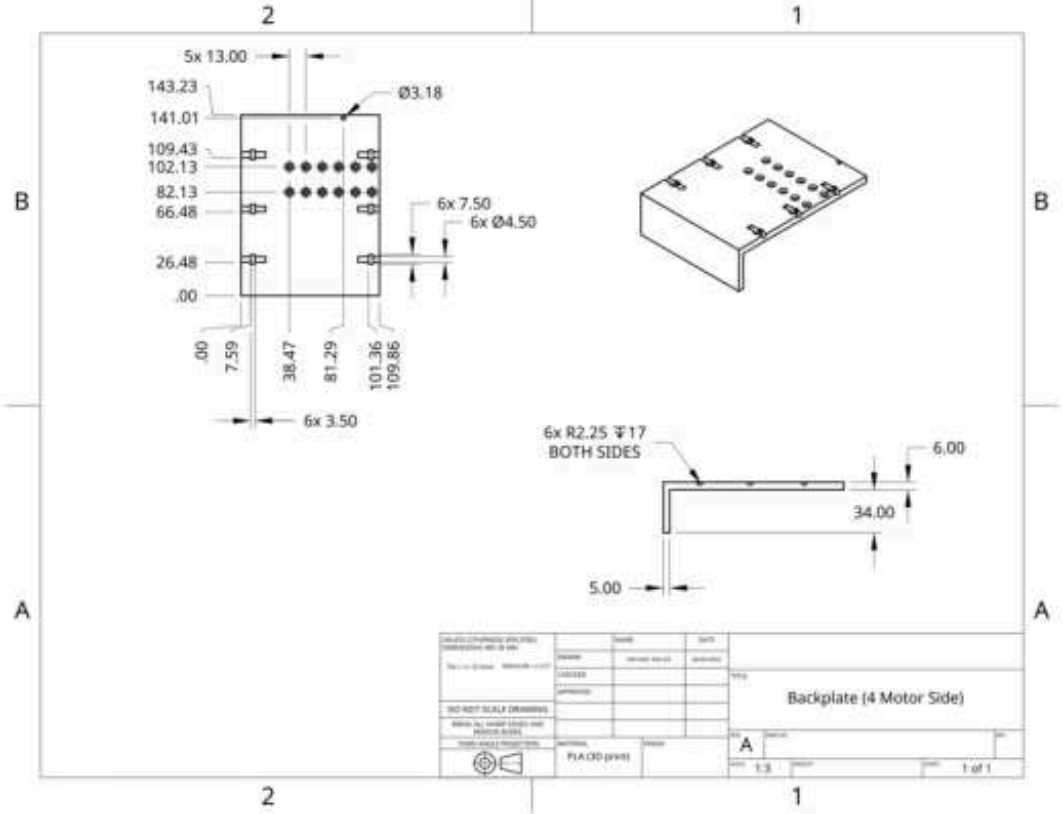


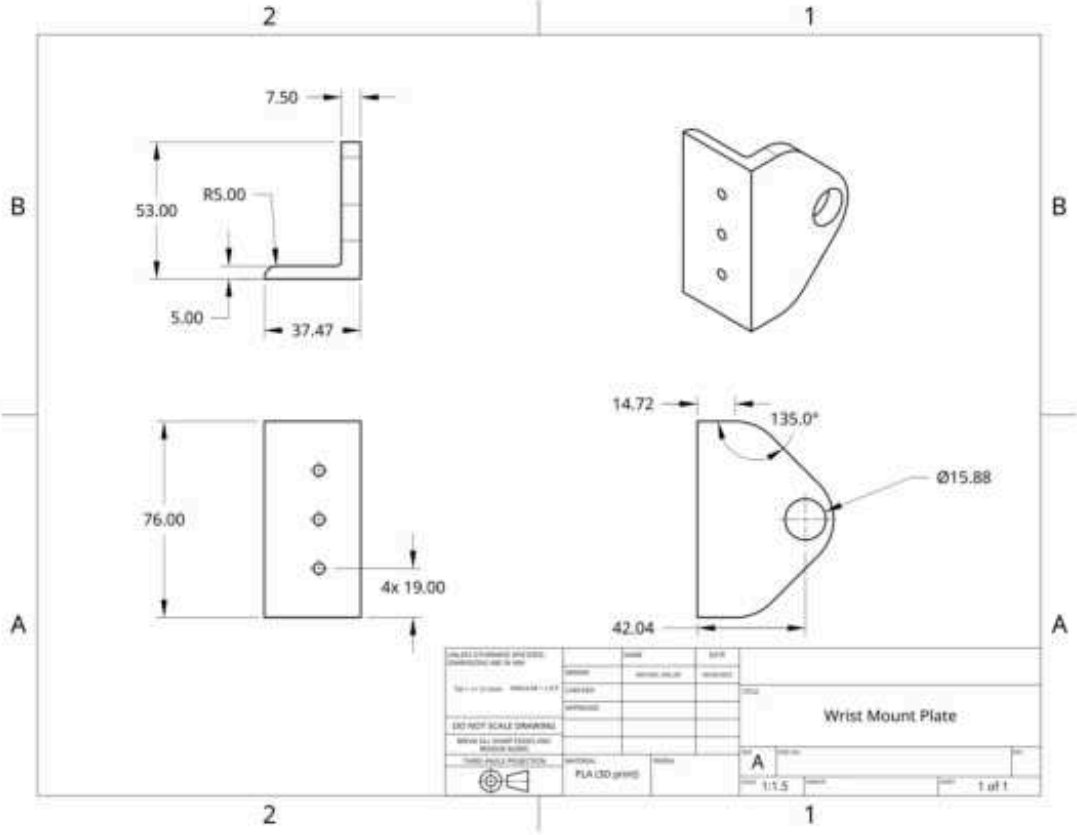

120.0°
2x .55
1.59
5.00
Ø9.53
Ø16.00
SEA Module Pulley
A
3:1
1 of 1

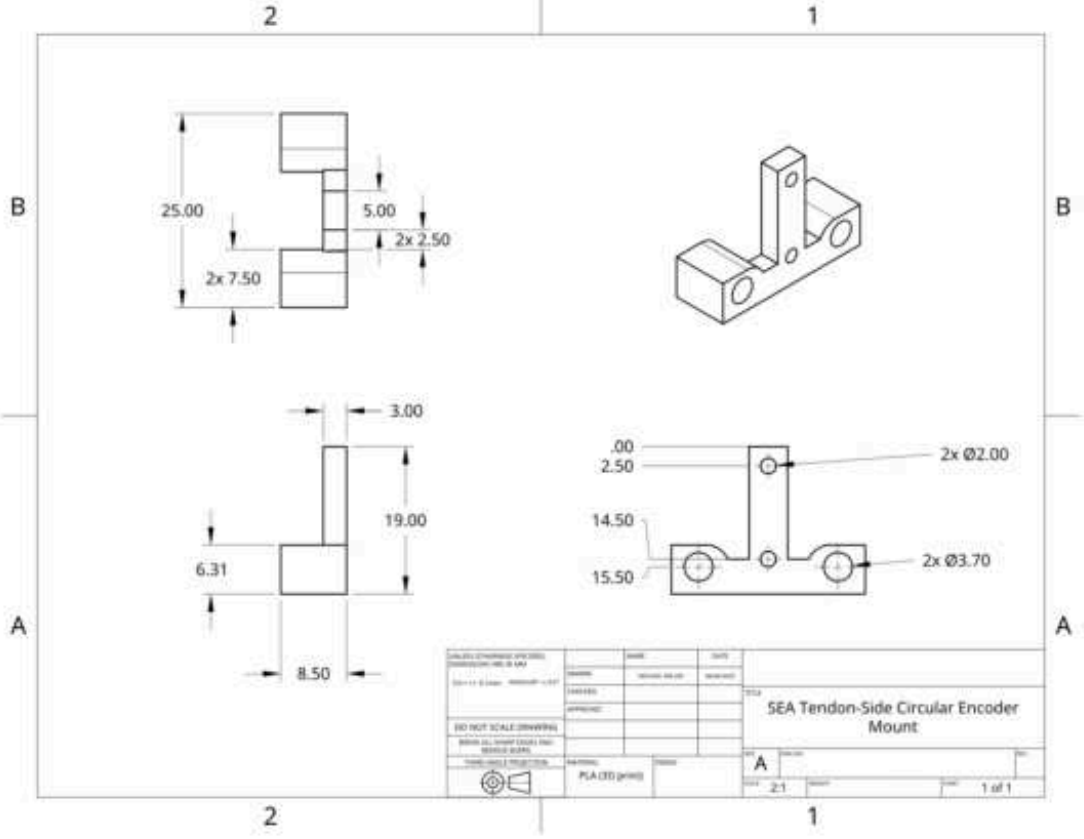

.00
5.00
37.47
.00
5.00
R5.00
165.00
3x Ø8.25
4x 19.00
21.24
136.27
96.27
53.32
52.57
32.57
5.00
.00
.00
36.00
52.51
65.51
76.00
3x Ø4.50
4x Ø3.40
Side Plate (Angled Side)
A
1:2
1 of 1

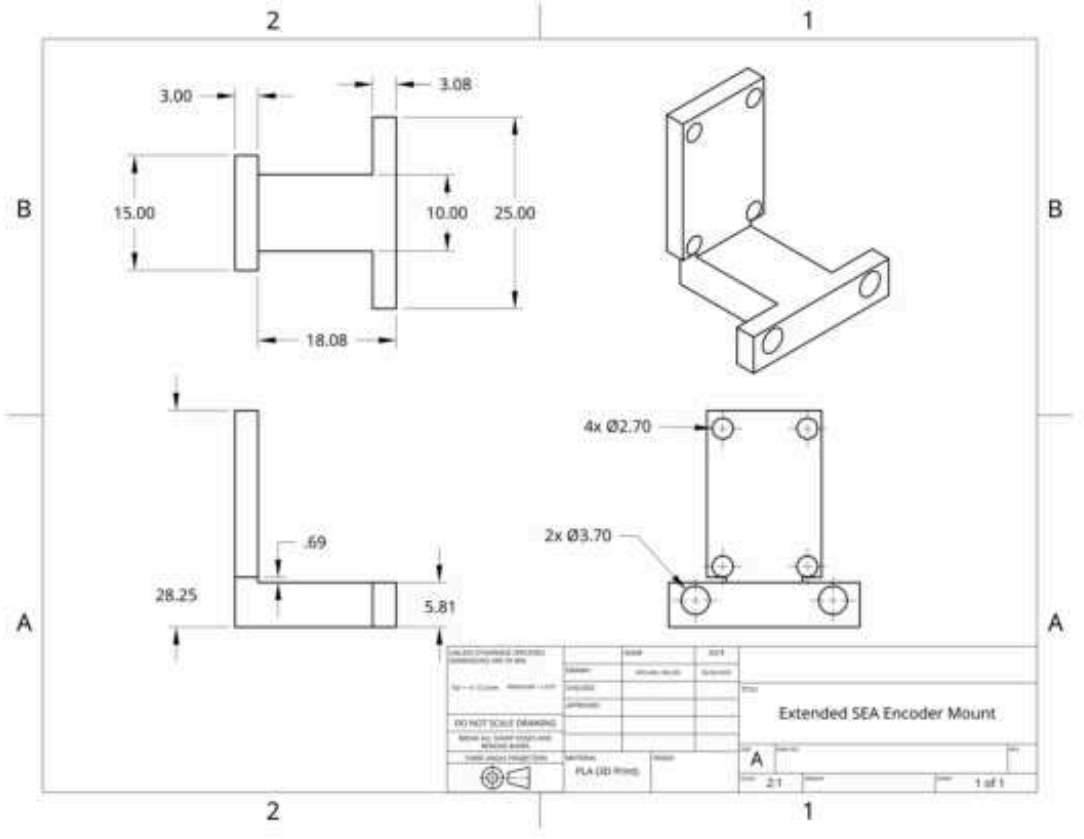

6.39
58.09
R2.00
5.00
218.00
3x Ø8.96
3x Ø8.25
Ø15.88
76.00
57.00
40.00
38.00
19.00
.00
.00
28.73
68.73
111.68
171.41
207.04
Side Plate (Flat Side)
A
1:3
1 of 1

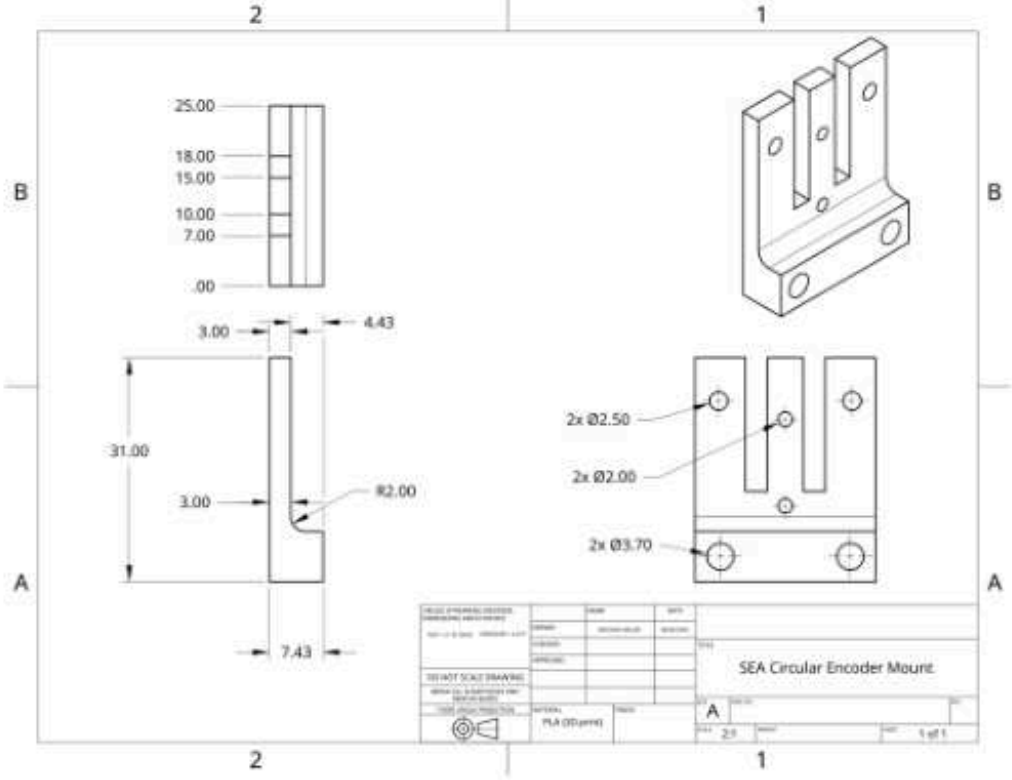

.00
7.59
32.97
81.29
101.36
Ø3.18 THRU
6x (3.50 x 7.50) THRU
141.01
107.93
20.00
64.98
24.98
5.00
.00
5x 13.00
5.00
6x R2.25 ↧ 17
BOTH SIDES
36.00
143.23
Backplate (3 Motor Side)
A
1:3
1 of 1

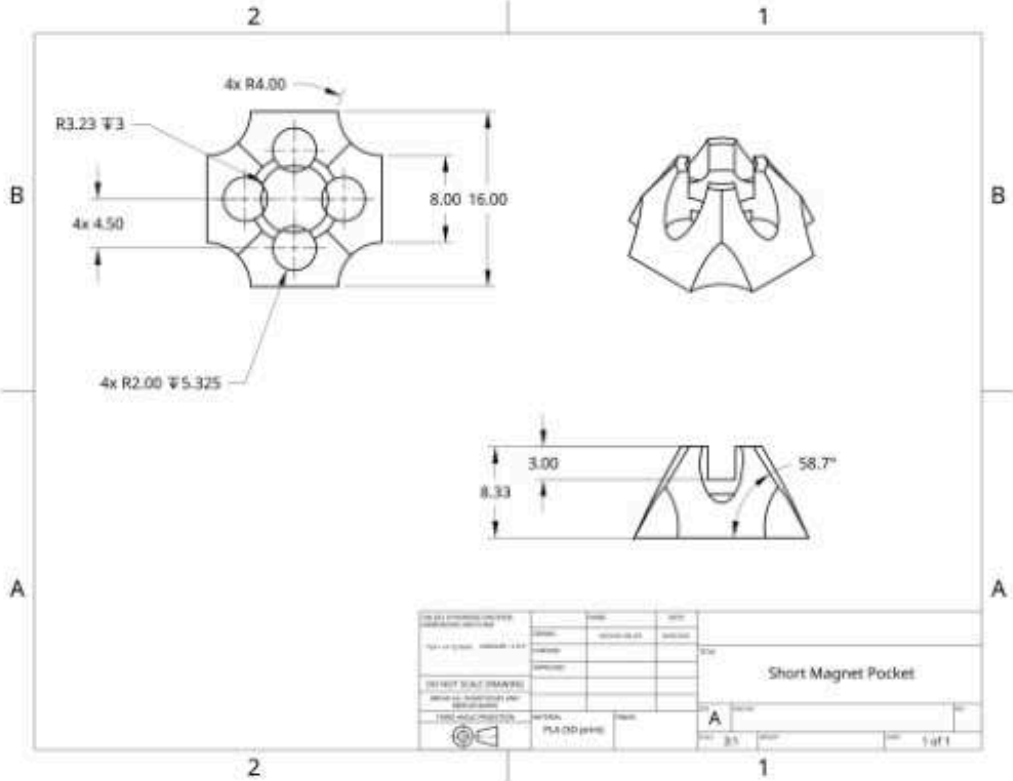

5x 13.00
143.23
141.01
109.43
102.13
82.13
66.48
26.48
.00
Ø3.18
6x 7.50
6x Ø4.50
.00
7.59
38.47
81.29
101.36
109.86
6x 3.50
6x R2.25 ↧17
BOTH SIDES
6.00
34.00
5.00
Backplate (4 Motor Side)
PLA (3D print)
A
1:3
1 of 1

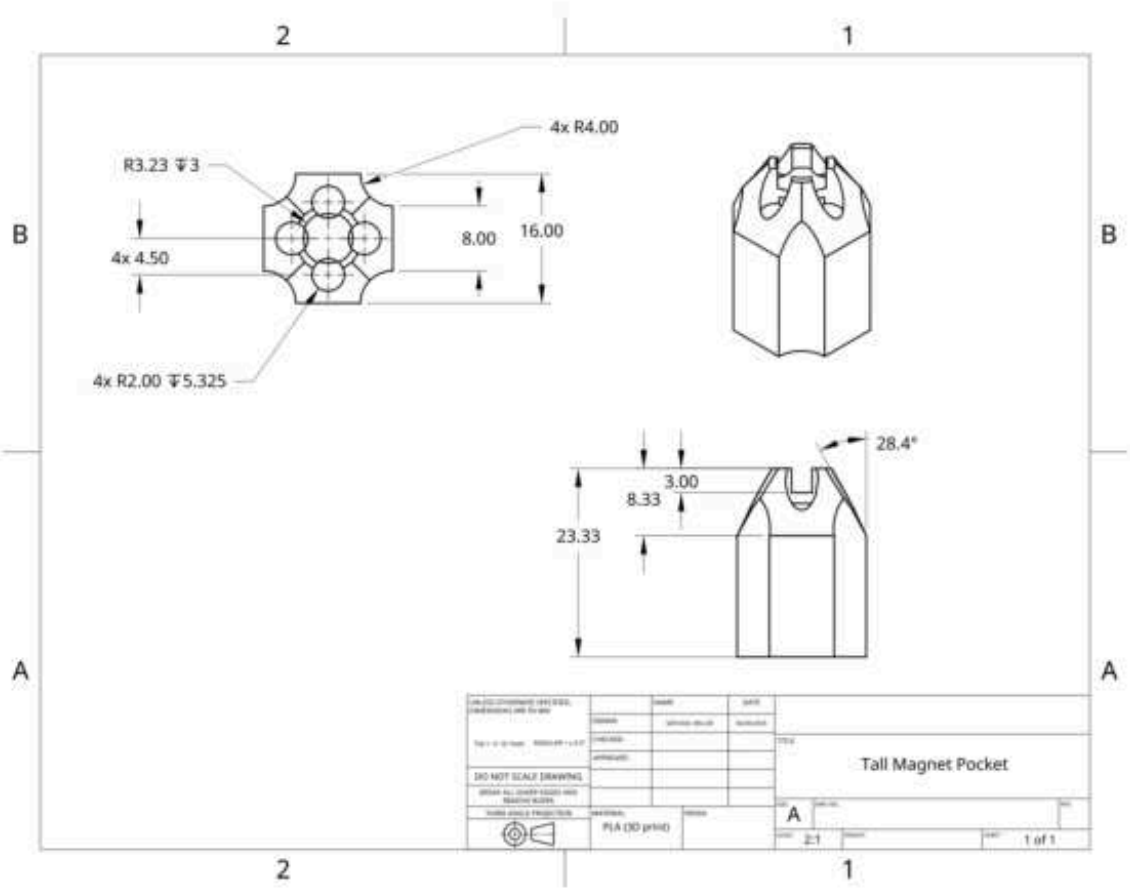

7.50
53.00
R5.00
5.00
37.47
76.00
4x 19.00
14.72
135.0°
Ø15.88
42.04
Wrist Mount Plate
PLA (3D print)
A
1:1.5
1 of 1


2
1
B
A
25.00
5.00
2x 2.50
2x 7.50
3.00
19.00
6.31
8.50
.00
2.50
2x Ø2.00
14.50
15.50
2x Ø3.70
SEA Tendon-Side Circular Encoder Mount
PLA (3D print)
A
2:1
1 of 1


2
1
B
A
3.00
3.08
15.00
10.00
25.00
18.08
.69
28.25
5.81
4x Ø2.70
2x Ø3.70
Extended SEA Encoder Mount
PLA (3D Print)
A
2:1
1 of 1


25.00
18.00
15.00
10.00
7.00
.00
3.00
4.43
31.00
3.00
R2.00
7.43
2x Ø2.50
2x Ø2.00
2x Ø3.70
SEA Circular Encoder Mount
PLA (3D print)
A
2:1
1 of 1


4x R4.00
R3.23 ↧3
4x 4.50
8.00
16.00
4x R2.00 ↧5.325
3.00
8.33
58.7°
Short Magnet Pocket
PLA (3D print)
A
2:1
1 of 1


2
1
B
A
4x R4.00
R3.23 ↧3
4x 4.50
8.00
16.00
4x R2.00 ↧5.325
28.4°
3.00
8.33
23.33
DO NOT SCALE DRAWING
PLA (3D print)
Tall Magnet Pocket
A
2:1
1 of 1

Wrist

RDS 2025:
Wrist Subsystem Documentation

All content is IP of Konrad Laudon
Developed 2/26/2025 - 6/13/2025

Table of Contents

1. Subsystem metrics & specifications
    a. https://docs.google.com/document/d/1BwJW530gXqWTnkT64ibqPX2wz35Pv5KS6G2aLIASCeQ/edit?tab=t.0
2. Design process & rationale
    a. https://docs.google.com/document/d/1zNVfcLTQ4HKjjtJZMww9NQ3Gw6aqYohs85vEPK-MaQg/edit?tab=t.0
3. Load cases & stress analysis
    a. https://docdds.google.com/document/d/1DYutICt1xy5BKwTTAVNAnzFqo1nM8-IeNO1agmZ2LxE/edit?tab=t.0
4. Kinematic coupling
    a. https://docs.google.com/spreadsheets/d/1_W_etTIFg6GL8CAcTprO9D5zbxdk_cDs8K6O2yhyiB0/edit?gid=0#gid=0
5. Routing guide
    a. https://docs.google.com/document/d/1Jat0kr1R8pEd4AbupItwJjovLlhkz1GH_te68fKOFbk/edit?tab=t.0
6. CAD
    a. https://docs.google.com/document/d/1vw6gM_GCkXcJd4n5BNM20DZox3gefYbFn88Az_UDt-4/edit?tab=t.0
7. Bill of materials
    a. https://docs.google.com/spreadsheets/d/1LQNLRPYjDFI5WkCr1GtSW9mjem4LHY9-pSs1lyUDlVY/edit?gid=0#gid=0
8. Manufacturing drawings

    a. https://docs.google.com/document/d/1XIQHqn3rEONQaDmgOXVloRaouMtXs9jKp13bZhw14HE/edit?tab=t.0
9. Reflection
    a. https://docs.google.com/document/d/13HDWBayEXA9zSdRoeNQN83PUT46X3-BzjM8b4B-kUFo/edit?tab=t.0

Palm

Palm

Kieran Cullen
Trevor Abbott

1. Anatomy

The palm spaces the two fingers so that their center axes are each spaced 24mm from the center axis of the wrist. If the dextrous finger is considered to be halfway between the pointer and middle fingers, and the power finger is considered to be halfway between the ring and pinky fingers, this spacing is only slightly larger than an average human hand. Because of the large size of the power finger plunger housing and the need to support tendon redirect pulleys in the space between the power finger and dextrous finger, the interfinger spacing could not realistically be reduced further.

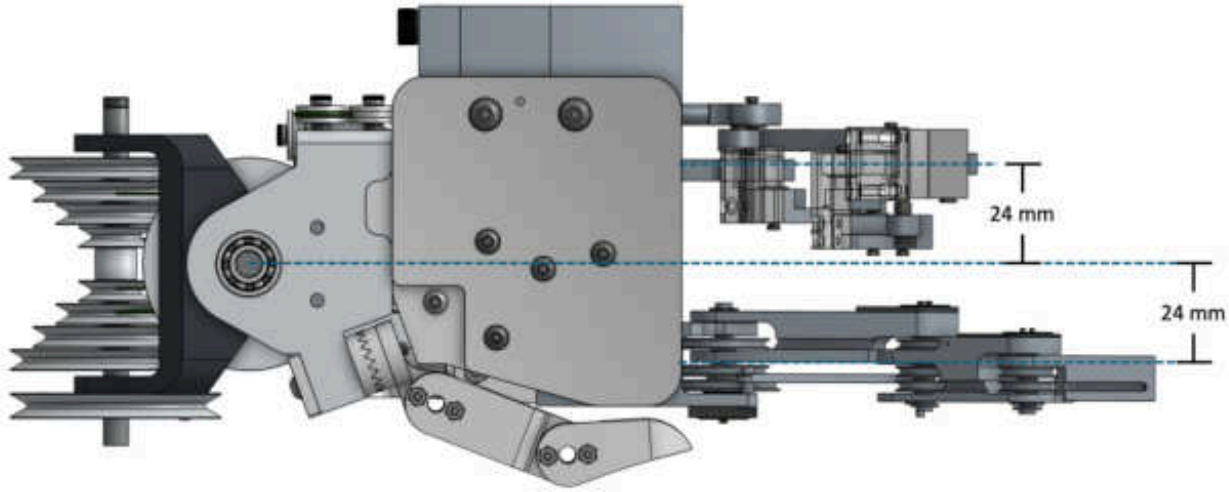


Figure P1: *Spacing of dextrous and power finger relative to wrist center axis*

The first joints of the fingers are as close to the wrist as possible to reduce the unhumanlike gap between the palm and wrist. The palm mounts the power finger with its back surface directly against the wrist structure, as shown in Figure P2.

The thumb originates from the palm in a location similar to that of a human thumb. As shown in Figure P3, it has an angled rolling axis modeled after the thumb on the NASA Valkyrie hand, which uses a similar low-DOF finger layout. The side of the palm is specifically contoured to allow the thumb to be stowed next to it if not in use.

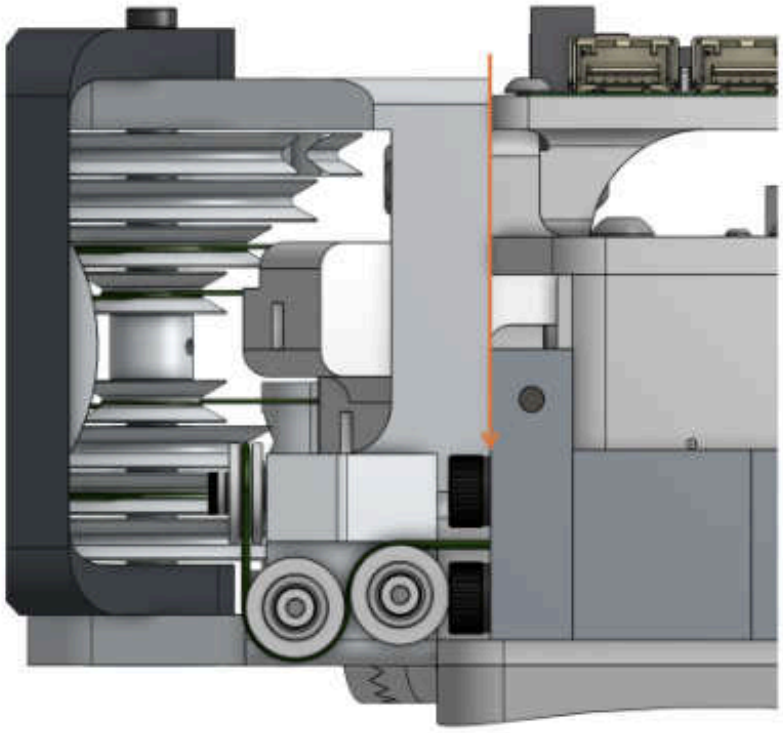


Figure P2: *Orange arrow showing that the back vertical surface of the power finger base is placed exactly at the boundary with the wrist mechanism. Further reduction of the wrist-palm gap would require more substantial modifications to the wrist.*

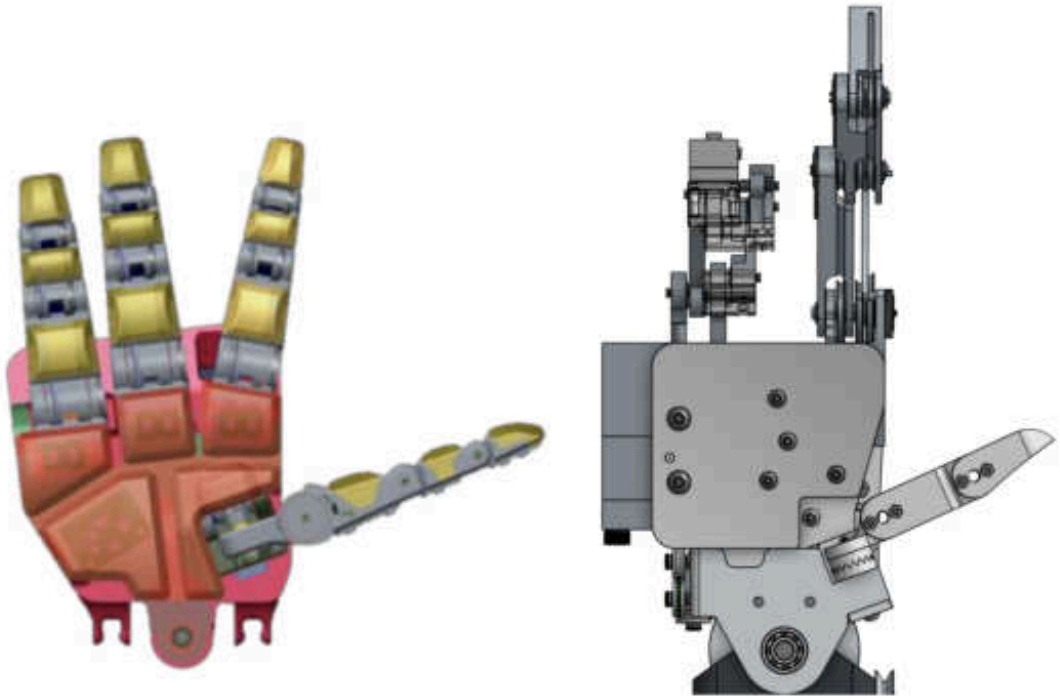


Figure P3: *The mounting location and rotation axes of the thumb are based on the NASA Valkyrie (left).*

2. Structure

The complexity, volume, and mass of the palm are minimized by using the existing structure of the power finger to provide most of the rigidity. The power finger is "sandwiched" between two parts - the Hand Structure Upper and Hand Structure Lower. These can be relatively thin 3D-printed plates because they are backed by the rigid power finger base. The sandwich structure also allows the dextrous finger to be inserted into the palm with its splay shaft already inserted, allowing the finger to be assembled completely independently of the palm.

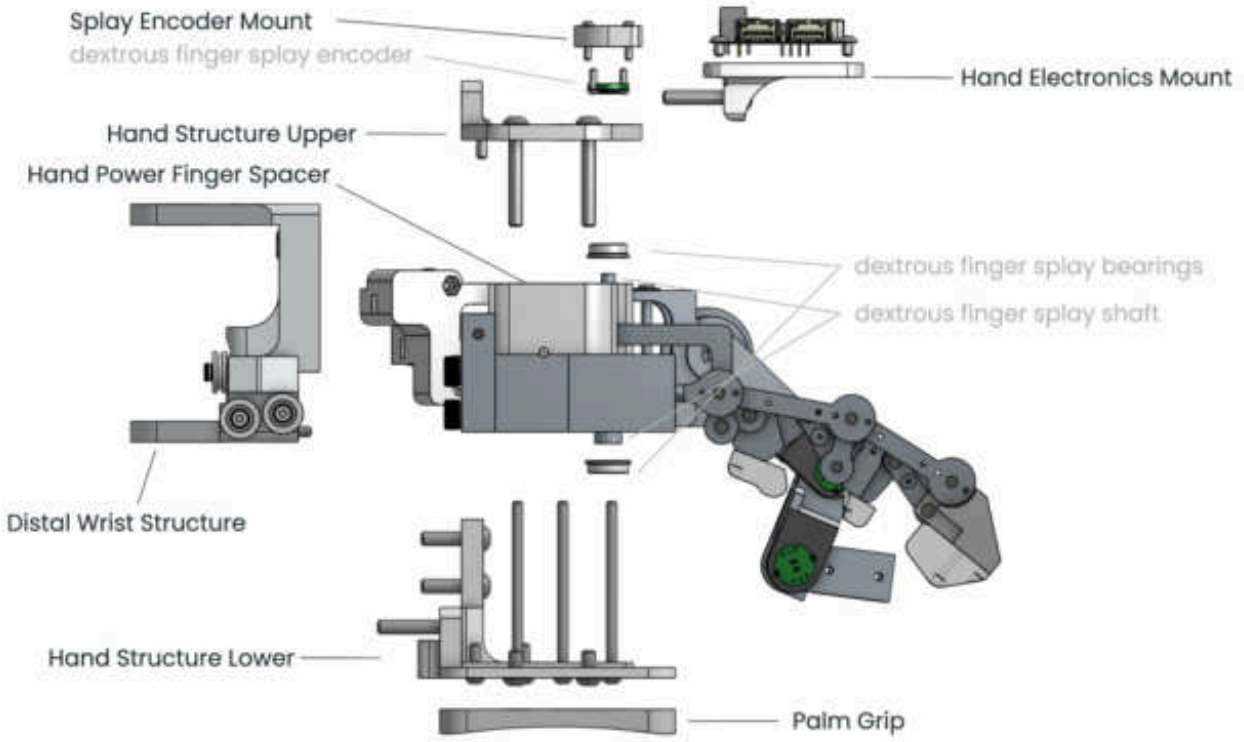


Figure P4: *Exploded view showing the "sandwich" design of the palm structure*

The power finger can be easily removed from the palm by removing the four M4 screws that hold it in place and sliding it out the side; the dextrous finger can remain in place with its tendons completely routed. Likewise, if the dextrous finger must be removed, it suffices to detach the either the Hand Structure Upper or Hand Structure Lower and lift the finger out of the palm; the power finger can stay assembled and routed in this case.

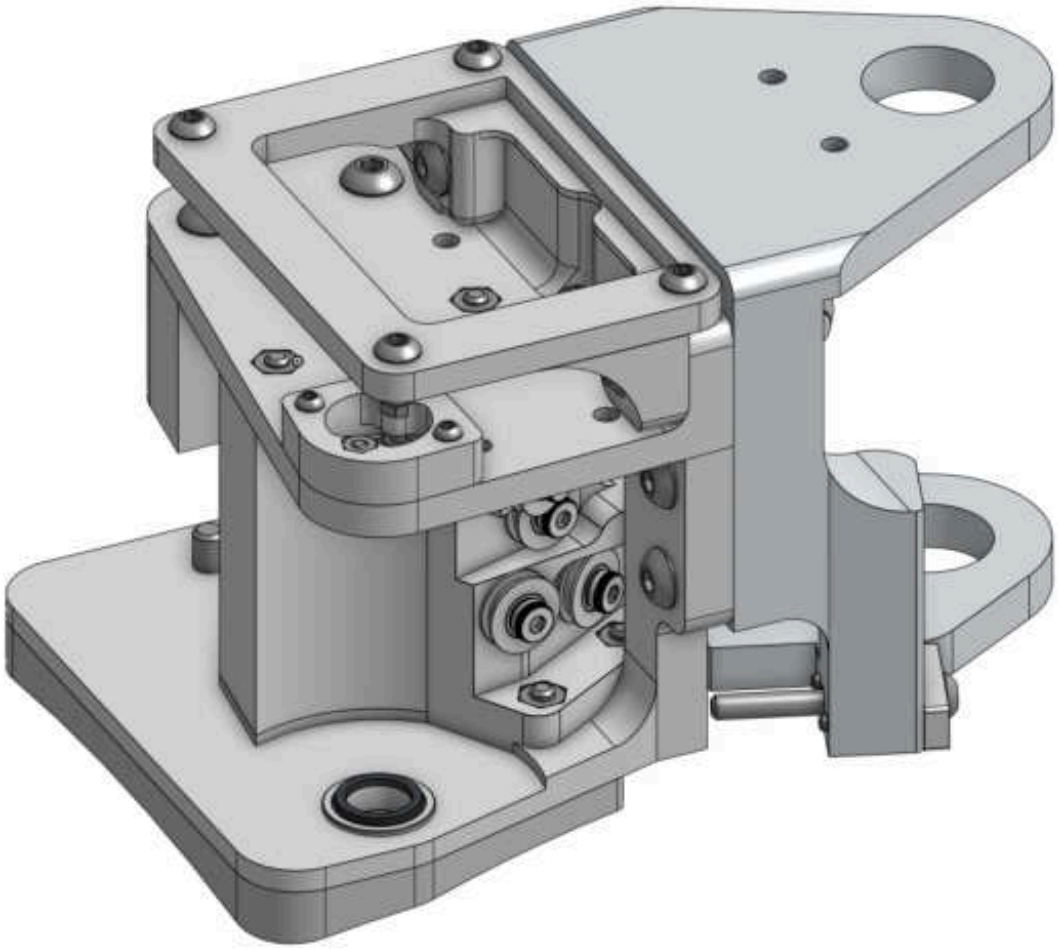


Figure P6: *Complete palm structure without fingers or wrist attached*

3. Tendon Routing

The Hand Redirect Block is a single part that accommodates eight pulleys for routing four tendons from the dextrous finger to the wrist. This block was designed deliberately with two features to reduce the difficulty of tendon routing:

I. All of the pulleys face towards the outside of the palm so that access to them is as unobstructed as possible. It isn't perfect because I had to work around the existing structure of the wrist, but it would be hard to do much better unless you're willing to make the palm significantly larger.

II. All the pulleys are cantilevered, and the tendons do not have to make full wraps around any of the pulleys. As a result, access to a free end of a tendon isn't required to route it on these pulleys. The tendon can be popped onto the pulleys with a pair of tweezers once it has been routed through the wrist and the finger.

All tendons can indeed be routed through the palm while it is completely assembled.

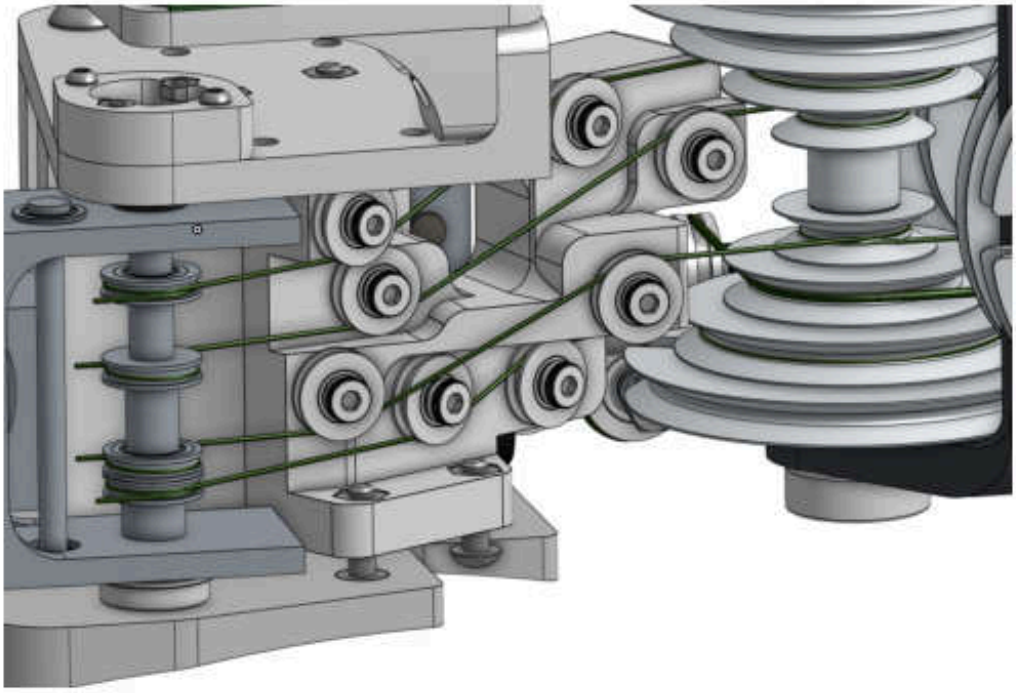


Figure P7: *Routing of tendons (green) from wrist to dextrous finger over the Hand Redirect Block. Some other palm parts are hidden for clarity. Consult the CAD model linked below for more detailed routing information.*

Routing for the power finger is accomplished similarly. I modified the structural part of Konrad's wrist that was closest to the palm to mount three pulleys on its exterior that route the power finger's single tendon. This placement of pulleys is very easily accessible for tendon maintenance. The modified wrist part also improves the wrist's compactness significantly; it is called Distal Wrist Structure.

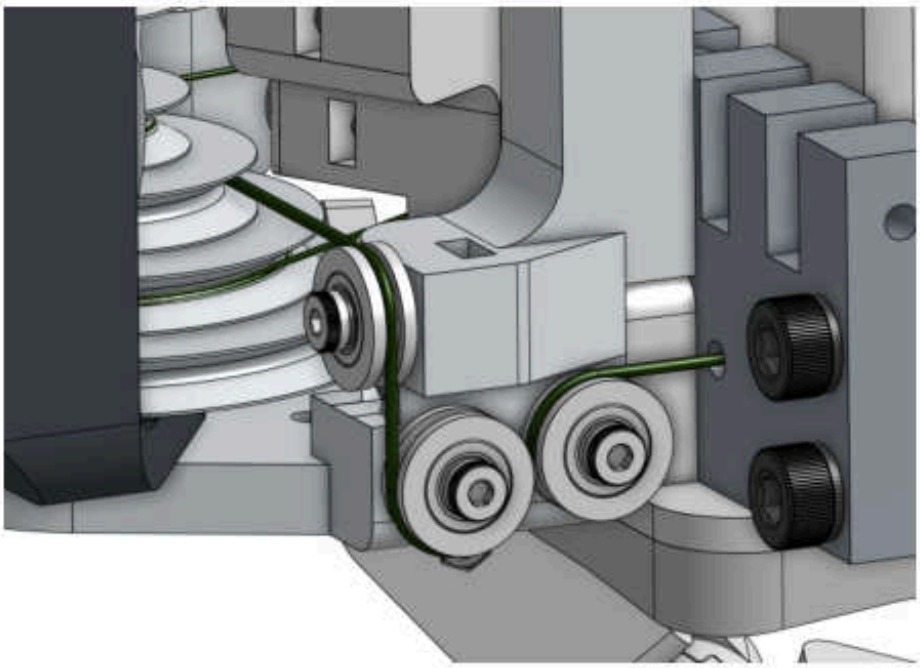


Figure P7: *Routing of tendon (green) from wrist to power finger with pulleys mounted to the modified Distal Wrist Structure*

All of the pulleys in the palm are mounted on standard M3 shoulder bolts instead of shafts. This makes assembly of the Hand Redirect Block very easy, eliminates a proliferation of shaft hardware like E-clips that would otherwise be necessary, and removes the need to manufacture a large number of high-tolerance small shafts, which other teams found to be difficult.

4. Thumb

Our project had no specific requirements for a thumb. Two thumbs were initially developed - a human-like fixed thumb and an adjustable thumb. Although the fixed thumb could be printed with TPU, fixing the thumb in a single position would have very limited usefulness in our testing because the thumb must adopt a large variety of positions when opposing the fingers in various grasps. Instead, I designed a thumb with three degrees of freedom that can be manually adjusted and locked in place. Removing a single M4 screw at a joint allows it to rotate freely, and tightening the screw locks the joint in place by squeezing two halves of a Hirth coupling together. The Hirth couplings are advantageous because they will not slip unless extreme forces (which would likely break other parts first) are applied to the thumb.

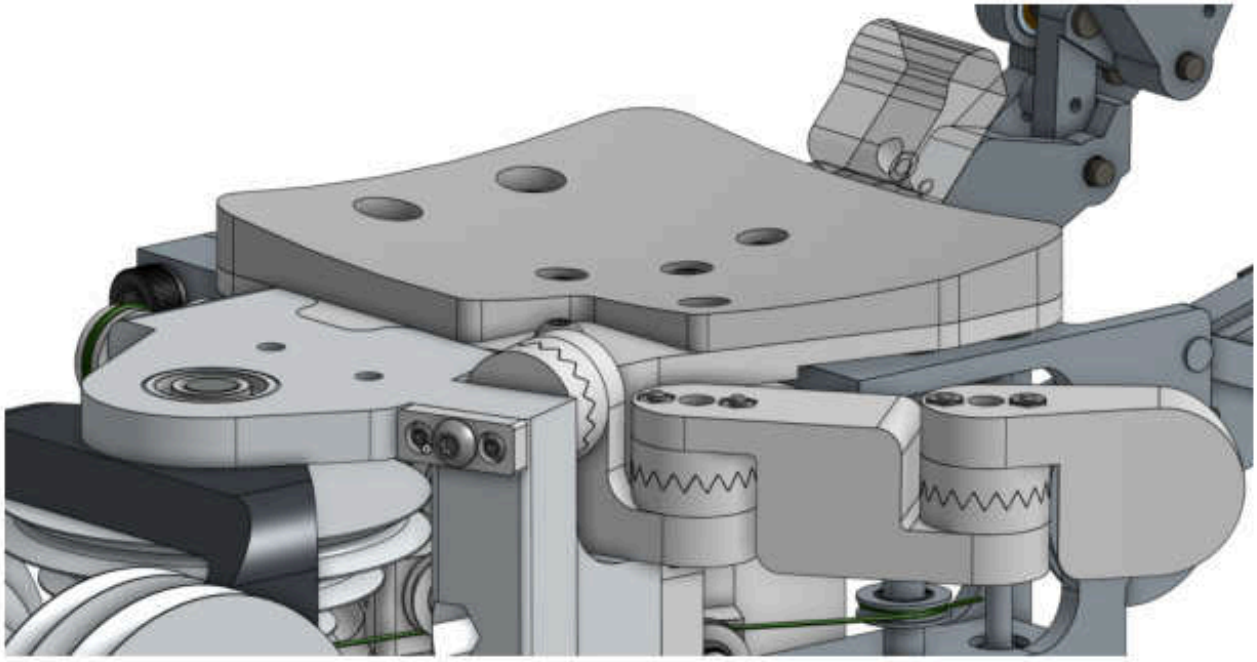


Figure P8: *Mounting of the thumb to the modified wrist structure*

The thumb mounts in a slot on the Distal Wrist Structure. Originally it was difficult to insert and remove the thumb while the entire palm was assembled, but this has been fixed with a part revision in CAD and on the physical build.

A tangential note about the thumb - many Hirth coupling models posted on the internet are modeled incorrectly, resulting in teeth that mesh imperfectly. One correct way to model each tooth is using a lofted cut between two isosceles triangles. See the CAD linked below for my fully parametric and correct Hirth coupling model.

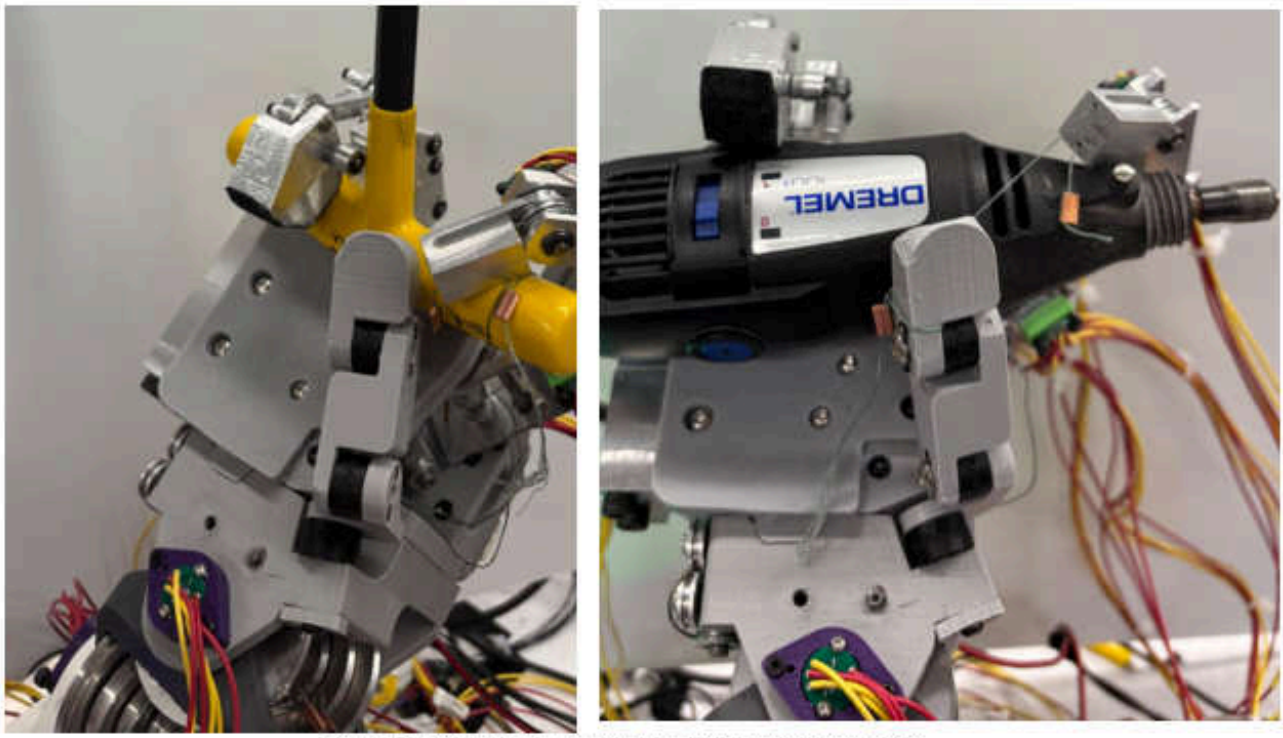


Figure P9: *The thumb involved in two different grasping poses*

5. Palm Grip

To make the palm surface compliant and increase friction with grasped objects, I made a custom silicone pad and adhered it to the Hand Structure Lower part. The pad has a curved, dish-like shape that mimics the contour of a relaxed human palm. I 3D-printed a mold and cast the pad using Ecoflex 00-30 silicone. Bonding silicone to plastic can be difficult, but I found that Scotchweld PR100 produced strong adhesion.



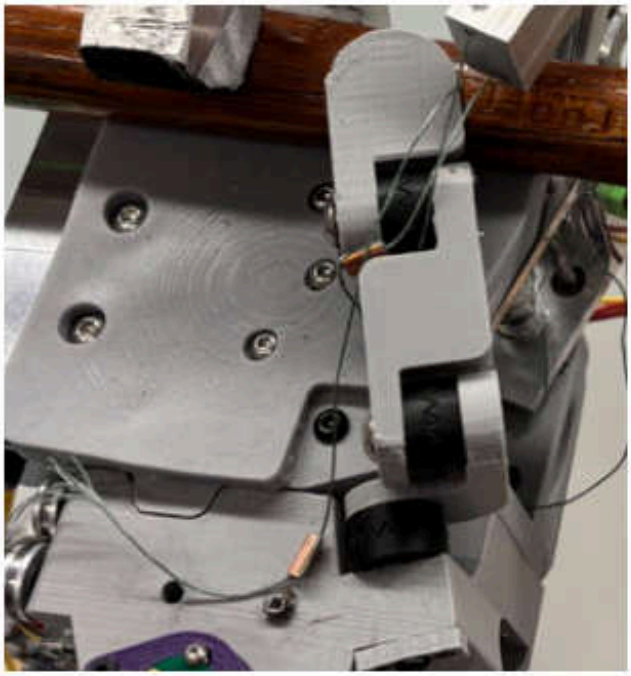


Figure P10: *Left: Casting the palm grip in a 3D-printed mold. Right: The gray silicone palm grip installed on the hand.*

6. Manufacturing

The hand redirect block, plates, and spacers were manufactured using 3D printing. Although the palm does need to accommodate some loads, strength is not an issue. Bearing and shoulder bolts were purchased from McMaster. Pulleys were manufactured similar to the dex finger. The critical dimension was the hole diameter to fit the bearing and, to a lesser extent, the thickness. The inner diameter was achieved using a reamer. A custom grooving tool with the exact pulley groove width was manufactured to make the pulley grooves. Using this tool, the operator could fix the position of the tool head and then move the tool inwards towards the center of the shaft until the desired outer pulley diameter was achieved. This removed any need to carefully position a generic grooving tool, which took a long time, and guaranteed a consistent pulley groove width. Once the inner hole and the groove were manufactured, the pulley was cut from the stock. It is critical to use lots of cutting oil during this process to prevent the small pulleys from heating up and warping. The final pulley was assembled with the bearings and other components. Any remaining looseness in the fit could be fixed with loctite. Lastly, one future improvement in the design is to make the pulley walls to be taller so that the tendons do not fall off easily.

7. Miscellaneous

The Hand Electronics Mount has the hole pattern for Han's palm PCB and attaches to the palm assembly with two screws. I chose to mount the PCB with a gap between its bottom surface and the top surface of the palm sandwich because the empty space could be useful for wiring.

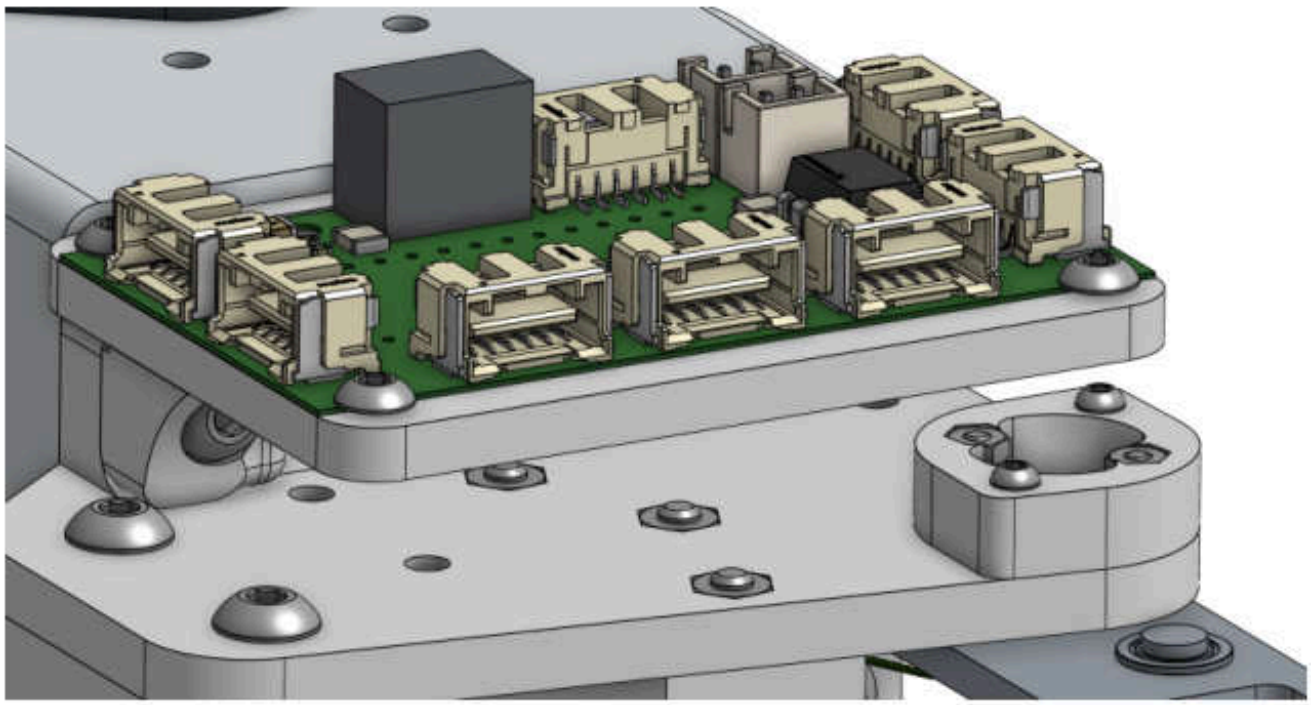


Figure P11: *Palm PCB mount*

The Splay Encoder Mount is a single part that places the circular encoder PCB as close to the top of the splay shaft as possible, leaving a 0.5mm gap between the shaft and the top of the encoder chip. The part can be easily swapped without unmounting the encoder by removing two M2 screws that fasten to trapped nuts on the underside of the Hand Surface Upper.

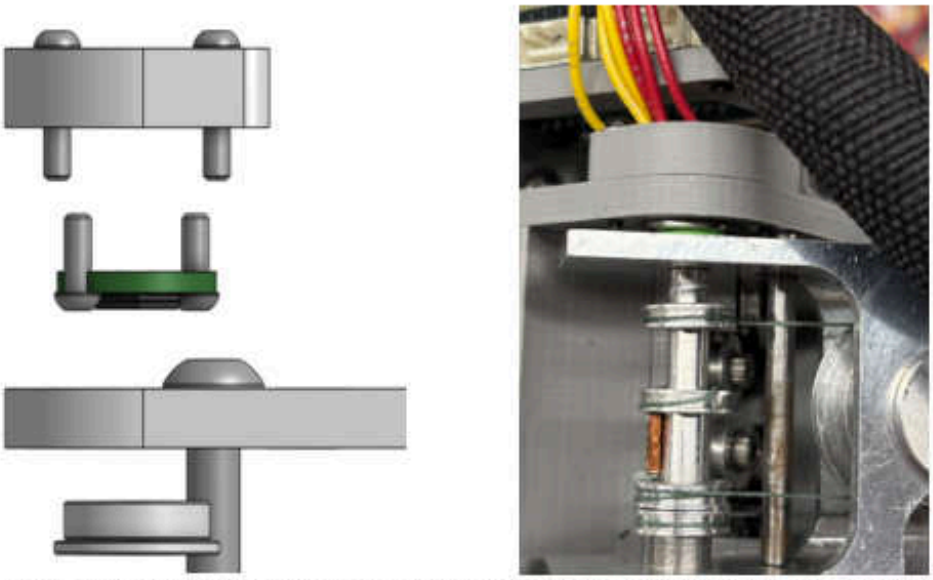


Figure P12: *Splay Encoder Mount exploded view (left) and real-world use (right). There are counterbores in the top surface of the Hand Structure Upper part to clear the encoder mounting screw heads.*

8. CAD, Drawings, and BOM

The Palm design exists in the following Onshape document:
https://cad.onshape.com/documents/002680511691l4ef722da114/w/5046039d8fc38cb24b4c0ba7/e/935f302befd0bb6de960d535

The complete assembly in the above document is called **Final Assembly.** That assembly includes all fasteners and has all tendon routing paths modeled in, so it should be treated as the master reference for assembly and repair of the palm. With the exception of the Distal Wrist Structure, all of the palm's custom parts were designed in a single Part Studio called **Hand Parts Master**. The modified wrist was designed in a separate Onshape document that contains Konrad's imported wrist CAD files, and is called **Distal Wrist Structure**:
https://cad.onshape.com/documents/283e82f4ef269efeefca99ad/w/c874baa9bc9a26eefe1f80f9/e/590342dd188ea4209f396edb

A full BOM of the palm is contained this spreadsheet, and all custom parts have drawings linked therein:
https://docs.google.com/spreadsheets/d/1WeRGOamJ1zUQiCC0IdDuals4DJPpDAvlK8Ju5Y5aRQs/edit?usp=sharing

7. Reflections

When working on the palm, a large design priority for me was avoiding as many sub-optimal characteristics as possible. In terms of structure, the palm places the fingers as close together as possible and as close to the wrist as possible so that we approach human-like anatomy, and uses relatively little material while still being very rigid. The volume of the palm is driven almost completely by the width of the power finger base and the height of the dextrous finger splay shaft - the palm-specific parts add very little volume, and the entire assembly remains compact enough to be smaller in cross-section than the wrist. Going through the palm is by far the easiest step of tendon routing and takes almost no time; it is comparatively much harder to route the tendons through the wrist and dextrous finger because they require full tendon wraps around non-cantilevered pulleys.

While its function might seem simpler than the other subsystems in our project, the palm required very substantial design work. The wrist and fingers were not designed with full-system integration in mind, and the palm design is very sensitive to even small design changes in any of the other subsystems. I went through four different iterations of the tendon routing paths within the palm as the dex finger team changed their desired arrangement of tendons going onto the splay shaft, and the forearm team changed their desired arrangement of tendons going onto the wrist. It turns out that there are only a few orderings of tendons on the wrist pulleys and dex finger splay shaft that can realistically be routed through the palm without unmanageable tendon crossings, so finding a working one after other subteams made design changes took a very significant amount of time. Many last-minute changes to almost every palm part were also required after Konrad needed to add a second drive pulley to the wrist, as I had designed the palm's modified wrist structure to be as close to the existing pulleys as possible to maximize compactness.

Modeling the palm using in-context references to the fingers and wrist was very helpful. I took an approach where I first modeled the tendon paths based on references to the finger and wrist pulleys, then chose the locations of the palm's redirect pulleys, and then finally designed the palm structure around the tendon paths and pulley locations. In the interest of optimization, this order of doing things is helpful when trying to include only the structure that is absolutely necessary to support routing pulleys.

Some potential future palm improvements:

- Finding a supplier for M3 shoulder bolts that have larger, tighter-tolerance shoulders would eliminate some wobble in the redirect pulleys. I don't think the wobble causes any issues, but the fit of the pulley bearings on the shoulder bolts we sourced from McMaster-Carr is somewhat looser than ideal.
- The Hand Structure Lower part has some geometry that makes it tricky to pull out from the rest of the palm assembly when the power finger is in place. It still is possible, and there aren't a lot of situations where you'd actually need to do this, but this was the only slight assembly difficulty I encountered that has not yet been addressed.
- There is an extra pulley available in the wrist that could route another tendon into the palm. In the future, this could be used to create a 1-DOF actuated thumb.
- The three core parts of the palm assembly - the upper and lower plates and the dextrous finger routing block - were originally intended to be machinable out of aluminum. I gave up on this

eventually because the palm design was so sensitive to the last-minute changes made to the fingers and wrist, and I didn't want to machine something that ended up being useless. Although their geometry is currently optimized for 3D printing and includes lots of curves and fillets, these parts could be easily modified for milling if aluminum versions were desired in the future.

Dexterous Finger

Dexterous Finger

Design Objectives

The following were set as the design objectives for the dexterous finger:

- 4 dof, 3 active; approx 90 deg ROM in plane, +/- 10 deg splay
- N+1 with active tensioning; do not require small tendon bend radii
- Tendons attached to distal and medial links, not proximal, and spring-loaded conformal grasping for remaining joint
- Continuous force: ~20 N at fingerpad at extension
- Speed: at least 1 ROM in 1 s
- Force controlled and backdrivable, retaining some backdrivability with power off
- Direct measurement of joint angles
- Tendons routed through carpal tunnel; ease of routing and maintaining tendons, and/or replacing whole finger (mechanical and electrical connections); role of steel cables, Bowden cables, other tendon materials
- Tendon evaluation: stiff, stretchable, or stiff plus an elastic element in line
- Size: human-sized (slim)
- Control objectives: trajectory-streaming position and force control (consider methods for measuring ground truth forces)

Specifications

The specifications for the dexterous finger are outlined in Table 1.

Table 1. Specifications for the Dexterous Finger

Motors Used*	RoboMaster M2006 P36
Motor Max Torque	1 Nm continuous
Tendons Used	Spiderwire Stealth Braided Fishing Line
Tendon Max Capacity	40 lb
Finger Length	155.43845 mm (Bottom of Base to Tip)
Finger Width	29.75901 mm
Finger Force at Tip (Extended)	37.33 N
Finger Degree of Motion Curling/Extension	~90 deg at each joint

Finger Degree of Motion Splay	~180 deg

Figure 1 below illustrates the dexterous finger's range of motion for curling. Note that the left image shows a greater range of motion than the final product because the linkage was not yet installed. The right image shows the actual angle at complete curling between the MCP and PIP with the linkage installed.



Figure 1. Dexterous finger curling range of motion

Videos of the finger moving can be found here.

* Worth noting is that the team used the above motors due to their shipping time and performance. The team previously did research on other motors (see this spreadsheet) and were going to purchase motors from a different vendor, but due to tariffs between the U.S. and China, the entire class had to pivot to these motors.

Design Summary

The dexterous finger has three phalanges and a base. There is a shaft between each phalange as well as a shaft on the base that allows for the finger's splay motion. Each shaft also has pulleys that allow for tendons to be routed at a particular radius, even as the tendons are tensioned by the motors. One other shaft exists on the base that redirects one tendon onto the splay shaft (this is referred to as the 'redirect shaft'). A metal linkage couples the PIP and MCP, leaving 3 independent degrees of freedom. While the linkage is supposed to be spring-like, the team decided to proceed with a metal linkage for reasons explained in the linkage section below.

Tendon Selection

During the design process, the team tried three different tendon options: coated steel cable (0.0468 in diameter), uncoated steel cable (0.024 in diameter), and fishing line (see Figure 2).

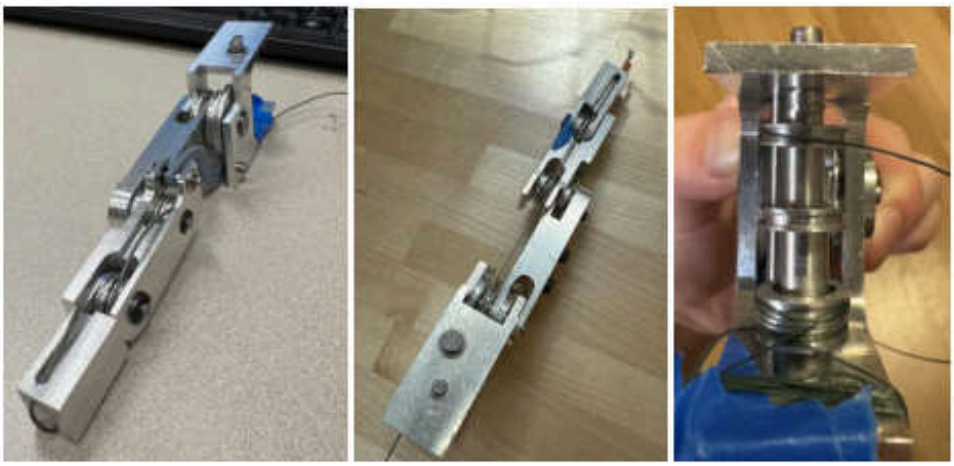


Figure 2. Coated steel cable (left), uncoated steel cable (center), fishing line (right)

Originally, the team was going to use coated steel cable, but it was realized after machining that the tendon would not be able to do complete wraps around the pulleys because the cable was too wide for the manufactured pulley groove. Complete wraps around the pulleys were necessary to prevent a tendon from lifting off the pulley and contacting other surfaces during operation.

Some basic concerns for the tendon are its strength and bend radius. The fishing line is rated to a breaking strength of 40lb or around 180N. This would have been sufficient for the old, original motor, but the new 1Nm motor is capable of exerting 200N arounds its r=5mm pulley, making it theoretically capable of snapping the fishing line. The tendon load means that it is desirable to have large pulleys on the finger so that less tendon tension is needed to reach the designed force. This breaking strength is not as much of a concern for the steel cables; the thin uncoated steel cable has a breaking strength of 70lb. However, the steel cables give recommended critical bend radii which are usually larger than the smallest radii on the finger, possibly reducing their effective breaking strength. Meanwhile, the fishing line has a negligible critical bend radius for the sake of this project. This being said, no fishing line tendons were snapped.

After discussing with instructor Oliver, the team moved to fishing line (see Table 1). However, the forearm team was concerned with creep, so the team also purchased uncoated steel cable, which was thinner than the coated steel cable. Ultimately, the team proceeded with fishing line because the uncoated steel cable kept unraveling as the team cut it, making it more likely for students to get metal splinters. The class also found that the fishing line was easy to terminate on the motors and had less creep than expected.

Linkage Coupling

The linkage placement was determined by moving the position of the endpoints incrementally and testing the movement of the finger. The linkage had to avoid interference with the pulleys while still allowing range of motion. Once the endpoints were finalized, several designs were tested.

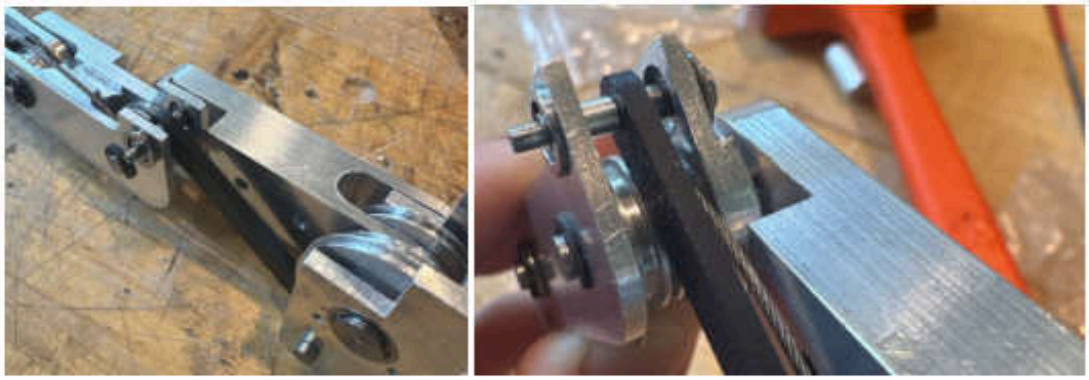


Figure 3. Straight linkage of PLA.

Initially, a straight linkage was modeled, printed, and tested to ensure the motion was as expected. However, the team knew from CAD that it would interfere with the pulleys when the finger curled slightly (see Figure 3). With this in mind, the team designed an S linkage such that the linkage would not touch the pulley as the finger flexed (see Figure 4).

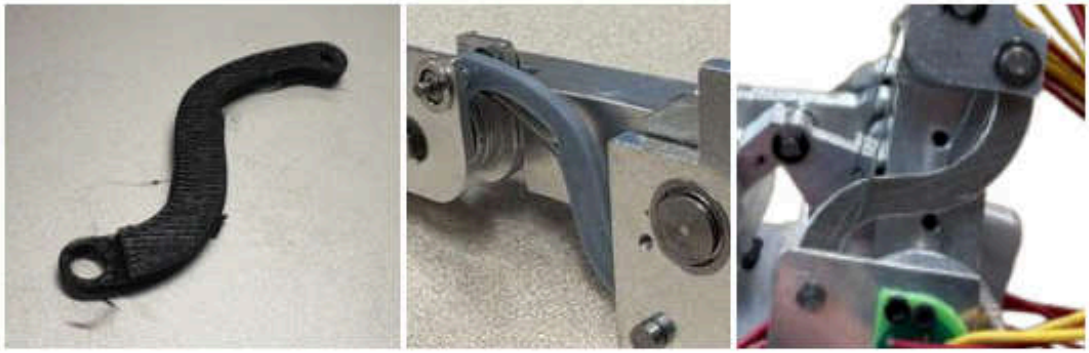


Figure 4. S linkage from TPU (left), PLA (center), and aluminum (right)

In consideration of the "spring-loaded conformal grasping" design objective, the coupling would need to change length so the team tested PLA and TPU as possible materials. The PLA had minimal, but noticeable, conformal behavior, while the TPU had high conformal behavior. Finally, the aluminum linkage was rigid, as expected. After speaking with the instructors, the team moved forward with the aluminum linkage. This makes the kinematics more straightforward, but arguably, the practical implementation is even more challenging, especially considering the tight packaging constraints and limited amount of time left in the project. A

simple design such as the one in figure 5 would become straight when stretched and could interfere with the pulleys, adding friction and wear. This means that, keeping current components in the same places, it would likely need to be some kind of compact linkage mechanism which moves in a carefully designed way. In addition to avoiding pulleys, it would need a compact lateral footprint to avoid getting caught in the tendons on either side which makes it hard to mount a spring or other elastic element in the tight space. A further difficulty with this requirement is that it adds another element which must be characterized for control. Should more "springiness" be desired, the linkage can be replaced with the TPU linkage.



Figure 5. Spring linkage. This provided the most spring-like behavior, but has not yet been characterized.

Manufacturing and Assembly

Perhaps the most time-consuming aspect of the project was manufacturing. It proved to be extremely challenging to machine tight tolerances (within a thousandth of an inch) on small components that are mostly designed for interference and transition fits. Moreover, all components except the bearings had to be manufactured from stock.

On the lathe, the small diameter shafts (particularly the longer shafts) would deflect from the cutting forces, usually resulting in significant deviation from indented diameter. In fact, all shafts required careful sanding with repetitive fit-checking to bring the part to an acceptable size. Other small details that can normally be overlooked for larger parts, such as the radius at the shoulder due the tool nose radius or tiny burrs necessitated additional post processing. Most critically, however, longer shafts would break when turning. To avoid this, the team eventually machined shafts starting from the smallest diameter moving up to the largest diameter. The smallest diameter would be machined, the shaft would be pulled farther out of the collet, and then the next section of the shaft would be turned down without touching the already machined smaller section(s). This process would be repeated until the shaft was ready to be cut from the stock. This method avoids any issues with shafts snapping.

For pulleys, the critical dimension was the hole diameter to fit the bearing and, to a lesser extent, the thickness. The inner diameter was achieved using a reamer, a boring bar, or a combination of both (which was needed for any counter bores). Although a standard grooving tool was initially used to manufacture the pulley grooves, the team eventually manufactured a custom grooving tool with the exact pulley groove width. Using this tool, the operator could fix the position of the tool head and then move the tool inwards towards the center of the shaft until the desired outer pulley diameter was achieved. This removed any need to carefully position a generic grooving tool, which took a long time, and guaranteed a consistent pulley groove width. Once the inner hole and the groove were manufactured, the pulley was cut from the stock. It is critical to use lots of cutting oil during this process to prevent the small pulleys from heating up and warping. The final pulley was assembled with the bearings and other components. Any remaining looseness in the fit could be fixed with loctite. Lastly, one future improvement in the design is to make the pulley walls to be taller so that the tendons do not fall off easily.

Spacers were cut from aluminum stock on the lathe. These also proved to be quite difficult at first as the small size of the bearings meant the spacers had to be cut from thin-walled tubes and most spacers themselves had to be very thin, from around 0.5mm to 1.1mm. Thankfully, the spacer's dimensions did not have to be as tightly controlled as other components. It was found that it was best to part very slowly using a good grooving tool. After careful deburring and a little sanding, the team found that the dimensional accuracy of the spacers was quite good and thickness within 0.1mm was easily achieved.

When milling links, a substantial amount of time was spent reducing the material to size and checking lateral thickness to ensure parts would line up later when assembling. To obtain the tolerances for the holes, a boring bar or a reamer could be used. However, the shop is not equipped with boring bars small enough for all the holes, leaving the reamer as the only option. While the reamer's size is accurate to within a few ten-thousands of an inch, they come in discrete sizes which are very close to their nominal size while bearings often require the housing to have a smaller-than-nominal hole for a tight fit. However, the holes still proved adequate for locating the bearings. In this and many other cases, Loctite retaining compound was again effective for locking loose parts together.

Finally, assembly was difficult due to the lack of visibility for alignment, tight fits between the shafts and bearings, and the fact that the stacks of spacers and pulleys fit with very little play between the walls created by the phalanges. Overall, this was time consuming but after experimenting (and shattering a few bearings), it was manageable. To keep the parts aligned, the team inserted an undersized screw through all the components and then pushed the screw out as the shaft was sequentially put through all the components. The shaft was usually tapped with a mallet until it was through all bearings, pulleys and spacers before finally being pressed all the way through using a machining vise.

Kinematics and Theoretical Performance

In this section, we will derive relationships between the motor angles and joint angles, motor and joint torques, and fingertip force. The team would like to acknowledge Luke for his guidance on this topic. **For numerical values, see the kinematics python notebook located in the student collaboration google drive under mechanical > dex finger.**

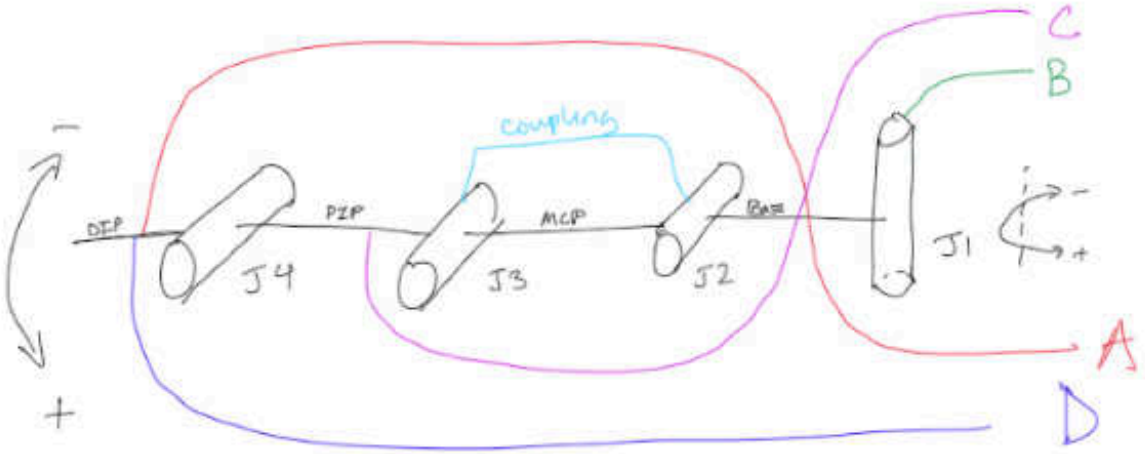


Figure 6. Tendon routing for the dexterous finger

Routing

Due to design requirements, the team was allowed to terminate tendons only on 2 of the 3 links on the finger and it was required to use a coupling between J2 and J3. The chosen routing scheme grants a few advantages. Firstly, since one tendon terminates splay and drives it independently, it reduces the number of tendons which must be routed through the rest of the finger, saving space. Secondly, placing two tendons on the bottom of the base joint (ie. J2) was a deliberate decision to bias the force capability in the curling/flexion (+) direction since it was anticipated that most actions performed by the dexterous finger, such as pulling a trigger or grasping would favor a design with strong flexion. During motor selection, the team found it would have been difficult to source a single motor with sufficient torque to give the 2Nm required at the base so putting 2 tendons in flexion was the only way to meet force requirements. Thirdly, the N+1 configuration makes it possible to run an auto-tensioning/calibration routine that removes the issues with tendon tensioning that would be present in an N design.

Motor selection

During motor selection, the team attempted to find a motor which would be able to provide sufficient torque at a reasonably low gear ratio, would be compact, and logistically feasible for our timeline. To determine the motor's output torque requirement, the team did some rough calculations as follows. First, we neglect splay forces as they are not required. This leaves J2 as the critical joint since it would have the longest moment arm of 10cm. With the extended fingertip force requirement of 20N, we have the torque requirement at J2: 20N * 0.1m = 2Nm. Therefore, each tendon/motor is responsible for delivering 1Nm in flexion. At the human-like size we are targeting, the maximum size for the J2 pulley would be roughly 10mm radius. Since it is unlikely that we could get a pulley much smaller than 5mm on the motor side while leaving room for the motor shaft and SEA, we estimated that a reasonable transmission ratio is 2:1. Therefore, the motor should have a max continuous torque of around 0.5Nm. Indeed, the finger was designed for this torque output.

After realizing that Maxon did not have options that could arrive on time, the team looked through the Moons' catalog and found that ECU16036H24-C063 with PG16M-0103 gearbox would have the necessary torque at a N=103 gear ratio while being compact and could be procured on time. Unfortunately, significant tariffs on China (where the Moons' motors are manufactured) coincided with the ordering schedule and made the motors significantly more expensive. As a backup, the instructional team ordered the Robomaster M2006 P36 motors which ended up being used. The main difference for kinematics is that they offer a higher maximum continuous torque.

Nomenclature

For the upcoming analysis, the following notation will be used.

ϕ	motor angle vector
θ	joint angle vector
l	tendon length vector
L_{ab}	physical distance between points on the finger, subscripts specify points.
R_j	matrix of joint pulley radii
R_m	diagonal matrix of motor radii
τ_j	joint torque vector
τ_m	motor torque vector

J_t	tendon Jacobian matrix, used to map speed/torque between motor and joints
J_f	finger Jacobian matrix, maps the speed/torque of joints to finger tip
$g(\theta_3)$	linkage relation where J3 is the driving joint
$h(\theta_3) = \frac{dg}{d\theta_3}$	derivative of the linkage relation, acts as the instantaneous transmission ratio between J2 and J3
f_t	tendon tension vector
F	fingertip wrench vector (moment and force)

Mapping motor-joint positions

First, we can briefly recall an N+1 configuration with no coupling simply has constant matrices relating the joint angles to motor angles, referred to in class as the structure matrix, and also has a constant matrix relating the joint torque and motor torque which we call the transmission matrix. If, during design, we ensure that we have an antagonistic pair of tendons for each joint, the only complication with an N+1 configuration comes with choosing motor torques so that all tendons are in tension using the null space of the transmission matrix. Adding a rigid coupling introduces a further complication which we will now handle.

When controlling the finger, we may be interested in commanding movement to a certain position. To do so, we will establish the relationship between the joint position and required motor angles. We can select angles for the 3 independent joints up to 90 degrees which determines the fourth angle through the 4-bar linkage. First, we derive the linkage equation using loop closure, as seen in figure 7. See the notebook for details of the loop closure solution.

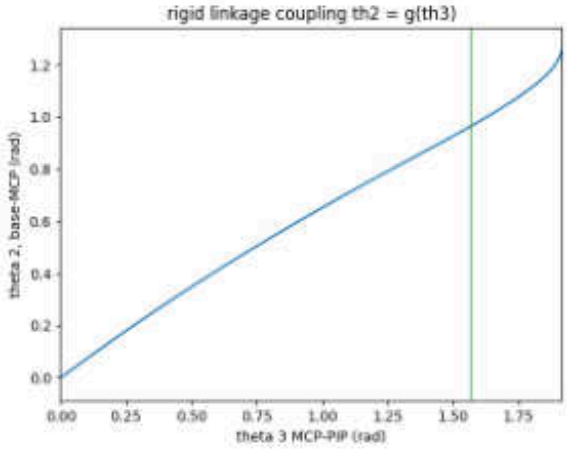


Figure 7. Relation between coupled joints. The green line indicates the 90 degree designed range of motion. The function is only slightly nonlinear in the operating region.

Let us denote the relationship between the joint as $\theta_2 = g(\theta_3)$. After taking the time derivative, we also have $\dot{\theta}_2 = \frac{dg}{d\theta_3}\frac{d\theta_3}{dt} = h(\theta_3)\dot{\theta}_3$, shown in figure 8. By power conservation, h can be regarded as an instantaneous transmission ratio, a quantity which will become important later.

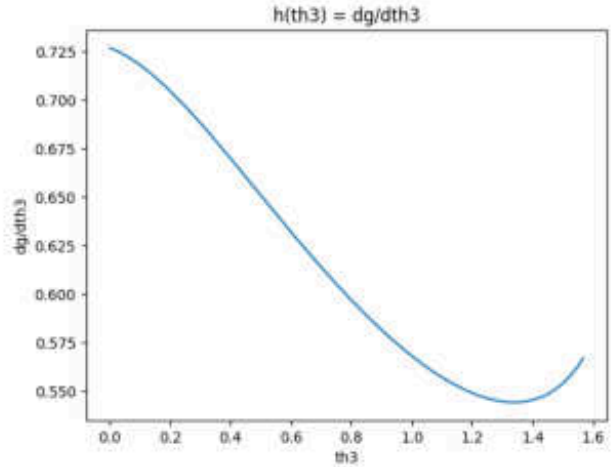


Figure 8. derivative of linkage relation used in the tendon Jacobian plotted up to theta3 = 90 degrees

To change the joint angle, we require the tendons in the finger to lengthen/shorten by a certain amount. This change in length is due to the tendon either unwrapping or wrapping around the joint pulleys. For a single joint, we have:

$$\Delta l = r\theta$$

Therefore, knowing the radii of each pulley, we can express the difference in the vector of tendon length, Δl by using a pulley radii matrix:

$$\Delta l = R_j\theta$$

Where we have defined R_j the 4x4 matrix of joint radii so that $l + \Delta l = l_{ref}$. This implies that shortening tendon (ie. wrapping onto the motor) is the positive sign convention.

Now, using the same principle and the sign convention that wrapping onto the motor is positive, we can construct the motor pulley radii matrix to obtain the compatibility condition for the tendon length change on the motor and finger.

$$\Delta l = R_j\theta = R_m\phi$$

So, for given joint angles, we obtain corresponding motor angles:

$$\phi = R_m^{-1}R_j\theta$$

We can also take the time derivative for the speeds. Furthermore, we can recast the equation in terms of the 3-vector of independent joints denoted with a subscript. We write the columns of R_j as r_1, r_2, etc.

$$\frac{dl}{dt} = R_m \dot{\phi} = \frac{d}{dt}(R_j \theta) = R_j \dot{\theta}$$

$$= R_{j,\,indep}(\theta)\dot{\theta}_{indep} = [r_1 \;\; (r_2 h(\theta_3) + r_3)\, r_4]\,[\dot{\theta}_1 \;\; \dot{\theta}_3 \;\; \dot{\theta}_4]^T$$

This gives us the so-called tendon Jacobian, where we use the pseudoinverse on $R_{j,\,indep}$:

$$\dot{\theta}_{indep} = R_{j,\,indep}(\theta_3)^{-1} R_m \dot{\phi} = J_t(\theta_3)\,\dot{\phi}$$

This formulation gives a set of compatible tendon lengths/motor angles. We can think of this as a set of tendon lengths which, if starting from a slightly tensed state, results in a desired movement while keeping every tendon barely in tension. If we had picked a set of motor angles at random, they would likely be incompatible.This would excessively tense or loosen pulleys, which is problematic as it may cause tendons to break or fall off the pulleys.

Finally, it should be mentioned that this system is valid only for the dex finger and does not account for wrist wrapping or SEA. Adding additional terms for the wrist pulley length changes is straightforward and the above equations should still hold after augmenting with 2 additional wrist angles and associated motor and joint radii. With SEA, we also need to account for the length change resulting from tension in the tendon. This analysis is valid in the unloaded, static case where the SEA experiences little force resulting in negligible length change. During grasping, it is better to use torque control on the motors. The following section will analyze how motor torques and joint torques are related.

Joint-Motor Torque Analysis

We will see that the relationship boils down to using the transpose of the previously derived tendon Jacobian. We start the derivation with power conservation:

$$\dot{\phi}^T \tau_m = \dot{\theta}_{indep}^T \tau_{j,indep}$$

$$\dot{\phi}^T J_t^T \tau_{j,indep} = \dot{\phi}^T \tau_m$$

So we see:

$$J_t^T \tau_{j,indep} = \tau_m$$

$$J_t^{-T} \tau_m = \tau_{j,indep}$$

We then recover the remaining torque using power conservations with the linkage equations.

$$\tau_2 = \frac{1}{h}\tau_3$$

Again, we use the pseudoinverse because J_t is a nonsquare (3 x 4) matrix. Since we have an N+1 system, we should again expect that J_t^{-T} has a 1-D null space. The physical interpretation of a null space in this jacobian is that there exists a 1-D space of motor torques. We can evaluate J_t^{-T} for a random value of θ and check that this is true in the notebook. Indeed, we observe that the null space of J_t^{-T} at $\theta_3 = 0$ is:

$$null(J_t^{-T}) = [0.38894668,\ 0.83328997,\ -0.05539662,\ 0.38894668]^T$$

Applying motor torques in proportion to the null space will result in no net joint torque.
If we obtain a solution for motor torques which will result in a tendon completely losing tension, that is, we obtain a value of $\tau_m < 0$, we can offset the solution using $\alpha[null(J_t^{-T})]$ where, α is a scalar we pick, so that all torques are positive. We can finally scale our new motor torque solution to ensure that the actuators are not saturated. Now that we can map joint and motor torque and also calculate the required motor torque command to generate a set of desired joint torques, we complete the analysis by obtaining the mapping to fingertip force.

Fingertip forces from joint torques

Now that we can find the finger joint torques, we want to see how these translate to the force at the end of the finger. To do this, we will introduce the finger Jacobian. From the specifications, we are interested in the case where the finger is fully extended. In the x-y plane, the splay joint J1 has no effect while all the other joints cause the fingertip to move in y. Only J1 causes motion out of the plane (in z), see figure 9.

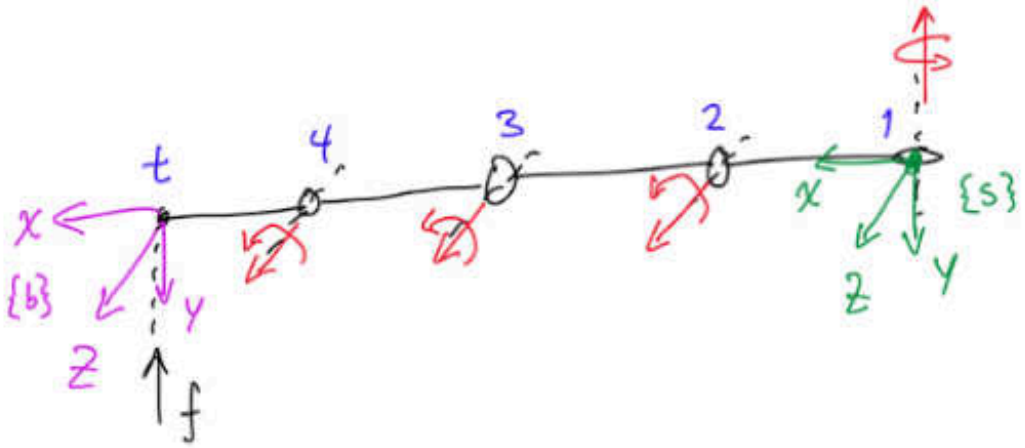


Figure 9. fingertip force and coordinate system diagram

The finger Jacobian maps between the joint speed and end effector speed. We handle the coupling in the same way as before to create an equation in terms of the independent joints. We can construct the Jacobian in the extended configuration ($\theta = 0$) by inspection.

$$[\dot{x}\ \dot{y}\ \dot{z}]^T_{tip} = [J_{f1}\ J_{f2}\ J_{f3}]_{trans}[\dot{\theta}_1\ \dot{\theta}_3\ \dot{\theta}_4]^T$$

$$J_{f1} = [0, 0, L_{1t}]^T$$

$$J_{f2} = [0, L_{2t}h(0) + L_{3t'}, 0]^T$$

$$J_{f3} = [0, L_{4t'}, 0]^T$$

Since we have revolute joints, we also need to account for the rotational component. Looking at the diagram, J2, J3, and J4 rotate about y and so will contribute to ω_z. The contribution from J2 will be added into the coefficients of J3 due to the coupling. J1 contributes to ω_y while none of the joints twist axially, so there is no contribution to ω_x. The construction is the same as for the forces and we should take care to include the coupling effect.

$$[\omega_x\ \omega_y\ \omega_z]^T_{tip} = [J_{f1}\ J_{f2}\ J_{f3}]_{rot}[\dot{\theta}_1\ \dot{\theta}_3\ \dot{\theta}_4]^T$$

Here, we will estimate the maximum fingertip force that can be exerted at the tip in flexion when the finger is fully curled. By applying power conservation and our tendon Jacobian, we have:

$$F = J_f^{-T} J_t^{-T} \tau_m$$

We know from the motor specs that the maximum continuous torque is 1Nm or 1000 N-mm. The maximum force in curling at the tip is always achieved by putting maximum tension on tendons C and D (figure 6). Therefore, we simply plug in $\tau_m = [0,\ 0,\ 1000,\ 1000]$ N-mm to get the end-effector wrench:

$$F = [m\ f]^T = [0,\ 0,\ 640,\ 0,\ 37.33,\ 0]^T$$

We have a z-moment of 640 N-mm and maximum continuous downward force at the tip of 37.33N which is significantly more than the requirement. However, this is due to the fact that the motors chosen are twice as strong as intended; if we had used the original motors, we would be a couple Newtons short. This is because we failed to account for the linkage in our rough analysis. The linkage effectively increases the transmission ratio between θ_3 and $\dot{x}_{tip}$ by causing both J3 and J2 to curl simultaneously, leading to faster fingertip velocity and thus reducing the force output by power conservation.

This deficiency could be fixed by decreasing the motor radii slightly but we can instead use the coupling to our advantage. Power conservation also directly links the torques at the 2 joints. Knowing this, another way to increase the fingertip force would be to increase R3 since τ_3 and τ_2 are proportional.

We can also find the finger jacobian in general for any configuration following the formulation in the Modern Robotics textbook ch5.1. First, obtain the body screw axes:

$$B_1 = [0\ \ -1\ 0\ 0\ 0\ L_{1t}]$$

$$B_2 = [0\ 0\ 1\ 0\ L_{2t}\ 0]$$
$$B_3 = [0\ 0\ 1\ 0\ L_{3t}\ 0]$$
$$B_4 = [0\ 0\ 1\ 0\ L_{4t}\ 0]$$

After using the Modern Robotics library to solve for the body Jacobian, make some slight modifications to rewrite the Jacobian in terms of the independent joint speeds:

$$[J_1 J_2 J_3 J_4][\dot{\theta}_1\ \dot{\theta}_2\ \dot{\theta}_3\ \dot{\theta}_4]^T = [J_1\ (h(\theta_3)J_2 + J_3)\ J_4][\dot{\theta}_1\ \dot{\theta}_3\ \dot{\theta}_4]^T$$

This logic is encapsulated in a function, make_finger_jac() in the kinematics notebook. With all the mappings, we can create some visualizations of the theoretical performance of the finger.

Performance

Achievable joint torques:

We observe a slight change in the achievable joint torques based on the position of theta 3.

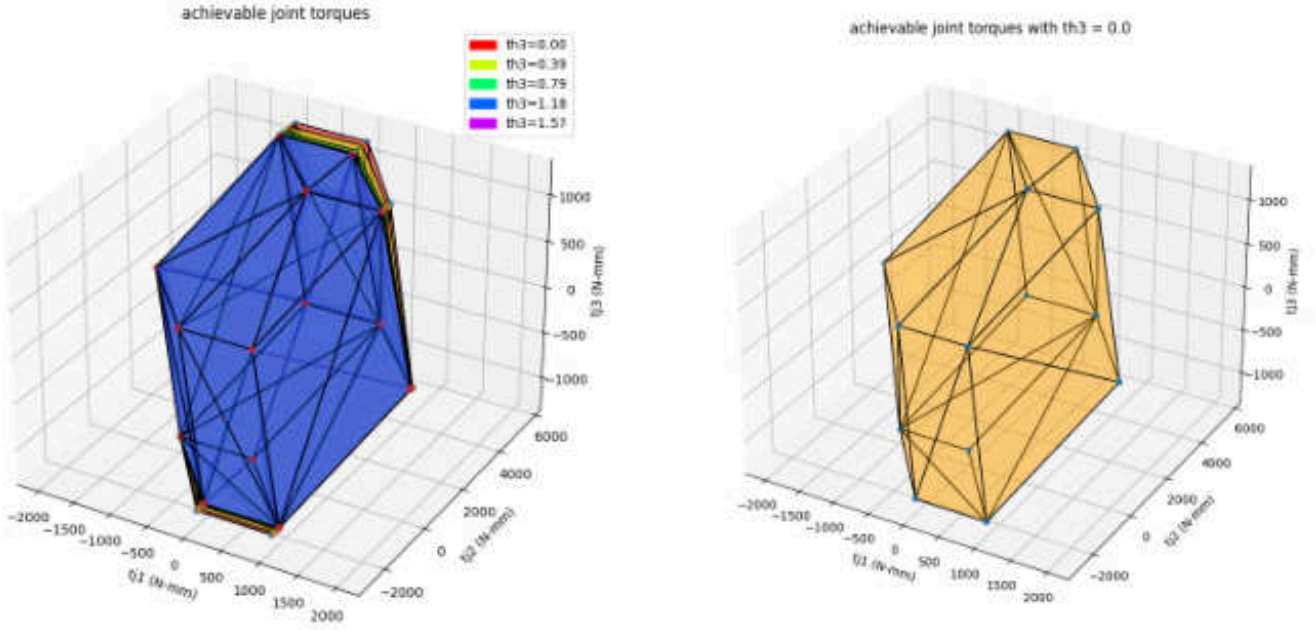


Figure 10. Achievable joint torques at each independent joint. Found by sampling the motor torque at each motor from 0 to 1000 N-mm and then plotting the convex hull.

Fingertip force magnitude vs joint angle:

The following plots (figure 11) are made by varying θ_3 while holding the other angles at 0 and then solving for the end effector wrench while flexing the finger as hard as possible. At first, the magnitude looks unrealistic: the peak is 300N (~70lbs) and the force rapidly increases as the finger starts to flex but it is explainable if we look at the components. We observe that the spike

is due entirely to axial force fx rather than a force normal to the fingerpad. We can recall that the fully extended position is a singularity where we cannot instantaneously move the tip in x but as the finger curls slightly, it brings the tip back in x slowly at first, resulting in a large force pulling in x, hence the negative sign on f_x. While it is large, this force is unlikely to be useful in most tasks. Instead, we are mostly interested in the f_y component, which is force normal to the fingerpad. f_y increases slowly and, if our analysis is to be believed, then reaches a steady-state of around 80N. This shows that while we didn't manage to satisfy the force target in the extended position, this design's force capacity increases greatly when slightly curled which is to the benefit of most tasks this finger will perform, particularly grasping objects and pressing triggers.

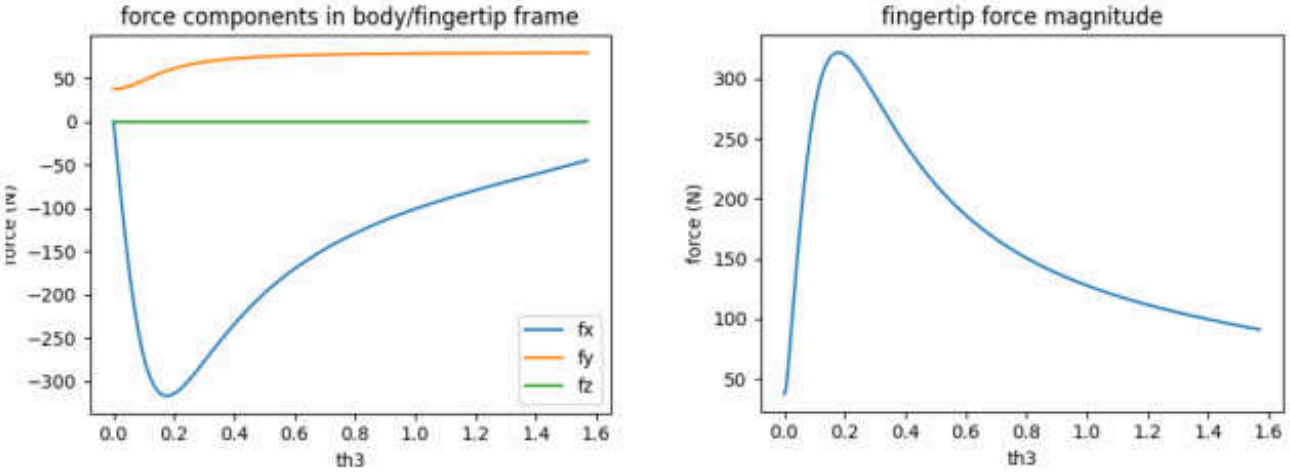


Figure 11. Maximum force output as J3 is curled while other joints are held at 0

Code for all topics mentioned in the kinematics section can be found in the notebook.

Engineering Drawings

All engineering drawings can be found hedre.

Misc. Items to Note

Encoders

Initially, the finger was designed to use two circular encoders and one slotted encoder. The base was then machined around the slotted encoder such that two M2 bolts could be used to mount the encoder to the part. However, after electrical issues, the team had to pivot and use a circular encoder at the base as well, so an adapter was designed and printed to have a circular encoder mount to the correct position and height (see Figure 12).

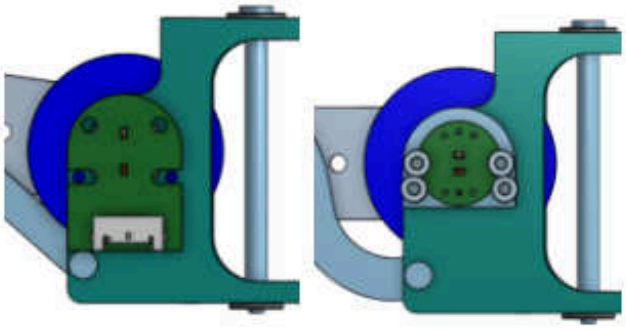


Figure 12. Slotted encoder (left) and circular encoder with the adapter (right).

Incomplete mounting holes in phalanges

The DIP does not have its M3 mounting holes like the MCP because these were initially neglected so that the assembly could be tested. Eventually, getting the finger and hand fully assembled and loctite-ed was a priority, so these holes were never added.

Tendon termination for splay

The tendon for splay is supposed to terminate on the pulley, but doing so with just the hole proved impractical since this required a very sharp change in direction for the tendon with nothing to guide it. So, a small slot was cut into the pulley using a Dremel to transition the tendon between the pulley and the hole. In the future, a better way to deal with this may be to anchor the tendon into the base link rather than directly on the pulley, which does not have much space.

Hardstops

The J4, and J3 have hardstops built in so that the finger cannot extend past straight. J2 stops against the base link but goes past straight while J1 has no dedicated hardstop at all.

Reflection and Future Work

The team identified a number of issues with the current design. Firstly, tendons fall off the pulleys easily when not in tension. During assembly and testing, replacing tendons takes a significant amount of time. The problem could be mitigated by using higher walls on the pulleys and possibly v-grooves. It may also be worthwhile to add a simple locking mechanism to isolate the tendons in the finger from those in other parts of the hand to facilitate testing without losing finger tension.

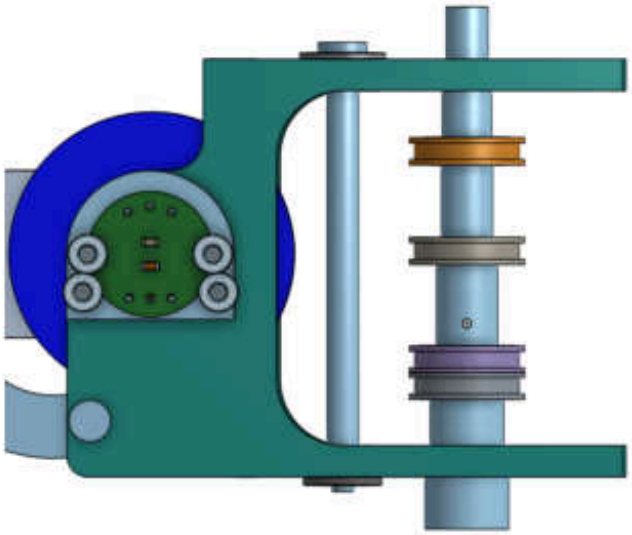


Figure 13. The splay pulley layout depends on the sizes of the J2 pulleys. As it stands, there is room to reduce the height (ie. vertical dimension in the picture) of the base link and could be reduced even more with some other design modifications.

Additional optimizations could be made to packaging, particular for the base link, and pulley sizing. As it is, the height of the base link could still be reduced until the top and bottom walls come nearly in contact with the splay pulleys (figure 13). The spacing of the splay pulleys is fully determined by the pulley radii at J2. As seen previously, the finger's maximum continuous force with current pulley sizes, given the final motors and linkage, is well above the required specification. So, reducing the size of the base pulleys and compensating by increasing the size of J3 pulleys is a viable option for packaging optimization while retaining force capability. Using smaller J2 pulleys makes it easier to bring J2 and J1 closer together to better resemble a co-located joint and allows the height of the base link to be reduced. Shortening the base link until it is about the same height as then would then allow the splay and idler shafts to be shortened significantly, resulting in easier manufacturing. Additionally, this opens up more possibilities for linkage mounting positions.

The rigid linkage coupling could also be optimized by reducing the values along the $h(\theta)$ curve. A small value of of $h(\theta)$ means a larger τ_2 relative to τ_3. If $h(\theta)$ is 0.5 this means that the linkage's transmitted torque balances the loads in static equilibrium. While the linkage nears this value around $\theta_3 = 1.3\text{rad}$ as the grip closes, it would ideally be closer to 0.5 for all values of θ_3. If instead we want conformal grasping, power finger's 5-bar design offers an interesting way to achieve this goal and it may be worth considering turning the MCP into a spring loaded 5 bar in a future design.

Weight reduction was not a focus on this project, but may be of interest in the future especially if more fingers are used. The design leaves a lot of room for weight reduction. The links are solid aluminum but would be just as functional if the inside material was removed to create a shell, retaining most of the strength while saving weight.

Manufacturing could be simplified by designing for pre-made parts. For instance, dowel pins are available in a variety of sizes and are precisely ground to within a few ten-thousandths of an inch. While it would lack shoulders to locate parts, this solution may be worth considering, as lateral spacing is less critical than achieving the right fit. Outsourcing more complex components like the PIP link may also be worthwhile. Additionally, while specialized cutting tools are not always necessary, it would be helpful to have a set of tools that were specific to RDS and not the general Ford shop, as the tools in the shop are often abused and don't leave good surface finishes. Due to the scale/size of the finger, these finishes were significant in terms of the parts fitting or not fitting.

The current design uses holes with a crimp to terminate the tendon. While this method is simple and reliable, it makes accessing the tendon more difficult, to, for instance, restring the finger after a tendon has fallen off. In the future, a removable clamp can be explored to improve tendon termination. Currently, the only way to get the required slack to restring a tendon is to wind the motors which is slow and cumbersome due to the gear ratio and the presence of electronics near the motors. To make matters worse, multiple tendons often lose tension at once during testing. This means it is necessary to loosen and then tighten each tendon by manually spinning the motors, which is a remarkably slow process. While software control of the motor to unwind one tendon could make this easier, it would be far easier if the free end of the tendon could be accessed by removing a clamp at the tip of the finger so that the tendon can be undone and restrung. The team found out the hard way that this is especially important if the tendon happens to get lodged tightly in a crevice between a pulley and spacer. When this happened, the loop resisted attempts to get pulled out and we ended up poking it with an x-acto knife to dislodge it. This operation is risky as it could have damaged the tendon and, when combined with restringing the other required tendons, took over an hour to carry out (it didn't help that this occurred at 4am the day of the demo!). This proposed system could be used to complement improved pulleys and

a tension-isolating system to reduce the chance of tendon malfunction and make it easier to reroute a tendon, saving a great deal of time overall.

It would have been beneficial to fully derive and analyze the kinematic model to begin with, if we did, we would have accurately hit the force target instead of just getting close. Doing so would have helped us better understand the design requirements and pick appropriate sizes for the elements. Looking back, we tunneled on getting a prototype ready for week 5 as per the original schedule which could be used to inform a second iteration, but due to the unexpectedly long manufacturing time and the tight schedule of the class, the kinematic analysis was put on hold for much longer than it should have. Then, somewhere along the way, we shifted to simply getting our existing design fully manufactured and did not get back to kinematics until later in weeks 9 and 10.

It would also be beneficial for the mechanical team to work more closely with the electrical and software team to design testbenches for each individual component of the system. While the dexterous finger was manufactured and ready for testing by around Week 7, the electrical team was not ready to test encoders. With this, the software team did not want to test the dexterous finger, especially with the SEAs and forearm not being ready either. Moving forward, if the class had made SEA modules and testbenches for each finger to be tested, the class likely would have resolved issues sooner. That being said, the forearm and SEA design changed around Week 8, so it is unknown how quickly the class would have been able to make these testbenches.

Bill of Materials

Table 2 shows the parts that make up the dexterous finger.

Table 2. Components for Dexterous Finger

Item	Quantity	Name	Material
1	1	Splay Shaft	1045 Carbon Steel
2	1	Base Phalange	6061 Aluminum
3	1	PIP	6061 Aluminum
4	2	6x10x3 Bearing	Bearing, As Purchased
5	7	4x7x2.5 Bearing	Bearing, As Purchased
6	1	Base Shaft	1045 Carbon Steel
7	1	ID7_R2 Pulley	6061 Aluminum

8	1	ID7_R2 Pulley	6061 Aluminum
9	1	DIP Shaft	1045 Carbon Steel
10	1	DIP	6061 Aluminum
11	6	5x8x2.5 Bearing	Bearing, As Purchased
12	1	PIP Linkage Mount	1045 Carbon Steel
13	1	MCP	6061 Aluminum
14	1	PIP Shaft	1045 Carbon Steel
15	2	J3_idler	6061 Aluminum
16	2	J4_pulley	6061 Aluminum
17	1	J3_pulley	6061 Aluminum
18	1	Large MCP Pulley	6061 Aluminum
19	1	Base Linkage Shaft	1045 Carbon Steel
20	2	4OD_innerrace_clearance	6061 Aluminum
21	1	5OD_innerrace_clearance	6061 Aluminum
22	1	4OD_innerrace_1.1	6061 Aluminum
23	1	Splay_D	6061 Aluminum
24	1	1.5x4x2 Bearing	Bearing, As Purchased
25	1	2x6x2.5 Bearing	Bearing, As Purchased
26	1	3x6x2.5 Bearing	Bearing, As Purchased
27	1	4OD_pulley_spacer	6061 Aluminum
28	1	PIP_linkage_spacer	6061 Aluminum
29	3	4-5_Eclilp	E Clip, As Purchased
30	1	Redirect Shaft	12L14 Carbon Steel
31	1	Base Spacer L2	6061 Aluminum

32	1	Base Spacer L3	6061 Aluminum
33	1	Base Spacer L4	6061 Aluminum
34	1	Base Spacer L5	6061 Aluminum
35	1	Base Spacer L6	6061 Aluminum
36	3	Magnet	Magnet, As Purchased
37	1	2x6x3 Bearing	Bearing, As Purchased
38	1	dex_encoder_slotted	Encoder, As Designed by Electrical
39	1	Splay_A	6061 Aluminum
40	1	Splay_A_D_Spacer	6061 Aluminum
41	1	Splay_B	6061 Aluminum
42	1	Splay_C	6061 Aluminum
43	1	Splay_B_C_Spacer	6061 Aluminum
44	3	Circular_encoder_Final	Encoder, As Designed by Electrical
45	1	Splay_Long_Spacer	6061 Aluminum
46	1	Splay_Short_Spacer	6061 Aluminum
47	1	Cap	6061 Aluminum
48	1	New Base Spacer	PLA
49	2	PIP Spacer	PLA
50	2	DIP Spacer	PLA
51	8	M2x6	Bolt, As Purchased
52	1	Linkage	6061 Aluminum
53	1	base_linkage_spacer	6061 Aluminum

The items purchased to make the dexterous finger are summarized in Table 3.

Table 3. Items Purchased for the Dexterous Finger

Part	Vendor	Part Number	Part Link	Unit Price	Quantity	Total Price
Steel Shaft (8mm diameter, 200 mm long)	McMaster	4138N81	https://www.mcmaster.com/4138N81/	$17.62	1	$17.62
Steel Shaft (8mm diameter, 400 mm long)	McMaster	4138N82	https://www.mcmaster.com/4138N82/	$20.60	1	$20.60
Steel Shaft (5 mm diameter, 100 long)	McMaster	1327K51	https://www.mcmaster.com/1327K51/	$4.97	1	$4.97
Neodymium Magnet (1/16" Thick, 1/16" OD)	McMaster	5862K409	https://www.mcmaster.com/5862K409/	$0.45	12	$5.40
1.5x4x2 Bearing	McMaster	57155K519	https://www.mcmaster.com/57155K519/	$13.66	6	$81.96
2x5x2.3 mm Sealed Bearings	Bearings Direct	F682-2RS	https://bearingsdirect.com/f682-2rs-miniature-flanged-ball-bearing-2x5x2-3-mm-sealed/?srsltid=AfmBOooNG41AmSWh8PzHKqIXd32juS58fkhdFPH4s4A	$4.38	4	$17.52

			eVHl15F-GlLPQ			
2x5x2.3 mm Sealed Bearings	McMaster	57155K526	https://www.mcmaster.com/57155K526/	$13.17	4	$52.68
2x6x2.5 Bearing	McMaster	57155K421	https://www.mcmaster.com/57155K421/	$15.20	3	$45.60
2x6x3 Bearing	Bearings Direct	692-ZZ	https://bearingsdirect.com/692-zz-mini-ball-bearing-2x6x3-shielded-r-620zz/?srsltid=AfmBOoqoVr-btbDZtO1iHyy7sKAgD_keWMfXlmoloLEd5aYixq3qM1Z_	$4.38	3	$13.14
2x6x3 Bearing	McMaster	57155K531	https://www.mcmaster.com/57155K531/	$14.16	3	$42.48
3x6x2.5 Shielded Flanged Bearing	McMaster	57155K538	https://www.mcmaster.com/57155K538/	$10.66	8	$85.28
3x6x2.5 Bearing	Bearings Direct	MR63-ZZ	https://bearingsdirect.com/mr63-zz-mini-ball-bearing-3x6x2-5-shielded-l	$4.38	3	$13.14

			-630zz/?srsltid=AfmBOopqLGrlWTGntlZEJJKdFDS_-aDdGertzOBQj3UnWml1P1M_wTWi			
4x7x2.5 Shielded Flange Bearing	Bearings Direct	MF74-2RS	https://bearingsdirect.com/mf74-2rs-miniature-flanged-ball-bearing-4x7x2-5mm-shielded/?srsltid=AfmBOorkU7EpjuoeOJBh1Se_Zxz5wbhypT5TYDqJGYmFZHSXfZmW5bK3	$4.38	7	$30.66
4x7x2.5 Bearing	McMaster	57155K551	https://www.mcmaster.com/57155K551/	$11.66	6	$69.96
5x8x2.5 Shielded Flange Bearing	Bearings Direct	SMF85-ZZ	https://bearingsdirect.com/smf85-zz-stainless-steel-mini-flanged-ball-bearing-5x8x2-5-shielded-sslf-850zz/	$6.24	9	$56.16
6x10x3 Shielded Flanged	Bearings Direct	SMF106-ZZ	https://bearingsdirect.com/smf106-z	$6.24	4	$24.96

Bearing			z-stainless-steel-mini-flanged-ball-bearing-6x10x3-shielded-sslf1060zz/			
Pulley Stock (6"x6" Sheet)	McMaster	89015K301	https://www.mcmaster.com/89015K301/	$9.09	1	$9.09
Large Pulley Stock	McMaster	4634T44	https://www.mcmaster.com/4634T44-4634T441/	$25.69	1	$25.69
Spacer Stock (12 mm OD)	McMaster	4634T37	https://www.mcmaster.com/4634T37-4634T371/	$4.56	1	$4.56
Aluminum Bar (6061 Aluminum Bar, 1" Thick x 2-1/4" Wide)	McMaster	5679N108	https://www.mcmaster.com/5679N108-5679N111/	$30.64	1	$30.64
Aluminum Bar (6061 Al, 3/4" Thick x 1" Wide)	McMaster	8975K14	https://www.mcmaster.com/8975K14-9140T147/	$19.50	1	$19.50
Thinner steel cable for tendon (7 x 19, 0.024" Diameter,	McMaster	3461T62	https://www.mcmaster.com/3461T62/	$43.75	1	$43.75

25ft)						
Tendon (Steel Cable, 18-8 Stainless Steel, 7 x 19, 0.032" Diameter, 25')	McMaster	8930T53	https://www.mcmaster.com/8930T53/	$44.25	1	$44.25
Rope Compression Sleeve for 3/64" Rope Diameter (25 pack)	McMaster	3633T51	https://www.mcmaster.com/3633T51/	$6.43	2	$12.86
Springs (1.125" Long, 0.3" OD, 0.049" Wire Diameter)	McMaster	5108N336	https://www.mcmaster.com/5108N336/	$18.02	1	$18.02
Wave Spring (4mm)	McMaster	7764N501	https://www.mcmaster.com/7764N501/	$1.32	3	$3.96
Side-Mount External Retaining Rings for 1-1.4 OD	McMaster	98543A050	https://www.mcmaster.com/98543A050/	$9.60	1	$9.60
E-Clip (4 mm-5 mm OD)	McMaster	98543A103	https://www.mcmaster.com/98543A103/	$3.80	1	$3.80
					SUM	$807.85

Worth noting is that several items were purchased as extra in case parts had to be remachined or components were lost. For example, although only one 1.5x4x2 bearing is used in the design, originally three were purchased in case two were lost. The team then lost two of these bearings, so three more were purchased just in case it was lost again.

The team purchased many bearings through Bearings Direct, which sold bearings at a lower price than McMaster, but took around one week for shipping. However, some bearings were needed ASAP, so some bearings were purchased from McMaster, which took around one day for shipping.

CAD

All CAD files for the finger were made in Onshape and are available in the final project folder under mechanical > dex finger. In this folder, there is "Four Bar Linkage," "Rough Dex Finger Model," "Rough Dex Finger Model - with Tendons," and "Dex Finger Model." The team was unable to delete items in the folder, so "Four Bar Linkage" and "Rough Dex Finger Model - with Tendons" can be ignored.

"Rough Dex Finger Model" is the design of the finger at the beginning of the quarter before the April 11 design review. Following the design review, the team decided to do a rework of the finger, making greater use of the global variable tool in Onshape, so the team created "Dex Finger Model." In this new model, the team created the "Variable Bible," which lists the dimensions for several key components of the finger, like the pulley radii, the width of phalanges, and more. The team used this so that any changes could be propagated throughout the finger without having to enter each individual part file.

Within the "Dex Finger Model" file, there are several part files, most of which are organized in folders (ie: hardware, spacers, phalanges). The full assembly of the finger can be found in the file "Final Finger." Worth noting is that as the team was creating the assembly, Onshape froze and crashed two times. This occurred as the team created the files "Finger Assembly" and "Finger Assembly Copy 1" (found in the "Ignore Assemblies" folder). As the team was assembling, Onshape would go into a loading screen that would exist forever. The team found that creating a copy of the assembly and working on the copy resolved the issue, so there exists three finger assembly copies. The final version is the assembly called "Final Finger."

Weekly(ish) Progress Presentations

The team's progress presentations to the class can be found here.

Power Finger

POWER FINGER

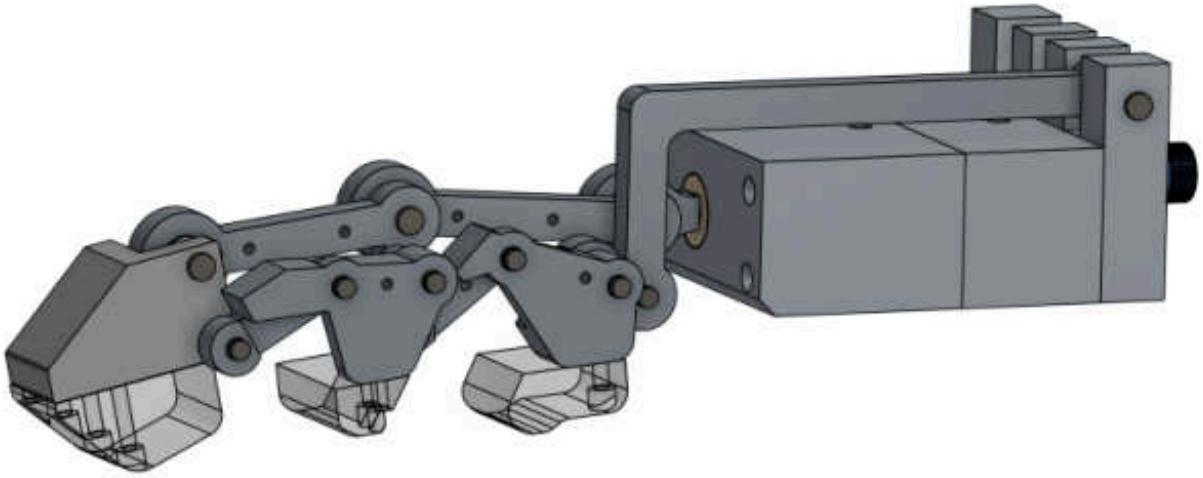


Figure 1: Power Finger Design

The Power Finger project was motivated by the need for a mechanically simple yet highly functional robotic finger capable of strong, adaptive grasping. Traditional robotic grippers often rely on complex, multi-motor actuation, leading to high power consumption, bulky designs, and limited compliance. Our goal was to create a tendon-driven finger with compliant degrees of freedom that could deliver high grasping force while maintaining mechanical simplicity and robustness.

This design has broad applicability in areas such as:

- **Prosthetics**, where low-power, high-force actuation and compliance are critical for everyday tasks.
- **Soft robotics**, where adaptability to diverse object geometries is essential.
- **Industrial gripping**, where durable, cost-effective fingers can streamline automation tasks.

The Power Finger is designed with the following objectives:

- **Deliver 40N continuous force** at the fingertip for strong grasps.
- **Maintain a grasp with minimal power consumption**, using passive mechanical compliance.

- **Employ a single actively driven degree of freedom (DOF)** with two passive compliant DOFs to reduce complexity.
- **Use robust tendon-based actuation** with stainless steel cables and spring-driven return to ensure reliable and repeatable performance.

This project integrates compliant mechanisms, tendon actuation, and linkage-based kinematics to create a powerful yet elegant robotic finger.

1. Specification Sheet

Degrees of Freedom	1 Active DOF 2 Compliant DOF
Length (mm)	Finger Length (palm to tip): 107 mm Overall Length: 170.5 mm
Width (mm)	52 mm
Height (mm)	34.75 mm
Motors Used	RoboMaster M2006 P36
Motor Max Torque	1 Nm continuous
Tendons	7x19 Coated 0.032" Stainless Steel
Tendon Max Capacity	20 lb, 89 N
Max Finger Force at Tip (extended)	10 N
Max Finger Force at Tip (full grasp)	30 N

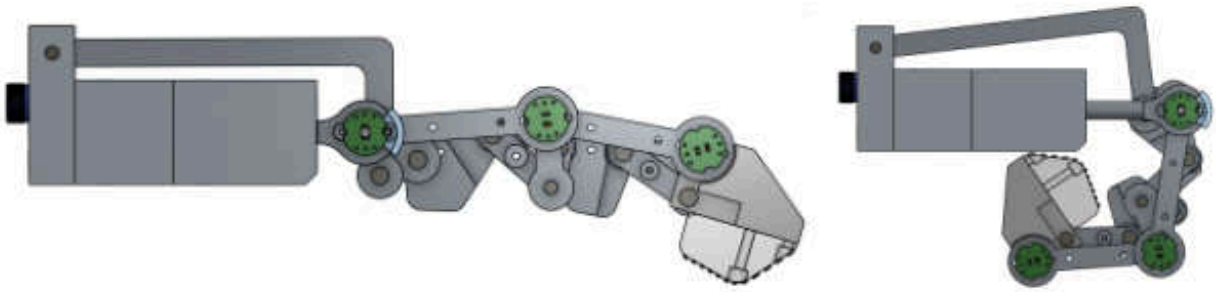


Figure 2: Extended and Curled Positions

2. Mechanical Design

2.1 4-Bar Linkage Design

The foundation of the Power Finger's motion is a **planar 4-bar linkage** that converts linear tendon actuation into coordinated angular motion at the MCP, PIP, and DIP joints. The original design used rigid links (A–B–C–D) and pivots to trace a biologically inspired curling trajectory, mimicking natural finger flexion.

This configuration allowed us to **fully couple the three primary joints** using a **single active degree of freedom**—the linear translation of the tendon. The key advantage was simplicity: by controlling one actuator, all joints move in synchrony, maintaining a natural grasp shape with minimal computation or feedback.

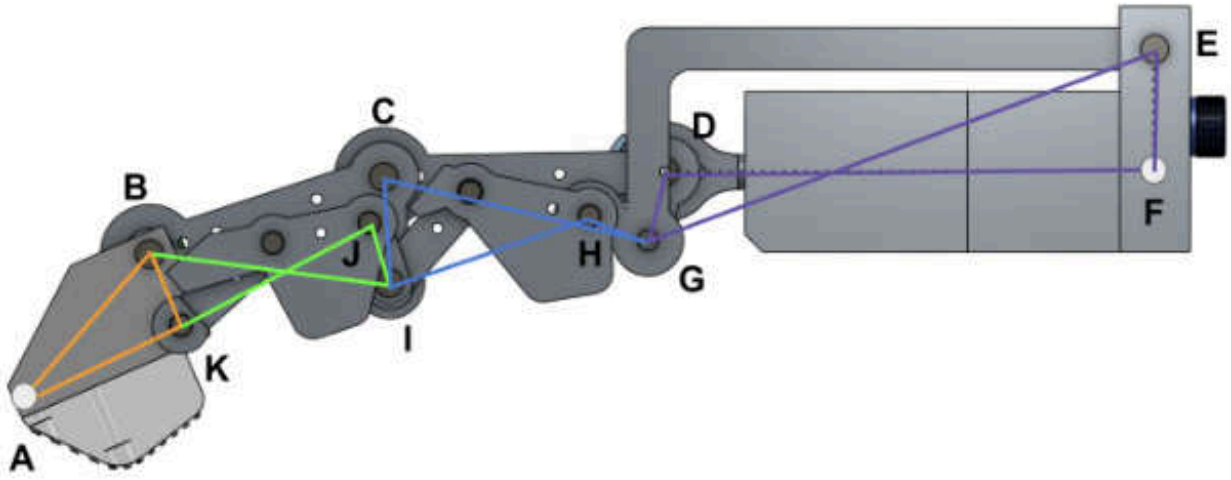


Figure 3: Labeled Joints

2.2 5-Bar Design with Compliance

While the 4-bar system offers precise joint coupling, it lacks adaptability when interacting with irregular or soft objects. To address this, we extended the design into a **5-bar linkage** by adding compliant elements—specifically, **torsional springs** at key joints and two additional links (I–J and H–G) as shown in white in the figure below. These links form a secondary path through the linkage that only activates under load.

In the absence of contact, the torsional springs hold the mechanism in its 4-bar behavior. Once the finger touches an object, **reaction forces cause links I–J-K and H–G-I to deflect**, triggering the 5-bar behavior. This adds **passive compliance**, enabling the finger to wrap around complex surfaces and distribute contact forces more evenly.

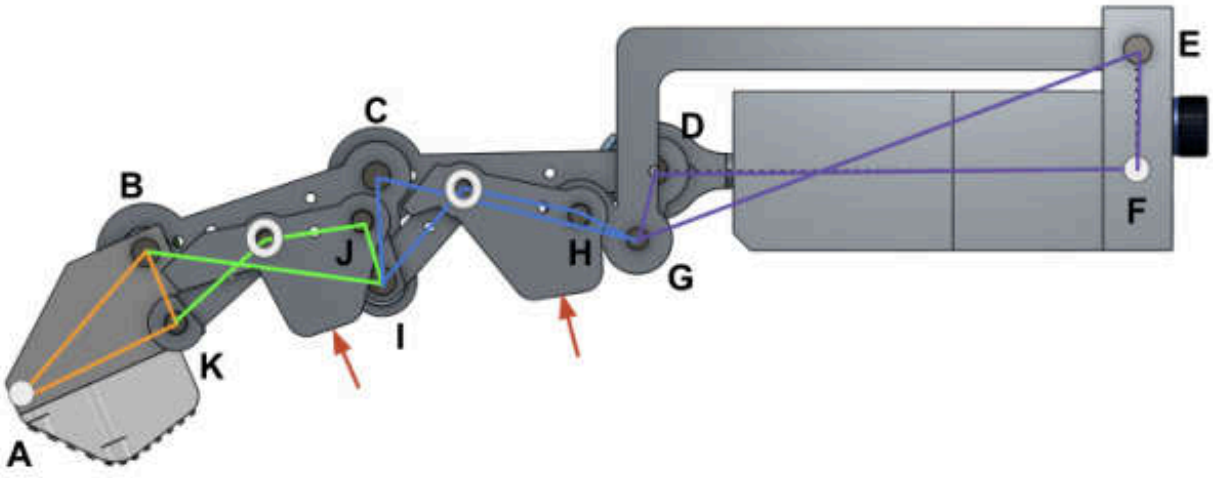


Figure 4: Reaction Forces Trigger 5-Bar Behavior

3. Actuation and Tendon Routing

To actuate the Power Finger, we used a **tendon-driven spring-return mechanism**. Our core design goal was to deliver a **strong grasp force** while consuming **minimal power during object holding**. To achieve this, we selected a **compression spring** preloaded in a piston to store mechanical energy. The spring drives the finger into a curled position, and the motor opposes the spring to open the finger for grasping.

Components

- **Motor**: RoboMaster M2006 P36: Provides sufficient torque (1 Nm continuous) to overcome spring force and extend the tendon.
- **Tendon**: 7x19 Coated Stainless Steel Wire Rope, 0.032" diameter: Chosen for flexibility, high strength (89 N), and routing efficiency.
- **Spring**: McMaster Part #9657K428
    - **Spring rate**: 5.1 lbs/in ≈ **0.896 N/mm**
    - **Free length**: 76.20 mm
    - **Fully compressed length**: 28.48 mm

- **Operating extension range**: 28.48 mm – 44.36 mm
- **Preload (at rest position):**
  $F = k * (Free\ Length - Initial\ Length) = 0.896 * (76.2 - 44.36) = 28.46N$
- **Max Force:**
  $F = k * (Free\ Length - Initial\ Length) = 0.896 * (76.2 - 28.48) = 42.76N$

To meet force requirements we used two springs in parallel, applying a total preload force of 56.92 N and compressed force of 85.51 N.

When selecting the spring we had to consider packaging (overall spring length, as the palm had limited space lengthwise), spring rate, and length the spring could compress (as the linkage has a specific range of motion and needs the spring to compress a specific distance to go from the extended to curled position).

Tendon Routing and Mechanical Advantage

The tendon is anchored at the fingertip and routed through the linkage joints to the motor. When the motor pulls, it **extends the spring**, which straightens the finger. Upon release, the spring contracts, curling the finger around the object.

This arrangement results in:

- **Passive grasping**: high holding force with no continuous motor power.
  Mechanical advantage through multi-joint routing: allows a lower motor force to produce larger distal finger forces.

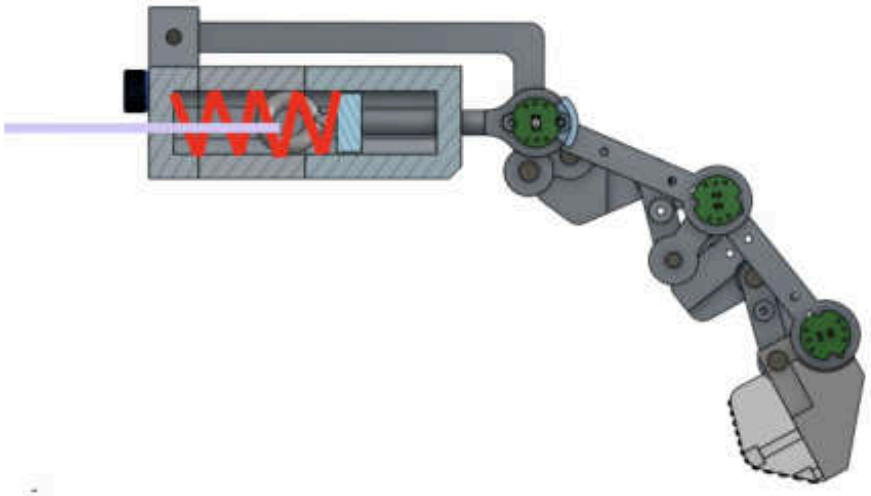


Figure 5: Tendon Routing and Spring

4. Kinematics

4.1 Forward Kinematics (4-Bar)

The forward kinematics of the Power Finger are defined by a closed-chain 5-bar linkage driven by spring extension. The system behaves as a **rigid 4-bar mechanism** until contact is made with an external object. Upon contact, compliance is introduced via torsional springs, transitioning the mechanism into a **5-bar configuration**.

Given an input spring extension Δx, we compute joint angles through sequential geometric vector loop closure:

1. Solve for θ_{GE} and θ_{GD} using loop constraints in the spring–motor linkage.

2. Propagate to the CG–GH loop to determine θ_{CG}, θ_{GH}, and subsequently θ_{IC}, θ_{IH}.

3. Use known offsets to get θ_{IB}, θ_{IJ}, and then solve for the remaining angles θ_{KB}, θ_{KJ}, θ_{AK}, θ_{AB}.

The MCP, PIP, and DIP positions are reconstructed from the angular chain, enabling full fingertip pose estimation.

We concatenate two kinematic regimes:

- **Pre-contact (pure 4-bar):** tendon force causes rigid curl.
- **Post-contact (5-bar):** external force deforms the structure, allowing object conformation.

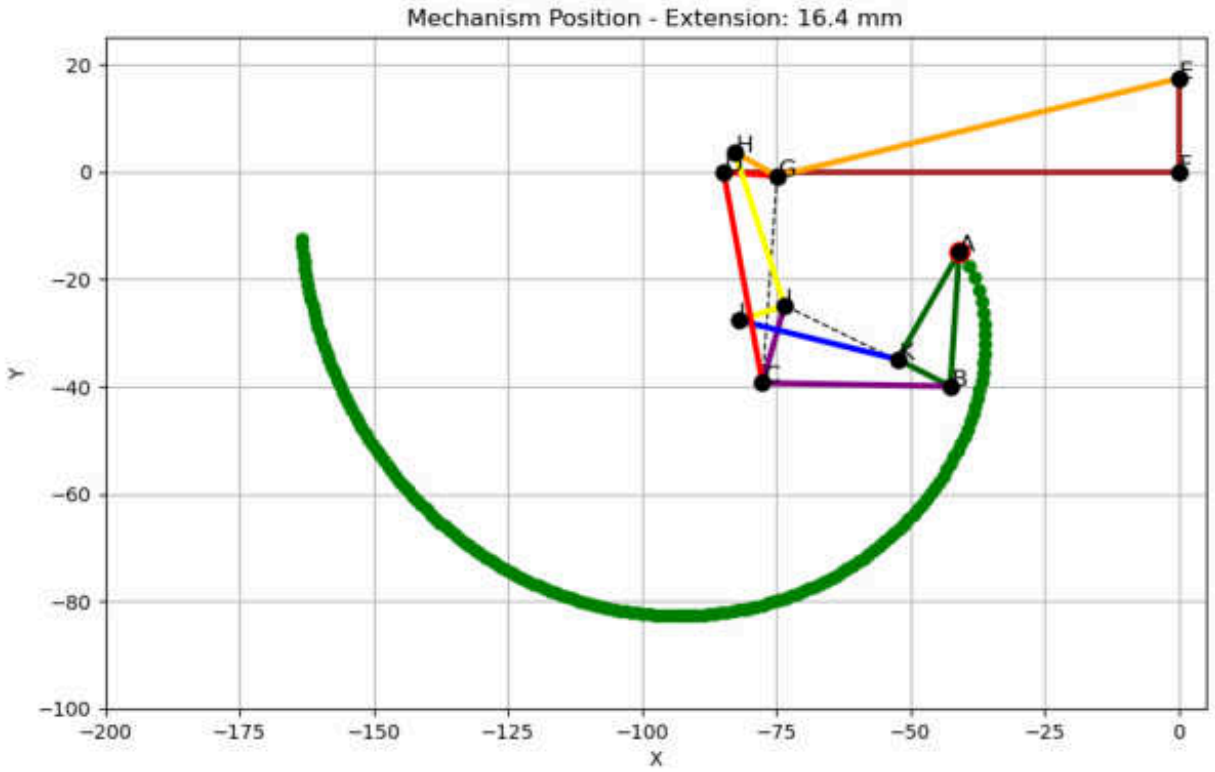


Figure 6: 4-Bar Position Graph

The derivation of vector loop for angle positions is below:

Loop 1: GE–GD–DF–FE

$$\vec{R}_{GE} = \vec{R}_{GD} + \vec{R}_{DF} + \vec{R}_{FE} \quad \Rightarrow \quad R_{GE}e^{j\theta_{GE}} = R_{GD}e^{j\theta_{GD}} + R_{DF}e^{j\theta_{DF}} + R_{FE}e^{j\theta_{FE}}$$

Euler's Formula

$$R_{GE}\cos(\theta_{GE}) = R_{GD}\cos(\theta_{GD}) + R_{DF}\cos(\theta_{DF}) + R_{FE}\cos(\theta_{FE})$$

$$R_{GE}\sin(\theta_{GE}) = R_{GD}\sin(\theta_{GD}) + R_{DF}\sin(\theta_{DF}) + R_{FE}\sin(\theta_{FE})$$

Physical Constraints

$$\theta_{DF} = 0 \rightarrow \cos(\theta_{DF}) = 1, \sin(\theta_{DF}) = 0$$

$$\theta_{FE} = \frac{\pi}{2} \rightarrow \cos(\theta_{FE}) = 0, \sin(\theta_{FE}) = 1$$

Full Equation for Loop 1

$$R_{GE}\cos(\theta_{GE}) = R_{GD}\cos(\theta_{GD}) + R_{DF}$$

$$R_{GE}\sin(\theta_{GE}) = R_{GD}\sin(\theta_{GD}) + R_{FE}$$

Loop 2: IC = IH + HG + GC

$$\vec{R}_{IC} = \vec{R}_{IH} + \vec{R}_{HG} + \vec{R}_{GC} \Rightarrow R_{IC}e^{j\theta_{IC}} = R_{IH}e^{j\theta_{IH}} + R_{GH}e^{j\theta_{GH}} + R_{CG}e^{j\theta_{CG}}$$

$$R_{IC}\cos(\theta_{IC}) = R_{IH}\cos(\theta_{IH}) + R_{GH}\cos(\theta_{GH}) - R_{CG}\cos(\theta_{CG})$$

$$R_{IC}\sin(\theta_{IC}) = R_{IH}\sin(\theta_{IH}) + R_{GH}\sin(\theta_{GH}) - R_{CG}\sin(\theta_{CG})$$

Physical Constraints

$$\theta_{GH} = \theta_{GE} + \angle HGE$$

$$\theta_{CG} = \theta_{GD} + \angle CGD$$

Loop 3: KJ–IJ–IB–KB

$$\vec{R}_{KJ} = \vec{R}_{IJ} + \vec{R}_{IB} - \vec{R}_{KB} \Rightarrow R_{KJ}e^{j\theta_{KJ}} = R_{IJ}e^{j\theta_{IJ}} + R_{IB}e^{j\theta_{IB}} - R_{KB}e^{j\theta_{KB}}$$

$$R_{KJ}\cos(\theta_{KJ}) = R_{IJ}\cos(\theta_{IJ}) + R_{IB}\cos(\theta_{IB}) - R_{KB}\cos(\theta_{KB})$$

$$R_{KJ}\sin(\theta_{KJ}) = R_{IJ}\sin(\theta_{IJ}) + R_{IB}\sin(\theta_{IB}) - R_{KB}\sin(\theta_{KB})$$

Physical Constraints

$$\theta_{IB} = \theta_{IC} + \angle BIC$$

$$\theta_{IJ} = \theta_{IH} + \angle JIH$$

Loop 4: AB–AK–KB

$$\vec{R}_{KB} = \vec{R}_{AK} + \vec{R}_{AB} \Rightarrow R_{KB}e^{j\theta_{KB}} = R_{AK}e^{j\theta_{AK}} + R_{AB}e^{j\theta_{AB}}$$

$$R_{KB}\cos(\theta_{KB}) = R_{AK}\cos(\theta_{AK}) + R_{AB}\cos(\theta_{AB})$$

$$R_{KB}\sin(\theta_{KB}) = R_{AK}\sin(\theta_{AK}) + R_{AB}\sin(\theta_{AB})$$

4.2 Joint Angles vs. Extension

To validate the kinematic solution, we plotted the evolution of joint angles across the full piston extension range. Each joint angle was solved symbolically and numerically using loop closure equations at every sampled displacement step.

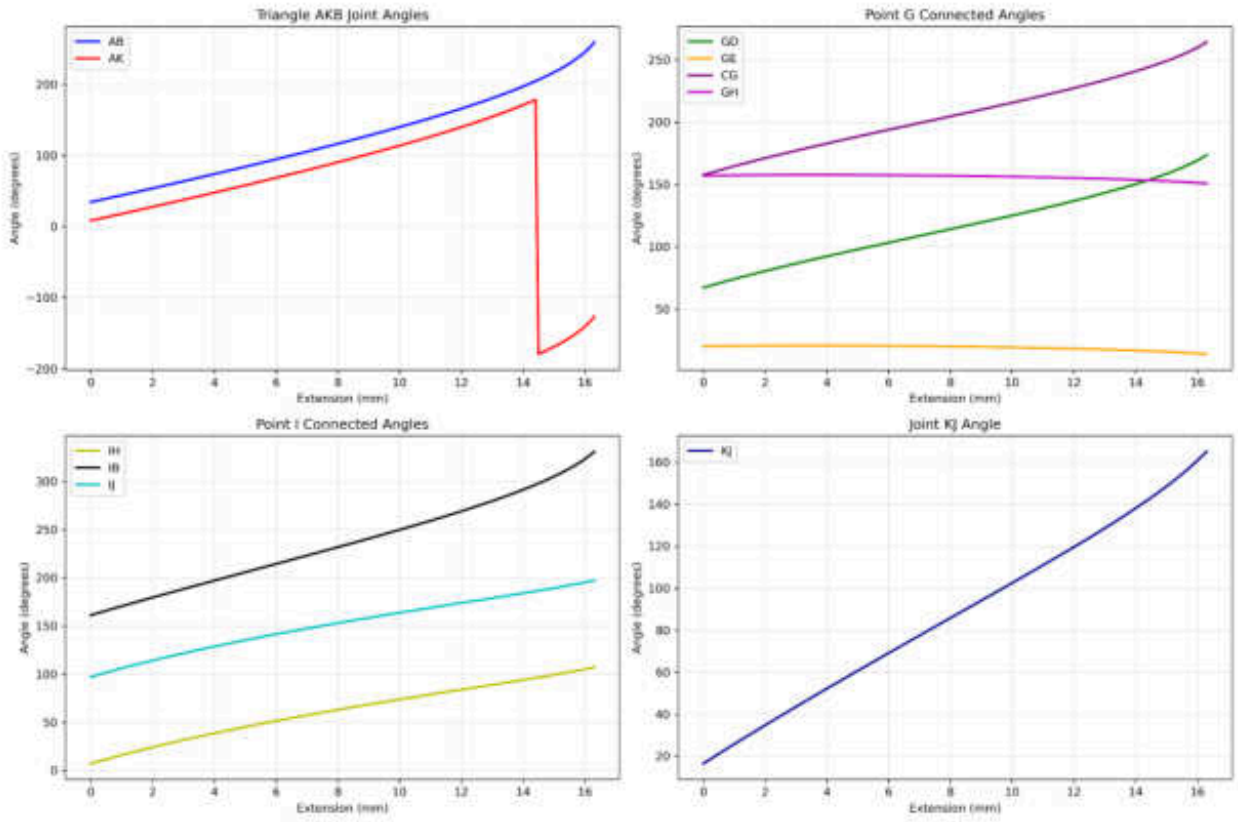


Figure 7: Joint Angles Plots

This visualization confirms consistent, monotonic motion during extension and highlights the coupling between joints due to the closed-chain constraint.

4.3 Joint Velocities

Angular velocities of MCP, PIP, and DIP joints were computed by differentiating angle trajectories with respect to time, assuming a constant linear extension rate of 1 mm/s.

Near the mechanical limits (e.g., full grasp), velocity spikes are observed due to nonlinear geometric sensitivity—small changes in piston displacement yield large angular displacements at the fingertip. This behavior confirms that we have a singularity near full grasp. Velocities are derived by taking the time derivative.

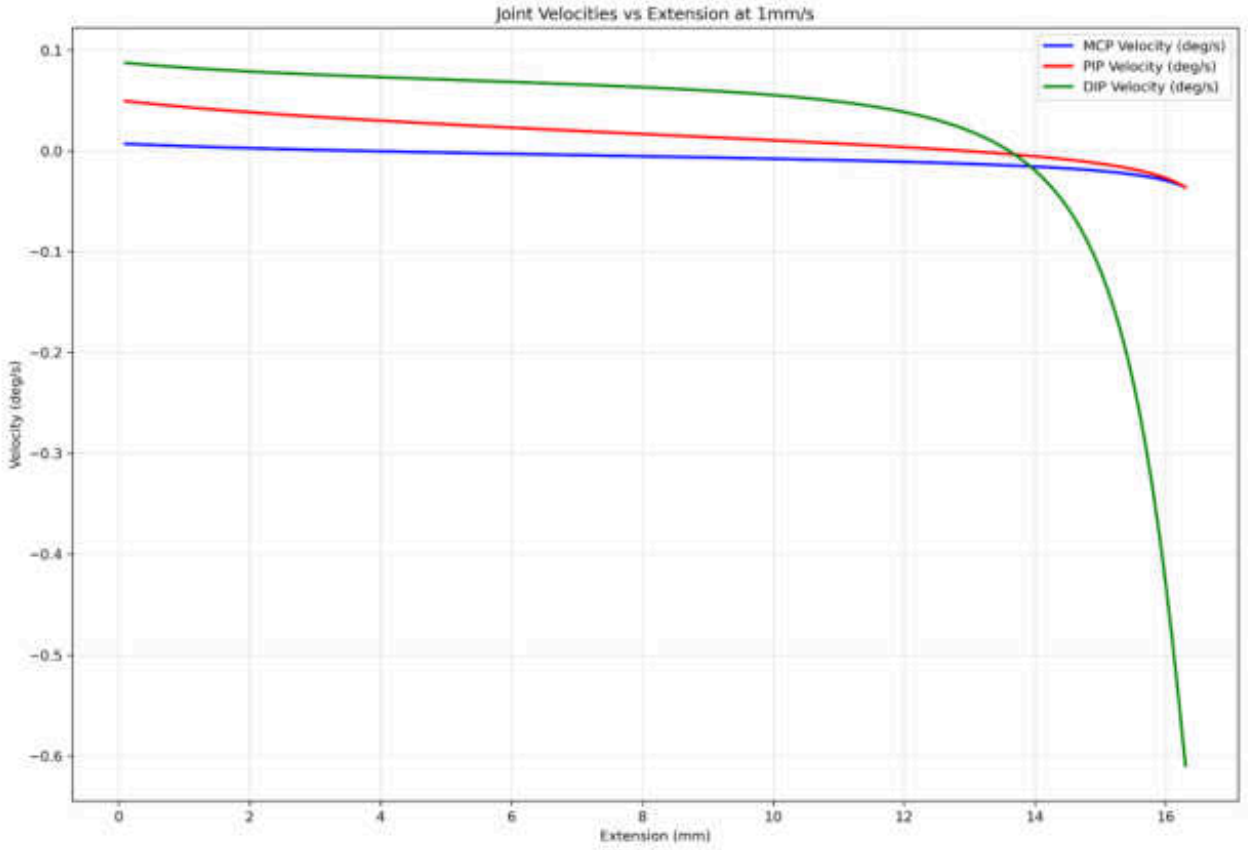


Figure 8: Joint Velocities Plot

This analysis is critical for control bandwidth estimation and actuator sizing, ensuring stable operation near kinematic singularities.

Derivation of Velocity using Vector Loop:

Loop 1: GE + GD + DF + FE

$$\vec{R}_{GE} = \vec{R}_{GD} + \vec{R}_{DF} + \vec{R}_{FE} \quad \Rightarrow \quad R_{GE}e^{j\theta_{GE}} = R_{GD}e^{j\theta_{GD}} + R_{DF}e^{j\theta_{DF}} + R_{FE}e^{j\theta_{FE}}$$

$$jR_{GE}\dot{\theta}_{GE}e^{j\theta_{GE}} = jR_{GD}\dot{\theta}_{GD}e^{j\theta_{GD}} + \dot{R}_{DF}e^{j\theta_{DF}}$$

$$R_{GE}\dot{\theta}_{GE}\cos\theta_{GE} = R_{GD}\dot{\theta}_{GD}\cos\theta_{GD} + \dot{R}_{DF}\cos\theta_{DF}$$

$$R_{GE}\dot{\theta}_{GE}\sin\theta_{GE} = R_{GD}\dot{\theta}_{GD}\sin\theta_{GD} + \dot{R}_{DF}\sin\theta_{DF}$$

Given

$\dot{\theta}_{DF} = 0$

$\dot{R}_{GE}, \dot{R}_{GD} = 0$

$\theta_{FE} = \frac{\pi}{2}$ (fixed)

$\theta_{DF} = 0$ (aligned with x-axis)

Unknown

$\dot{\theta}_{GE}$

$\dot{\theta}_{GD}$

Loop 2: IC–IH–GH–CG

$$\vec{R}_{IC} = \vec{R}_{IH} + \vec{R}_{HG} + \vec{R}_{GC} \Rightarrow R_{IC}e^{j\theta_{IC}} = R_{IH}e^{j\theta_{IH}} + R_{GH}e^{j\theta_{GH}} + R_{CG}e^{j\theta_{CG}}$$

$$jR_{IC}\dot{\theta}_{IC}e^{j\theta_{IC}} = jR_{IH}\dot{\theta}_{IH}e^{j\theta_{IH}} + jR_{GH}\dot{\theta}_{GH}e^{j\theta_{GH}} + jR_{CG}\dot{\theta}_{CG}e^{j\theta_{CG}}$$

$$R_{IC}\dot{\theta}_{IC}\cos\theta_{IC} = R_{IH}\dot{\theta}_{IH}\cos\theta_{IH} + R_{GH}\dot{\theta}_{GH}\cos\theta_{GH} + R_{CG}\dot{\theta}_{CG}\cos\theta_{CG}$$

$$R_{IC}\dot{\theta}_{IC}\sin\theta_{IC} = R_{IH}\dot{\theta}_{IH}\sin\theta_{IH} + R_{GH}\dot{\theta}_{GH}\sin\theta_{GH} + R_{CG}\dot{\theta}_{CG}\sin\theta_{CG}$$

Given

$\dot{R}_{IC}, \dot{R}_{IH} = 0$

$\dot{\theta}_{GH} = \dot{\theta}_{GE}$ (rigid link)

$\dot{\theta}_{CG} = -\dot{\theta}_{GD}$ (opposite orientation)

Unknowns

$\dot{\theta}_{IC}$

$\dot{\theta}_{IH}$

Loop 3: KJ–IJ–IB–KB

$$\vec{R}_{KJ} = \vec{R}_{IJ} + \vec{R}_{IB} - \vec{R}_{KB} \Rightarrow R_{KJ}e^{j\theta_{KJ}} = R_{IJ}e^{j\theta_{IJ}} + R_{IB}e^{j\theta_{IB}} - R_{KB}e^{j\theta_{KB}}$$

$$jR_{KJ}\dot{\theta}_{KJ}e^{j\theta_{KJ}} = jR_{IJ}\dot{\theta}_{IJ}e^{j\theta_{IJ}} + jR_{IB}\dot{\theta}_{IB}e^{j\theta_{IB}} - jR_{KB}\dot{\theta}_{KB}e^{j\theta_{KB}}$$

$$R_{KJ}\dot{\theta}_{KJ}\cos\theta_{KJ} = R_{IJ}\dot{\theta}_{IJ}\cos\theta_{IJ} + R_{IB}\dot{\theta}_{IB}\cos\theta_{IB} - R_{KB}\dot{\theta}_{KB}\cos\theta_{KB}$$

$$R_{KJ}\dot{\theta}_{KJ}\sin\theta_{KJ} = R_{IJ}\dot{\theta}_{IJ}\sin\theta_{IJ} + R_{IB}\dot{\theta}_{IB}\sin\theta_{IB} - R_{KB}\dot{\theta}_{KB}\sin\theta_{KB}$$

Given

$$\dot{\theta}_{IB} = \dot{\theta}_{IC}$$

$$\dot{\theta}_{IJ} = \dot{\theta}_{IH}$$

$$\dot{R}_{KJ}, \dot{R}_{KB}, \dot{R}_{IB}, \dot{R}_{IJ} = 0$$

Unknowns

$$\dot{\theta}_{KJ}$$

$$\dot{\theta}_{KB}$$

Loop 4: AB–AK–KB

$$\vec{R}_{KB} = \vec{R}_{AK} + \vec{R}_{AB} \Rightarrow R_{KB}e^{j\theta_{KB}} = R_{AK}e^{j\theta_{AK}} + R_{AB}e^{j\theta_{AB}}$$

$$jR_{KB}\dot{\theta}_{KB}e^{j\theta_{KB}} = jR_{AK}\dot{\theta}_{AK}e^{j\theta_{AK}} + jR_{AB}\dot{\theta}_{AB}e^{j\theta_{AB}}$$

$$R_{KB}\dot{\theta}_{KB}\cos\theta_{KB} = R_{AK}\dot{\theta}_{AK}\cos\theta_{AK} + R_{AB}\dot{\theta}_{AB}\cos\theta_{AB}$$

$$R_{KB}\dot{\theta}_{KB}\sin\theta_{KB} = R_{AK}\dot{\theta}_{AK}\sin\theta_{AK} + R_{AB}\dot{\theta}_{AB}\sin\theta_{AB}$$

Given

$$\dot{R}_{AK} = \dot{R}_{AB} = 0$$

$\dot{\theta}_{KB}$ carried over from previous loop

Unknowns

$$\dot{\theta}_{AK}$$

$$\dot{\theta}_{AB}$$

Summary of Relationships

Loop	Unknowns	Relations Used
1	$\dot{\theta}_{GE}, \dot{\theta}_{GD}$	$\dot{R}_{DF}$ given, θ_{DF}, θ_{FE} fixed
2	$\dot{\theta}_{IC}, \dot{\theta}_{IH}$	$\dot{\theta}_{GH} = \dot{\theta}_{GE}, \dot{\theta}_{CG} = -\dot{\theta}_{GD}$
3	$\dot{\theta}_{KJ}, \dot{\theta}_{KB}$	$\dot{\theta}_{IB} = \dot{\theta}_{IC}, \dot{\theta}_{IJ} = \dot{\theta}_{IH}$
4	$\dot{\theta}_{AK}, \dot{\theta}_{AB}$	$\dot{\theta}_{KB}$ known from Loop 3

5. Force Analysis

5.1 Static Force Analysis

To understand the finger's behavior before introducing compliance, we first analyze the static force transmission in the original 4-bar linkage. This setup features a single degree of actuation through a tendon routed over the distal phalanx. The objective is to quantify how spring tension translates to output force at the fingertip.

Assumptions:

- The spring applies a tension force F_{Spring} along the FD direction.
- All links are rigid and connected via ideal pin joints.
- The system is in static equilibrium.

Moment Balance About Point G

To solve for the output force at the fingertip, we perform a moment balance about the base joint G. The spring force induces a torque about G via link GD, while the fingertip force F_{Perp} (perpendicular to distal link AK) generates a counteracting moment through the position vector GA.

$$F_{\perp} = \frac{(\vec{r}_{GD} \times \vec{F}_{\text{spring}})}{(\vec{r}_{GA} \times \hat{n}_{\perp})}$$

$\vec{F}_{\text{spring}}$ is the spring force vector along $\overrightarrow{FD}$

$\hat{n}_{\perp}$ is the unit vector perpendicular to distal link $\overrightarrow{AK}$

$\vec{r}_{GD} = \vec{D} - \vec{G}$

$\vec{r}_{GA} = \vec{A} - \vec{G}$

This formulation uses the principle of virtual work: the torque created by the spring must be balanced by torque due to the fingertip force.

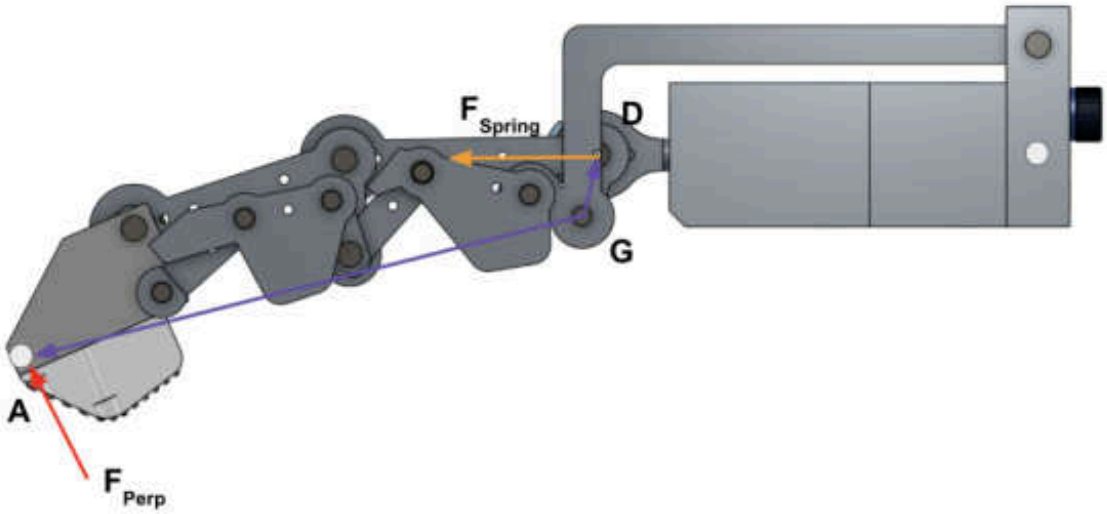


Figure 9: Free Body Diagram

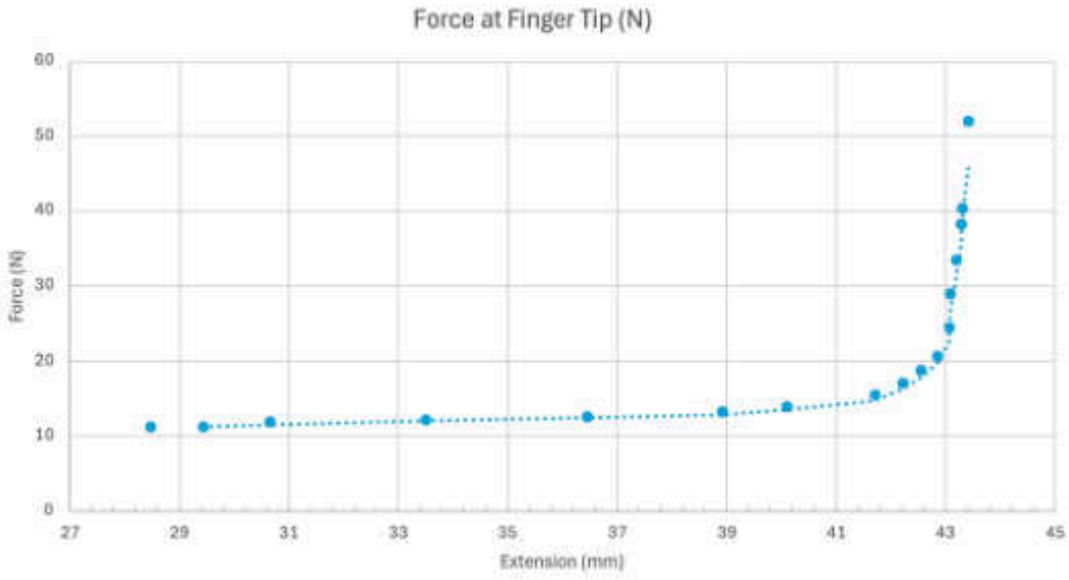


Figure 10: Fingertip Force Graph

7. Manufacturing

7.1 Linkages

We initially attempted to fabricate the finger linkages using waterjet cutting. However, this method proved unsuitable due to two key issues: (1) many of our linkage components involved angled or non-planar features that the waterjet could not accurately reproduce, and (2) the dimensional tolerances were too loose for our tight-fit assemblies, resulting in poor mating between joints. As a result, we transitioned to CNC milling, which allowed for much greater precision and consistency. While this shift introduced a learning curve—especially in toolpath generation and workholding strategies for small aluminum parts—it significantly improved both part quality and system reliability. All linkages were milled from 6061 aluminum to maintain strength while minimizing weight.

7.2 Shafts

The rotational shafts that served as pin joints were manufactured from steel using manual lathe operations. We chose steel for its higher strength and wear resistance, especially given the repeated loading cycles these joints would undergo. The lathe allowed for precise control of shaft diameter and shoulder lengths, ensuring a snug and consistent fit with both the linkage holes and the spring mounts. Light chamfers were added to assist with assembly and reduce edge stress concentrations.

7.3 Spring Assembly

The spring extension system required careful consideration due to the high cantilever forces experienced during finger actuation. Initially, we intended to use aluminum for the extension rod component due to its machinability. However, finite element analysis and early prototypes indicated significant deflection under load. We ultimately switched to a steel rod, which provided superior stiffness and better load-bearing characteristics. Although the spring mounts could have been produced using a vertical mill, we opted for CNC milling to streamline fabrication and achieve cleaner profiles and consistent tolerances.

7.4 Pads

The fingertip pads were fabricated using TPU filament on a Prusa i3 MK3S+ printer. We printed with 0% infill to maximize compliance and grip conformity. Higher infill percentages were tested but resulted in excessive stiffness, reducing the pad's ability to conform to varied object geometries. The soft TPU provided sufficient surface friction, but we also considered experimenting with epoxy resin casting or multi-material silicone molding to further increase grip and durability in future iterations.

8. Testing

8.1 Peg Test

To test the conformity of the 5-bar linkage design we performed a peg test. This test involved using screws as pegs to demonstrate the conforming nature of the linkage against various shapes. The results of this test are shown in the images below. The finger had no difficulties conforming to different grasp positions as forced by the pegs.

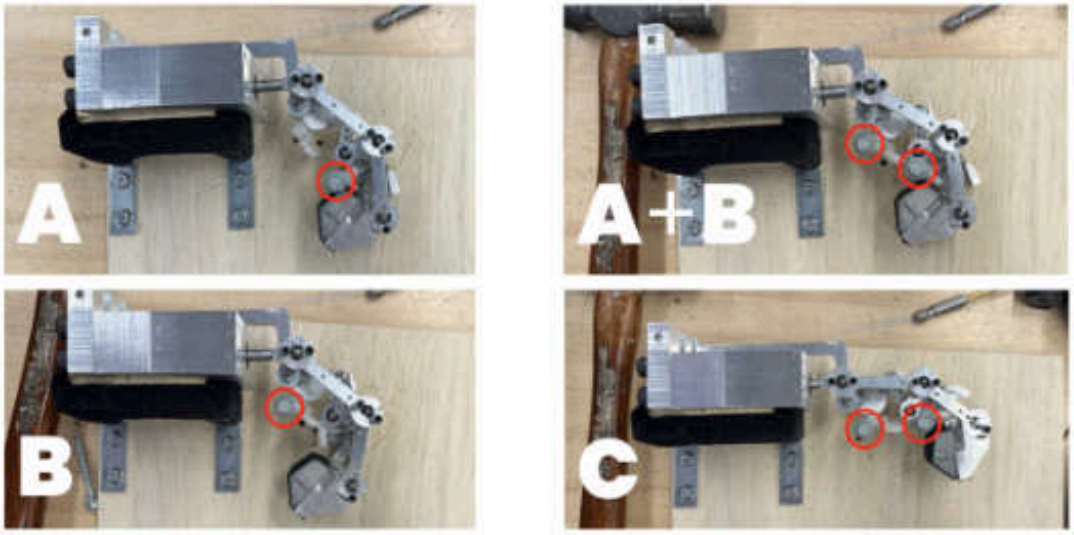


Figure 11: Peg Test

8.2 Grasp Force Test

In this test we determined the force applied at the tip of the finger at different grasping positions.

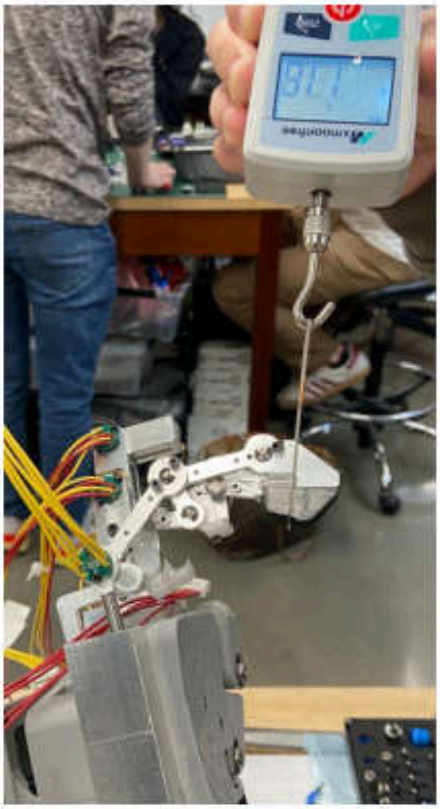


Figure 12: Grasp Force Test Setup

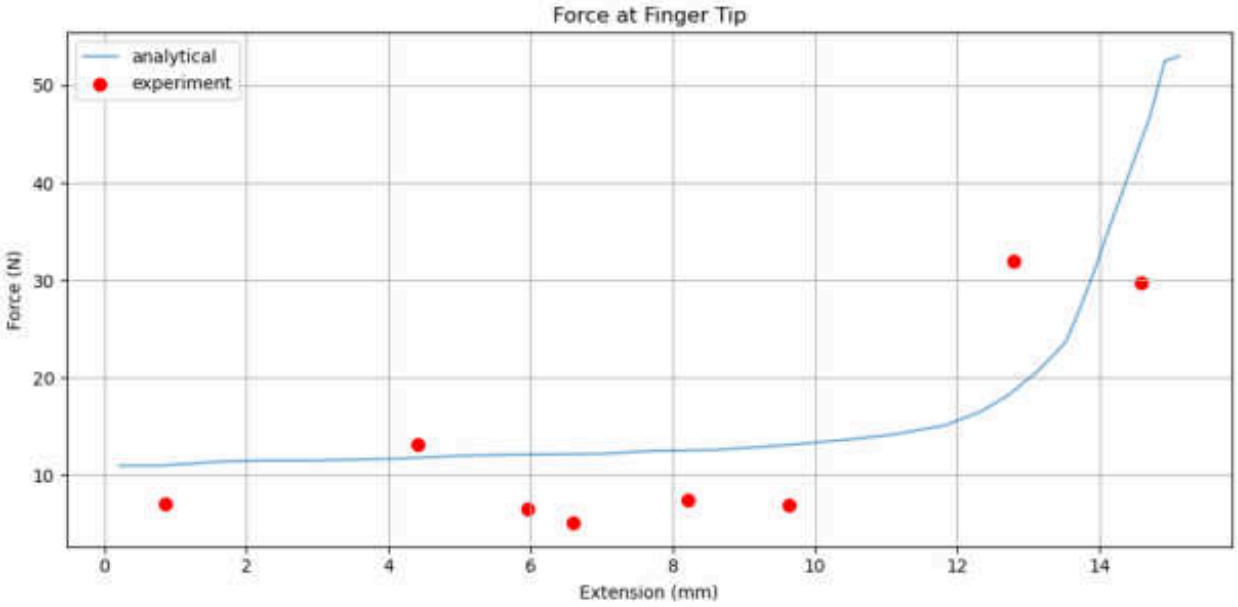


Figure 13: Grasp Force Test Results

8.3 Cylinder Grasp Test

To test the grasp strength around different sized objects we performed a cylinder grasp test, measuring the force required to ungrasp a cylinder linearly out of the grasp of the finger (varying from 20mm to 70mm in diameter, in increments of 10mm). The test setup and the graph of the results are shown below. This test measure grasp force due to measuring the normal force due to the grasp times friction of the pads. We were unable to test beyond 70mm due to being unable to grip without substantial support from the palm. From the graph we can see that the grasp strength of the finger is much greater for smaller objects than larger objects. The strength greatly depended on the friction in the system. We used sandpaper or grip tape to increase the friction and make it easier to grip.



Figure 14: Cylinder Grasp Test Setup

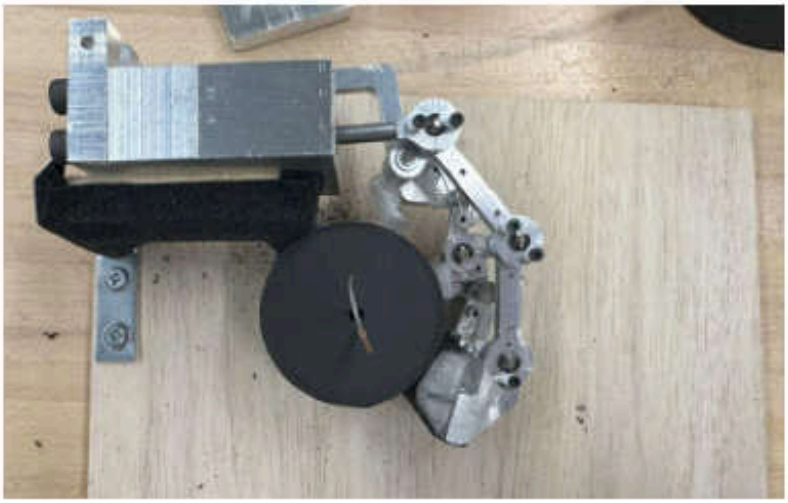


Figure 15: Cylinder Grasp Test Setup

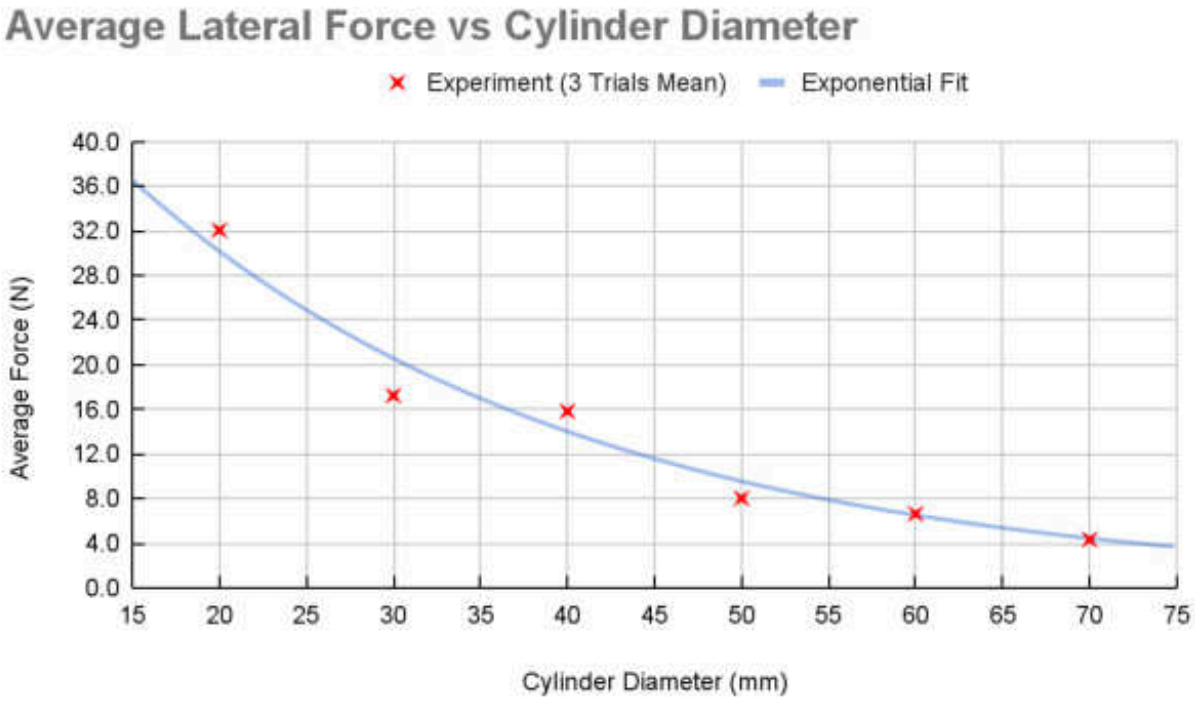


Figure 16: Cylinder Grasp Test Results

8. Reflection and Future Work

8.1 Workspace and Conforming Behavior Optimization

Future iterations should explore optimizing the finger's curl trajectory and workspace

coverage. The current design exhibits limited adaptability to irregular object geometries. By redesigning the linkage geometry or tendon routing, the finger could achieve more biomimetic curling and improved surface conformity during grasping.

8.2 Grasp Force Optimization

Testing revealed that grasp force peaks at full curl and drops significantly when the finger is more extended. This non-uniform force profile limits grasp stability during precision tasks. Adjustments to tendon pathing, spring preload, or linkage lengths could help re-balance the force distribution to maximize fingertip force across a wider range of configurations.

8.3 Pad Material Optimization

The cylinder grasp test confirmed that pad material critically affects friction and thus grasp strength. The current 0% infill TPU pads perform well in compliance but may benefit from a dual-material strategy—combining a soft core with a higher-friction surface layer. Exploring elastomers, silicones, or even castable resins could significantly improve grip strength and conformity.

8.4 Shell Design

A protective outer shell remains an important design milestone. It would shield internal linkages from impact or contamination, allow better integration of the pads, and give the finger a more anthropomorphic appearance. A modular, snap-fit shell could also improve assembly and maintenance.

8.5 Mechanical Redesign to Reduce Stress and Cantilever

Several components, particularly the extension rod and distal joints, experience high bending moments due to excessive cantilever lengths. Redesigning to minimize unsupported spans—by repositioning the actuation path, using thicker cross-sections, or introducing reinforcement features—could improve longevity and reduce mechanical failure risk.

8.6 Weight Optimization

Although the current prototype prioritizes rigidity, there's clear opportunity to reduce weight without sacrificing performance. This could involve switching to lighter alloys, hollowing non-critical features, or using topology optimization to remove unnecessary

material. A lighter finger would enable faster actuation and lower energy consumption in robotic applications.

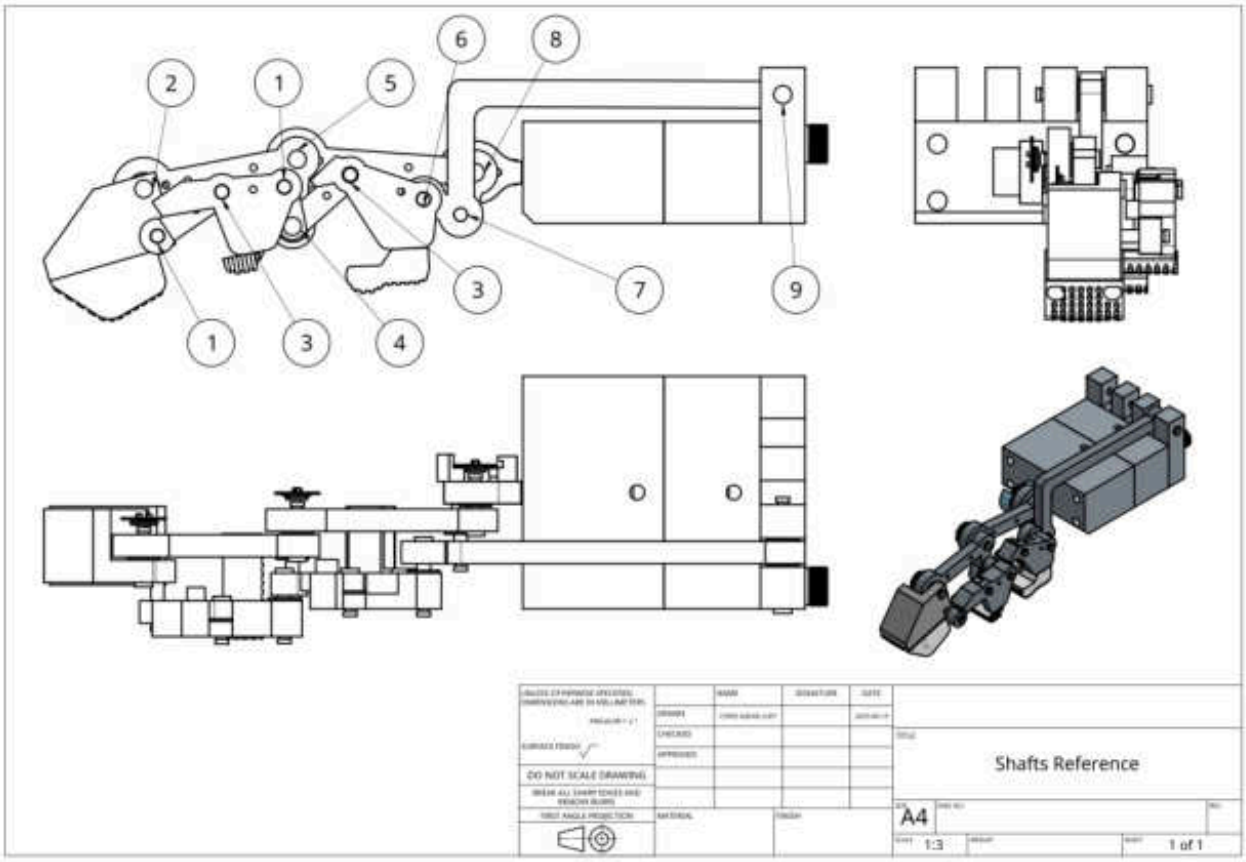
7. Mechanical Drawings and CAD

The final CAD can be found on the Onshape here. All of our designs are saved in the Power-Grasp Finger folder. The final design is called 5-Bar Design.

The drawings are located here:
https://drive.google.com/drive/u/0/folders/1Nbyotr8MVJPOeGSryV5drSJtldHeL9R0

Kinematic Analysis Code: https://github.com/ChristopherLuey/FingerForceAnalysis

7.1 Drawings of Shafts



https://drive.google.com/drive/u/0/folders/1Nbyotr8MVJPOeGSryV5drSJtldHeL9R0

8. Bill of Materials

Ordering Sheet

Item	Vendor	Part #	Unit Price	QTY	Price
6061 Al Rod (1-3/8" diameter, 1/2')	McMaster	8974K17	12.09	1	12.09
6061 Aluminum Bar (1-1/2" x 1-1/2" x 1')	McMaster	9008K46	27.7	1	27.7
6061 Aluminum Bar (10 mm x 40 mm x 1 ft)	McMaster	9146T69	15.76	1	15.76
Aluminum Bar (1 ft)	McMaster	9008K14	12.05	1	12.05
Aluminum Bar (5mm x 40mm x 3ft)	McMaster	9146T44	18.83	1	18.83
Bearings (3mm)	McMaster	57155K538	10.66	26	277.16
Bearings (4mm)	McMaster	57155K554	14.16	8	113.28
Compression Spring	McMaster	9657K428	8.79	1	8.79
Double Return Torsion Springs	Amazon		4.99	1	4.99
Dowel Pins	McMaster	91595A023	10.66	1	10.66
Eyebolt	McMaster	9686T71	9.1	1	9.1
Low-Carbon Steel Bar 5 x 25mm x 1ft	McMaster	6775T57	8.27	1	8.27
Multipurpose Aluminum Sheet, 1ft length	McMaster	9146T62	13.19	1	13.19
Multipurpose Aluminum Sheet, 1ft length	McMaster	9146T78	24.73	1	24.73
Rope Compression Sleeve for 1/16" (25 pack)	Mcmaster	3633T2	6.4	2	12.8
Shoulder Bolt	McMaster	92981A120	1.75	5	8.75
Shoulder Bolt	McMaster	92981A746	3.32	2	6.64
Sleeve Bearing	McMaster	2868T309	2.58	2	5.16
Sleeve Bearing	McMaster	2938T752	2.43	2	4.86
Socket Head Screw	McMaster	91290A199	6.64	1	6.64
Spring	McMaster	3630N201	13.43	1	13.43
Stainless Steel Ball Bearing	McMaster	7804K104	7.17	5	35.85
Steel Shaft 3mm (1 ft)	McMaster	5544T222	4.9	1	4.9
Steel Shaft 4mm (1 ft)	McMaster	5544T232	5.1	3	15.3
Steel Shaft 4mm (3 ft)	McMaster	5544T232	9.87	1	9.87
Tendon (25 feet)	McMaster	3423T32	56.25	1	56.25
Tight-Tolerance 12L14 Carbon Steel Rod, Ultra-Machinable, 5 mm D x 1 ft	McMaster	5544T242	5.67	1	5.67
Torsional Springs Assortment Kit	Amazon		12.98	1	12.98
Wave Spring Washers M3	McMaster	92161A049	10.8	1	10.8
				Total:	**766.5**

Software

Software

Software documentation can be found in the README of the project's github.